

**Soil Moisture and Drought Monitoring Using Remote Sensing  
I: Theoretical Background and Methods**

David L.B. Jupp, Tian Guoliang, Tim R. McVicar, Qin Yi and Li Fuqin

**Final Report Australia-China Joint Science and Technology Commission Project  
1992-1997**

**EOC Report, 1998.1**

© 1998 CSIRO Australia, All Rights Reserved

This work is copyright. It may be reproduced in whole or in part for study, research or training purposes subject to the inclusion of an acknowledgment of the source. Reproduction for commercial usage or sale purposes requires written permission of CSIRO Australia.

## Authors

David L.B. Jupp<sup>1</sup>, Tian Guoliang<sup>2</sup>, Tim R. McVicar<sup>3</sup>, Qin Yi<sup>4\*</sup> and Li Fuqin<sup>5\*</sup>

1 CSIRO Earth Observation Centre, PO Box 3023, Canberra, ACT, 2601, Australia  
david.jupp@eoc.csiro.au

2 Institute of Remote Sensing Applications, Chinese Academy of Sciences, Beijing China  
tiangl@irsa.irsa.ac.cn

3 CSIRO Land and Water, PO Box 1666, Canberra, ACT, 2601, Australia  
tim.mcvicar@cbr.clw.csiro.au

4 School of Physics, The University of New South Wales Sydney, 2052, Australia  
qinyi@newt.phys.unsw.edu.au

5 Environmental Science, Murdoch University, Western Australia, 6150, Australia  
li@qnim.murdoch.edu.au

\* previously affiliated with 2

**ISBN 0 643 05463 4**

### **For bibliographic purposes, this document may be cited as:**

Jupp, D.L.B., Tian, G., McVicar, T.R., Qin, Y. and Fuqin, L., 1998. Soil Moisture and Drought Monitoring Using Remote Sensing I: Theoretical Background and Methods, EOC Report 1998.1, pp. 96.

### **For additional copies of this publication please contact:**

Publication Enquires  
CSIRO Earth Observation Centre  
PO Box 3023  
CANBERRA  
ACT 2601  
AUSTRALIA

enquiries@eoc.csiro.au

<http://www.eoc.csiro.au>

## CONTENTS

<b>CONTENTS</b>	<b>3</b>
<b>SUMMARY</b>	<b>i</b>
<b>1 INTRODUCTION</b>	<b>1</b>
<b>2 DROUGHT AND SOIL MOISTURE</b>	<b>5</b>
<b>3 MONITORING SOIL MOISTURE USING THE WATER BALANCE</b>	<b>7</b>
<b>4 USING REMOTELY SENSED INFORMATION</b>	<b>9</b>
<b>5 SIMPLE INVERTIBLE MODELS RELATING DAYTIME SURFACE TEMPERATURE AND EVAPOTRANSPIRATION</b>	<b>13</b>
<b>5.1 One Layer Models</b>	<b>13</b>
<b>5.2 Two-Layer REBM Model</b>	<b>16</b>
<b>5.3 Constrained Two-Layer Models</b>	<b>19</b>
<b>5.4 Available Energy</b>	<b>21</b>
5.4.1 Low cover or bare soil	21
5.4.2 Vegetated case	23
<b>5.5 Performance with Data</b>	<b>25</b>
<b>6 ESTIMATING METEOROLOGICAL DATA AT THE TIMES AND ON THE DATES OF AVHRR OVERPASSES FROM STANDARD DATA</b>	<b>29</b>
<b>6.1 Air Temperature</b>	<b>29</b>
<b>6.2 Humidity / Vapour Pressure</b>	<b>32</b>
6.2.1 Daytime humidity from daily meteorological data	32
6.2.2 Interpolating vapour pressure	34
<b>6.3 Solar Radiation</b>	<b>40</b>
6.3.1 A simple daily model	40
6.3.2 The Bristow-Campbell model for daily total transmittance	42
6.3.3 Estimation of solar radiation at the times of overpasses	48
6.3.4 Estimation of diffuse fraction	54
<b>6.4 Wind Speed</b>	<b>56</b>
6.4.1 Influence of wind speed on daily $ET_p$ calculations	56
6.4.2 Influence of wind speed on instantaneous $ET_a$ , $ET_p$ and $m_a$ calculations	58
6.4.3 Influence of wind speed when inverting $T_s$ from the REBM when $m_a$ is known	63
<b>6.5 Daily Potential Evaporation</b>	<b>65</b>

<b>6.6 Application to Yucheng Data</b>	<b>67</b>
6.6.1 Modelling of individual terms and $ET_a$	67
6.6.2 Comparing modelled $ET_a$ with measured $ET_a$	69
6.6.3 Modelling Net Radiation	71
<b>7 INTEGRATING THE METHODS AT AVHRR OVERPASS TIMES</b>	<b>76</b>
7.1 Image based Products	76
7.2 Calibrating the Water Balance	77
<b>8 CONCLUSIONS</b>	<b>77</b>
<b>9 ACKNOWLEDGMENTS</b>	<b>78</b>
<b>10 REFERENCES</b>	<b>80</b>
<b>11 APPENDIX: SOLUTION OF THE TWO LAYER ENERGY BALANCE EQUATIONS WHEN RESISTANCES ARE GIVEN</b>	<b>86</b>
11.1 Basic Equations	86
11.2 Defining Equations	86
11.3 Solution when resistances are known	88
11.4 The Error Function and its Partial Derivatives	89
11.4.1 Special Case (1) - PET	92
11.4.2 Special Case (2) - Infinite resistance (no water!)	94

## **SUMMARY**

In many parts of the world, including China and Australia agricultural production is limited by the availability of water and severely affected during times of natural drought. Satellite remote sensing has the capacity to monitor both plant available moisture and land cover type and condition at regional scales over extended periods. It provides an excellent strategic monitoring tool to assess the level of drought stress and to indicate the need to respond at a regional scale.

In recognition of this background, a cooperative international project combining satellite remote sensing measurements with regional water balance modelling has been carried out in China and Australia between 1991 and 1997 under the framework of the Australia-China Joint Science and Technology Commission. It has been implemented by CSIRO Land and Water and the CSIRO Earth Observation Centre in Australia and the Institute of Remote Sensing Application of the Chinese Academy of Sciences. The objective of the work has been to investigate and demonstrate the potential for an operational system based on satellite and other geographic data.

This Report is one of two which comprise the final reports of this Project. They describe the methods developed and demonstrated in this Project and show how satellite data may provide routine monitoring of the distribution of regional moisture availability from space.

This first Report introduces the theoretical basis for combining meteorological data and surface energy balance models to estimate the moisture availability (measured here as the ratio of actual to potential evapotranspiration) based on remotely sensed measurements of surface temperature. When the surface cover is a complete vegetation canopy then the moisture availability is a function of the available water in the root zone. When there is partial cover, the moisture availability is a combination of near surface soil evaporation and transpiration by the plants. One objective of the modelling is to separate these effects in the data. It is shown that a simple two-layer surface energy balance model with suitable access to meteorological data and linked to a water balance model can provide effective means to link the satellite data and plant available moisture.

The first Report also discusses how to make best use of daily meteorological data to provide necessary ancillary meteorological data to the surface energy balance models at the AVHRR overpass times which allow the models to be run. The minimum daily meteorological data sets consists of daily maximum and minimum air temperatures and daily rainfall. From this minimum data set methods to derive air temperature, relative humidity and solar radiation at the AVHRR overpass times have been tested. The influence of wind speed has also been assessed. Finally, the sensitivities of these two methods are tested against intensive field data collected at the Yucheng Research Station, Shandong Province, China.

In the second Report the use of methods developed in the first are applied using AVHRR data in an operational Geographic Information Systems (GIS) setting to monitor the level of drought in the North China Plain, which affects the winter wheat crop, and in the Murray-Darling Basin. Such assessments can be used as regional measures of drought stress, or as tools for planning water allocation, or as indicators of the efficiency with which water is being used. These measures, taken together with estimates or records of yield, provide very powerful management tools in the task of maximising production in the face of limited or costly water availability.



## **1 INTRODUCTION**

In this first Report, and Part II, the application of AVHRR thermal data to monitoring drought and soil moisture effects at a regional scale is investigated in China and Australia. Part I describes the theoretical methods we have used in order to construct a demonstration system for monitoring. Part II describes the implementation and application of the theory using satellite and meteorological data covering the Murray Darling Basin (MDB) (Fig 1) and North China (or Huang Huai Hai) Plain (NCP) (Fig 2) of China where the work has developed (Jupp *et al.*, 1990, Jupp *et al.*, 1992, McVicar *et al.*, 1991, McVicar *et al.*, 1992, McVicar *et al.*, 1993, Tian *et al.*, 1989, Tian, 1991, Tian, 1993, Yang and Tian, 1991).

The MDB covers 1.063 million square km of Southeast Australia and sustains a high proportion of Australia's dryland and irrigated agricultural production. Extensive clearing of natural vegetation and intensive irrigation have greatly altered the water balance of the MDB. Exacerbated by the effects of land degradation, the economic return from agricultural industries can be severely reduced during drought. In China, the NCP is the alluvial plain of the Huanghe (Yellow River), Huaihe and Haihe rivers. The NCP is one of the great plains of China and includes most parts of five provinces (Hebei, Henan, Shandong, Anhui and Jiangsu) and two autonomous cities (Beijing and Tianjin). The NCP covers an area of about 350,000 sq km with an area of arable land of 178,000 sq km. It is an important agricultural region of China accounting for up to 40% of national production in many of the major cereal crops. However, the NCP has for some time also been facing problems of drought, waterlogging and salinisation which to an increasing extent are limiting the maintenance of current agricultural production. The onset of drought is a particular problem since both natural and managed water resources are in great shortage, especially in spring when the winter wheat crop is developing.

Remotely sensed data can be used in regional monitoring and management in two main ways. The first is to monitor changes in land surface type and condition. Land cover type and condition as well as the temporal series of greening of crops can be monitored using a variety of satellite borne instruments (such as Landsat TM, SPOT and AVHRR) at a range of spatial and temporal scales. Out of this use of remotely sensed data can come estimates of land cover type (such as forest or grassland) and the condition of the cover (such as green or dry). The second use involves converting the remotely sensed data to physical measurements of the earth and using them to resolve environmental parameters. This may lead to estimates for parameters of the cover (such as Leaf Area Index or LAI, cover fraction and reflectivity) as well as geophysical parameters such as the surface radiometric temperature and albedo. It is this second aspect that will be the focus of these Reports. In particular, the Reports focus on the utility of thermal radiance data as measures of surface temperature. The temperatures of the land surface components are determined by the balance of available energy from the sun and its conversion to other forms of energy. In particular, the flux of water is a component of exchanges determining the surface temperature which thereby provides an indirect measure of moisture availability.

The NOAA AVHRR/HRPT data record provides a relatively long term environmental satellite based time series with available global coverage between 1983 to the present and will continue into the future. A number of satellite based sensors with similar characteristics are also being developed and deployed by countries other than the US. The five bands of the AVHRR measure visible, near infrared and three thermal bands of radiance. This allows the average radiant temperature of the earth's surface over an approximately 1 km pixel to be estimated at basically regular (albeit drifting) day and night time passes. The success rate of this measurement is determined by the cloudiness of the target area with the varying cloud cover resulting in a temporally 'gappy' series of surface temperature images being available for many areas of the world.

The opportunity for using the AVHRR data in environmental monitoring exists in both its day time and night time imagery. For low cover of vegetation, thermal response as expressed by high daytime temperatures and high differences between day and night temperatures (called the "thermal inertia", Price, 1982) depends on the soil moisture level in upper soil layers and provides an opportunity for remote sensing to estimate potential plant moisture stress when actual plant growth is low and soil moisture status when vegetation is not present. When there is more complete cover, the stomatal behaviour of the plants during the day can indicate the state of the plant available soil moisture stores. Higher than expected canopy temperatures are indicators of plant moisture stress and precede the onset of drought. This thermal response to lowered moisture availability occurs even when the plants are green and the leaf area still unaffected. This is due to leaf stomatal closure through which the plants minimise water loss. Some of the work reported here was originally motivated by satellite thermal imagery showing significant differences in stress between irrigated and rain fed crops that were not visible in greenness indices.

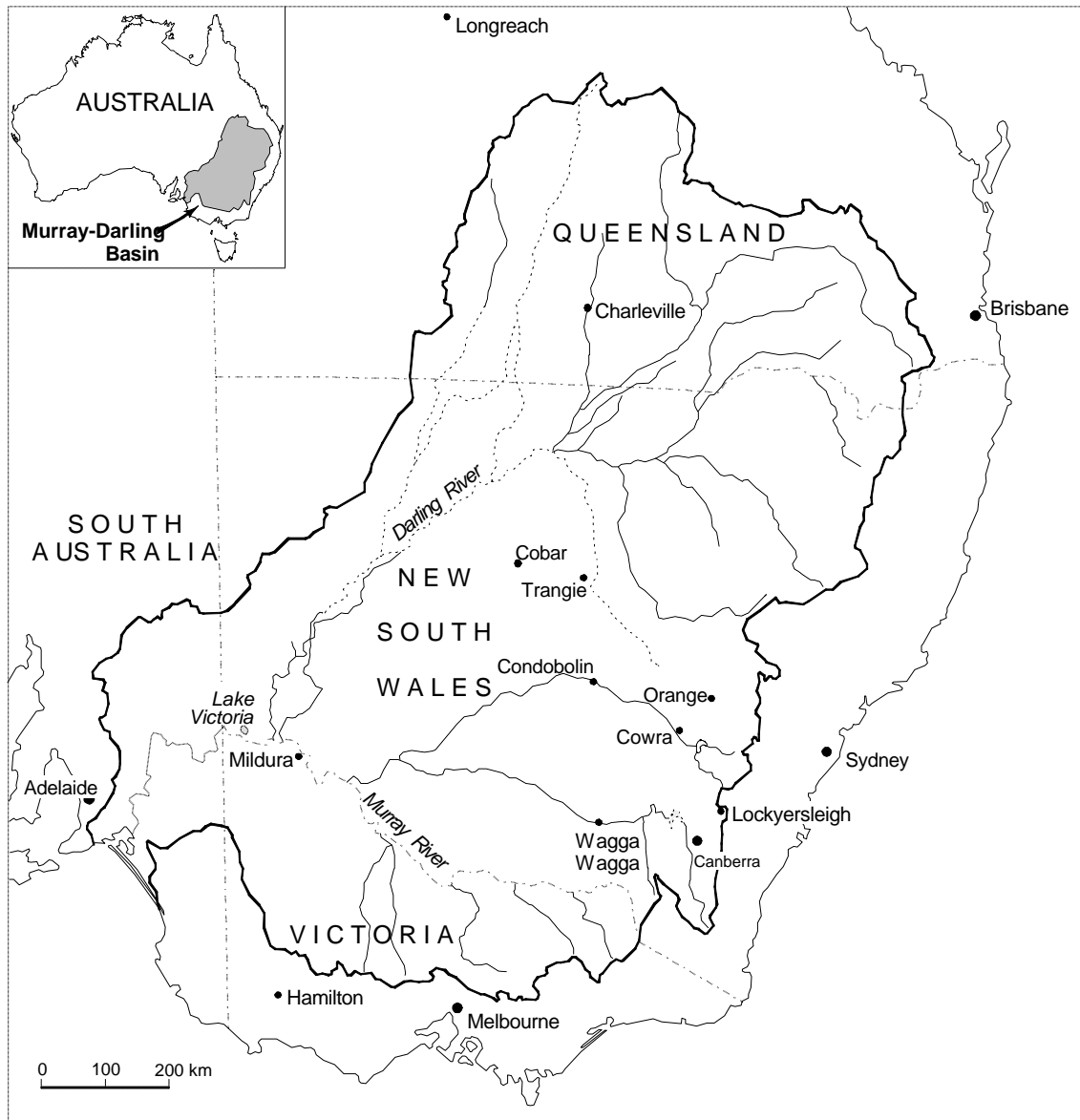


Figure 1. Location of the Murray-Darling Basin and field sites.

Plant moisture stress occurs when the demand for water exceeds the plant available soil moisture level and the potential for stress exists when the water in the soil storages is not enough to sustain the current growth. This is especially serious for crops as the consequence is reduced yields. For this case, Jackson *et al.* (1981, 1983) and Jackson (1982) pioneered methods, which are now used routinely, for assessing crop health and establishing irrigation scheduling at the field scale using measured canopy radiometric temperature as the primary data source. The temperature was measured by a thermal radiometer. The work reported here essentially applies those methods at the regional scale using AVHRR data. The scale issue - especially integrating the differing scales of the data sources needed - has been the most difficult issue in this application. The aim, however, is to establish a remote sensing based system which is as routinely applicable at the broad regional scale as the thermal methods are at the field scale. In this report the focus is on thermal data. For a comprehensive review of the current and potential uses of more general remotely sensed data (including reflective, thermal and microwave) for drought see McVicar and Jupp (1998).



Figure 2. Location of the North China Plain and field sites.

## **2 DROUGHT AND SOIL MOISTURE**

Severe drought in China and Australia can devastate crops and create hardship for the people who depend on the growth and health of crops and/or livestock for food or economic return. From this viewpoint, drought occurs when the balance between rainfall, evapotranspiration and discharge leaves less available water in the soil storages accessible by plants than they and/or animals which depend upon them need to maintain health. The key role of available soil moisture in the root zone in providing food for people and animals places accurate monitoring and effective responses as central issues in food security.

In this view of drought, low soil moisture is not the only factor. Drought here must be considered as a combination of moisture deficit and land use. It is a condition where the available moisture is at or below a point where harm is caused to vegetation (including crops) and/or stock and thereby to people and/or animals that depend on it. Drought can obviously be avoided if land utilisation can adapt to low soil water availability by reducing the demand on water when it is scarce or increasing the efficiency of water use. On the other side of drought, when rains arrive and soil moisture increases, the actual end of a drought will also be a function of land use. The drought stress is only past when the effects on the vegetation and the people and/or animals which depend on it are past. The lag between soil moisture replenishment and the response of the vegetation and the dependent animals and people (who may live in other regions) is a significant aspect of drought.

Recognising these complexities, White (1990) describes how drought has been classified into different types and presents a thorough analysis of the issues involved. Modifying his discussion slightly for the purposes of this Report, we will consider four broad overlapping categories:

- *Climatic Drought*, where periods of lower rainfall result in soil moisture and stored water being “significantly” less than the climatic equilibrium values for a given season;
- *Agricultural Drought*, where soil moisture deficiencies in the root zone lead to loss of production by crops and/or orchards beyond what is reasonably expected for the region;
- *Pastoral Drought*, where low soil moisture leads to lack of available feed for livestock and/or reduction in available stored surface water leads to lack of drinking water; and
- *Hydrological Drought*, where rainfall is reduced over a period to the extent that natural and man-made water storages such as dams, streams and even groundwater become scarce or depleted.

Climatic Droughts are characteristic of an environment and human land use must clearly adapt to them. The consequence of climate change may well be a change in the way people need to adapt to the different regional environments of the world. Of more acute consequence, Agricultural, Pastoral and (to some extent) Hydrological Drought

occur through the interactions between climate and land use. Their economic and human consequences demand effective monitoring and effective responses (such as improved water use efficiency, the provision of extra irrigation or reduction in pressure on the land) to their onset. The opportunity remote sensing provides for this task has been the motivation for the Project reported here.

### **3 MONITORING SOIL MOISTURE USING THE WATER BALANCE**

Setting aside, for the present, the potential for use of remotely sensed data, a general water budget for the root zone of the soil can be written (cf. Yang and Tian, 1991):

$$\frac{dW}{dt} = (P + I) - E - R + D - G \quad (1)$$

where:

- $W$  is water content of the root zone (cm);
- $P$  is Precipitation (cm);
- $I$  is Irrigation (cm);
- $E$  is Evapotranspiration (cm);
- $R$  is Runoff (cm);
- $D$  is Discharge from the groundwater (cm); and
- $G$  is Recharge to the groundwater (cm).

Incorporating recharge and discharge into a single soil “bucket” and combining irrigation with rainfall, this rate equation can be integrated over days or weeks resulting in a simple difference equation for the incremental change in the soil water storage:

$$W_t - W_{t-1} = P_t - E_t - R_t \quad (2)$$

Total soil moisture thereby increments by the net of rainfall ( $P_t$ ) minus evapotranspiration ( $E_t$ ) and runoff ( $R_t$ ) over the time period from  $t-1$  to  $t$  resulting in a total at time  $t$  of  $W_t$ . Since  $E_t$  can have contributions from evaporation from the soil or at open water surfaces or by transpiration from vegetation it is referred to as “Evapotranspiration” and abbreviated to “ET” in the following.

Despite the apparent simplicity of this water budget, ET and runoff are difficult to measure or characterise and the need to separately estimate recharge and discharge cannot be ignored if the issue of interest is soil moisture in the root zone of vegetation and crops rather than the whole soil system. Plant available soil moisture seems at one level to be a stable, integrated and simply computed parameter. However, it can easily become a relatively small residual component which is difficult to derive after surface/groundwater interactions have occurred and ET and runoff have accounted for most of the rainfall. Such residual terms are difficult to measure and are subject to considerable error. Despite its importance, soil moisture therefore remains one of the principal unknowns in climate and other environmental models.

Typically, an information system for estimating soil moisture will utilise meteorological data to provide rainfall and the atmospheric demand for water. This demand can be estimated in various ways from records of air temperature, solar radiation, humidity and wind speed (Monteith and Unsworth, 1990). It can then be used with allowance for land cover type and condition (which could be supplied by the analysis of remotely sensed data) to compute a potential evapotranspiration ( $E_p$ ). This is the response of the current land surface to the atmospheric demand for water if soil water is not limiting. The ratio of the actual ET ( $E_t$ ) to this potential ET ( $E_p$ ) is called the “moisture availability” ( $m_a$ ):

$$m_a = \frac{E_t}{E_p} \quad (3)$$

A simple water balance can be computed if an initial water store is known ( $W_0$ ) and if relationships between the water balance moisture availability ( $m_a(WB)$ ) and ‘runoff fraction’ ( $r_r$ ) and soil moisture are defined. These relationships are often called “operating characteristics” for the area being modelled. For example:

$$m_a(WB) = E / E_p = f((W_t - W_w) / W_{max}) \quad (4)$$

and

$$r_r = R / P = g(W_t / W_f)$$

Here,  $W_f$  is the water which would be available in the soil profile at field capacity when further precipitation creates only runoff,  $W_w$  is an amount of water in the profile at which ET stops and plant growth ceases.  $W_w$  is called the permanent wilting point.  $W_{max}$  is the extractable water which is usually taken to be equal to  $W_f - W_w$ . In the work reported in this Part I and the Part II, it has been sufficient (but not necessary) to use the simplest linear forms of these equations and in particular (Manabe, 1969):

$$m_a(WB) = \max[0, \min[1, \mathbf{b}(W_t - W_w) / W_{max}]] \quad (5)$$

where  $\mathbf{b}$  is parameter defining the sensitivity of  $m_a(WB)$  to changes in soil moisture in the upper layers.

The behaviour of the moisture availability as defined above with respect to changes in soil moisture could also be generated by a model and take into account plant uptake, plant cover and separate evaporation and transpiration. However, for our discussions and investigations here this simple model will be used. Hence, leaving aside recharge and discharge, the application of Equation (2) or some generalisation of (2) in which the total water store is broken into more ‘buckets’ results in a time series for the water available in the root zone and consequently a time series of moisture availability and actual evapotranspiration over the time step of the model.

Matching the available moisture series so computed with the demand or needs that the vegetation has for water, as outlined in Yang and Tian (1991), can provide a drought index for the area over which the water balance applies with the form:

$$D = (W_t - W_w) / W_r \quad (6)$$

where  $W_w$  is the permanent wilting point and  $W_r$  is the water requirement of the vegetation for normal growth. Deriving such a drought index (which is obviously closely related to  $m_a$ ) would thus need adequate meteorological data and GIS spatial information about the hydrological properties of soils and the nature of the land cover. Clearly, if  $m_a$  (and therefore its related index D) can be observed at various periods by remote sensing technology, the data could provide a calibration for the water balance parameters and operating characteristics. It is this general opportunity that is being investigated and evaluated in these two Reports.

## **4 USING REMOTELY SENSED INFORMATION**

There are many technical issues to consider to bring about successful operational use of water balance based methods in drought monitoring. Among them are two particularly important ones:

- 1 As a combination of soil water status and land use, an effective agricultural drought index ( $D$ ) will have a high degree of spatial variability. Since weather stations are often located away from the areas of most interest and decisions must often be made at different scales for different purposes, the spatial issues are critical. The unknown spatial variation of irrigation only adds to this spatial issue
2. There is little opportunity to compute the components of Equations (1) and (2) at a regional scale nor to validate or calibrate regional operating characteristics because of the spatial paucity of rainfall, runoff and meteorological data. Therefore the validity of applying the mass balances is questionable. Validation by field studies at selected sites is necessary but limited due to the high spatial variability addressed in point 1 (above). The resulting time series data are very sensitive to the choice of the operating characteristics and parameters such as  $W_f$  and  $W_w$  and even more sensitive to the greater number of (generally unknown) parameters of more complex water balance models.

Remote sensing data, being a “gappy” series of observations of the land cover and state cannot by themselves overcome these problems. However, the spatial coverage offers many ways to improve the situation. An effective combination of GIS processing and image processing of remotely sensed satellite data could provide an operational means to ameliorate the problems. Clearly, the need for information on the spatial distribution of soils, land use, access to irrigation and interpolation or extension of data over regions makes the use of an established regional environmental GIS essential as the base for such operational monitoring. Also, because of the high spatial and temporal variations that characterise the system, remote sensing from a range of platforms, including satellites and aircraft operating at a range of heights may be needed. However, by using different forms of remotely sensed data based on similar physics, issues of spatial and temporal scale can be addressed in a consistent way over large areas and at specific points in the region.

At the heart of the opportunity being investigated here is the use of remotely sensed thermal data as an observation of the surface energy balance. If  $R_n$  denotes net (total downward minus total upward) all wavelength radiation (units  $W m^{-2}$ ) and  $G$  denotes the heat flux into the soil or other storages (units  $W m^{-2}$ ), there is a net available energy ( $A$ ) at the earth's surface of  $A=R_n-G$  for conversion to other forms of energy in the surface boundary layer. In the models being used with remotely sensed data, the available energy at the earth's surface can be partitioned as:

$$\begin{aligned} A &= R_n - G \\ &= IE + H \end{aligned} \tag{7}$$

where:

$E$  is the Evapotranspiration (ET) flux ( $m \text{ sec}^{-1}$ ) of water vapour;  
 $I$  is Latent heat of vaporisation of water ( $J \text{ m}^{-3}$ ); and  
 $H$  is sensible heat flux ( $W \text{ m}^{-2}$ ), or the energy involved in the movement of the air and its transfer to other objects (such as trees, grass etc).  
 $IE$  is the flux of water as water vapour expressed as the energy used to change the water from liquid to vapour.

The energy (latent heat) component of the ET can be computed by writing the energy balance equation (Monteith and Unsworth, 1990) in the form:

$$IE = (R_n - G) - H \quad (8)$$

It follows that an avenue to computing the ET through its occurrence in the energy balance is to provide models for  $G$  and the sensible heat flux,  $H$ . The energy balance components may be computed in various ways using ‘resistance’ models (Monteith and Unsworth, 1990) of differing levels of complexity. These models are functions of the degree of detail introduced into the land surface structure and cover. In each case, the sensible heat flux is driven by the differences that exist between the distribution of temperatures among the surface components and the air temperature at different levels of the canopy.

For simple ‘one-layer’ models or more complex models with sufficient constraints (e.g. as described in Jupp, 1990) the remotely sensed radiometric surface temperature is an observation of effects due to the actual contact temperatures of the cover components. With sufficient ancillary knowledge, this observation may be sufficient to obtain an estimate for ET from a remotely observed radiometric surface temperature or (conversely) estimate an apparent surface temperature when the moisture status is known. Not all energy balance models, however, contain explicit relationships between soil moisture and the surface component temperatures. Many of those that do are complex and may contain many parameters (such as vertical profiles of soil and canopy properties) which are difficult to specify or even measure.

Most models, however, can be solved for the case when soil moisture is at field capacity and the crop functioning properly so that water does not limit the model in any way. The effective ET corresponding to a situation where soil water and vegetation condition are not limiting but the atmospheric demand and land cover type and structure are the same as the given case, is denoted  $IE_p$  and is called the *potential* ET. The (Energy Balance) moisture availability at other times (when soil water is below this field capacity) is then defined as:

$$m_a(EB) = IE / IE_p \quad (9)$$

For crops, Jackson *et al.* (1981, 1983) and Jackson (1982) used an integrated version of this quantity as measure of stress and defined the Crop Water Stress Index (CWSI) as:

$$\begin{aligned}
CWSI &= 1 - m_{ad} \\
&= 1 - \frac{E_d}{E_{pd}}
\end{aligned}
\tag{10}$$

where the subscript 'd' denotes that the quantity is integrated over a day. That is, the CWSI is based on the average moisture availability over a day.

A variety of empirical models exist relating the actual evaporation (and hence  $m_a$  and  $CWSI$ ) to available moisture in the soil matrix down to the rooting depth as well as the land cover type. For the water balance, these provide the operating characteristics that allow them to be computed. *Remote sensing therefore provides information for the water balance since the water and energy balances are linked through the ET as a common term.* If the daily water balance moisture availability  $m_a(WB)$  and the instantaneous (Energy Balance) moisture availability  $m_a(EB)$  can be effectively related, then the energy balance and the water balance operating characteristic can be directly coupled - even for the simplest energy and water balance models.

Establishing consistency between the remotely sensed  $m_a(EB)$ , the water balance moisture availability ( $m_a(WB)$ ) based on the observed surface temperatures, albedo, land cover type and the meteorological data based water balance provides a means to use remotely sensed data to validate and calibrate the water balance model at a scale common and appropriate to them both.



## **5 SIMPLE INVERTIBLE MODELS RELATING DAYTIME SURFACE TEMPERATURE AND EVAPOTRANSPIRATION**

### **5.1 One Layer Models**

For this work, it is critical to be able to relate remote observations of surface temperature and the moisture availability in relatively simple but accurate ways that will allow “inversion” of either surface temperature to evapotranspiration or evapotranspiration to an effective temperature. The models chosen must obviously be able to be computed using remotely sensed data and available meteorological data.

The style of model we have used is one where the interactions in the land surface layer are “closed” by meteorological data at a reference height above the land surface and in the top layer of the soil by some condition of the soil heat flux. The meteorological data assumed to be known at the reference height are air temperature, water vapour density (measured in one of a variety of ways), wind speed and short and long wave solar radiation. In the land surface layer it is also assumed that parameters such as plant cover, Leaf Area Index (LAI) and radiative properties such as albedo and emissivity of the surface components are also known. In the case of cover, LAI and albedo terms the estimates can be provided by remotely sensed data, either from simple land type and condition information or as parameter estimates. For example, empirical relationships have been developed which allow regional reflective remotely sensed indices to be scaled to estimates of LAI for needle-leaved canopies (Nemani and Running, 1989), broad-leaved canopies (McVicar *et al.*, 1996c) and grasses (McVicar *et al.*, 1996a, McVicar *et al.*, 1996b).

The least complex model of this type which still provides an adequate model for the near surface processes involved is the one-layer Resistance Energy Balance Model (REBM) or in a linearised form, the Penman-Monteith formula (Monteith, 1981, Monteith and Unsworth, 1990). The REBM treats the surface as a single, composite entity, assumes equilibrium of the fluxes and concentrations, is “external” in that it only includes fluxes of heat and water vapour external to the effective surface and does not include water balance components.

In this model, the sensible heat flux ( $H$ ) is modelled using a ‘resistance’ formulation (Monteith and Unsworth, 1990) by:

$$H = r C_p \frac{(T_e - T_a)}{r_a} \quad (11)$$

where:

- $T_e$  is an effective temperature for the composite surface;
- $T_a$  is air temperature at the reference height (usually 2 metres) above the surface;
- $r C_p$  is the volumetric heat capacity of air; and

$r_a$  is a term describing the resistance to transport of sensible heat between the surface and the reference height.

If a model for the resistance term ( $r_a$ ) is available and computable then the REBM proceeds by identifying  $T_e$  with the (remotely) measured surface temperature  $T_s$  to obtain H and using equation (1) to compute the ET as:

$$LE = R_n - G - H \quad (12)$$

which assumes that the soil heat flux  $G$  and net radiation  $R_n$  have been adequately modelled. In our work, for the one layer case we modelled these as:

$$R_n = (1 - \alpha) R_s + \epsilon \sigma (e_a T_a^4 - T_s^4) \quad (13)$$

where:

$\alpha$  is the albedo of the surface  
 $R_s$  is the shortwave solar irradiance  
 $\epsilon$  is the surface emissivity  
 $\sigma$  is the Stefan-Boltzmann constant  
 $\epsilon_a$  is the effective atmospheric emissivity  
 $T_a$  is air temperature at reference height, and  
 $T_s$  is the surface temperature.

Some account for fractional vegetation cover was used to estimate emissivity and albedo as linear combinations of values for vegetation and soil but the temperatures of the vegetation and soil are not differentiated in the one layer case.  $R_s$  and  $T_a$  must be measured or estimated at the reference site and a good (clear sky) approximation for  $\epsilon_a$  is due to Brutsaert (1975):

$$e_a = 1.24 (e_a / T_a)^{1/7} \quad (14)$$

where  $e_a$  is vapour pressure in millibars and  $T_a$  is air temperature in Kelvin. Both are assumed to be available or estimated at the site of application.

When vegetation cover is present and for daytime modelling, it is possible to use one of a number of simple closing conditions on  $G$  which take account of the vegetation cover. Choudhury *et al.* (1987) proposed that  $G$ ,  $R_n$  and the ‘‘hemispherical’’ fractional cover of vegetation ( $f_v$ ) could be usefully related by:

$$G = G_f R_{ng} \quad (15)$$

Where  $G_f$  is an empirical factor.  $R_{ng}$  is the net radiation at the soil which in that paper was estimated simply as:

$$R_{ng} = (1 - f_v) R_n \quad (16)$$

An alternative, and similar, empirically measured equation for crops which was used for the Chinese work was:

$$G = (0.1 - 0.042h)R_n \quad (17)$$

where  $h$  is the height of the crop.

The empirical factor  $G_f$  was used with a default value of 0.4 as found by Choudhury *et al.* (1987) but was also fitted to data at sites in both China (Yucheng Station) and Australia (Lockyersleigh Experimental site) These data confirmed the strong correlation but showed variations in the value of  $G_f$  in both directions from the default. When a fairly high level of vegetation cover is present none of these choices affects the estimates of ET or  $T_s$  by very much. With partial canopies (significant bare soil areas visible) both the measurement and application of this relationship becomes more difficult and soil heat flux becomes an important consideration (see Section 5.4.1)

From a range of choices, the approximation to  $r_a$  due to Choudhury *et al.* (1986) and Choudhury (1989) was shown to be very satisfactory from experiments by Kalma (1989) using data from a CSIRO Division of Water Resources experimental site at Lockyersleigh in NSW (Kalma *et al.*, 1987). It takes account of vegetation cover and has been used in the work reported here.

The ET can also be expressed in resistance form as:

$$LE = \frac{r C_p (e_s(T_e) - e_a)}{g (r_a + r_s)} \quad (18)$$

where

- $e_s(T_e)$  is saturated vapour pressure at temperature  $T_e$ ,
- $e_a$  is vapour pressure at the reference height
- $\gamma$  is the psychrometric constant and
- $r_s$  is a composite 'surface' resistance.

The surface resistance expresses both the intrinsic capacity to extract water through the composite surface and the available water in the root zone and near surface.

The temperature  $T_e$  is an effective canopy temperature which is sometimes called the "mid-canopy air stream" temperature. If  $T_e$  is identified with  $T_s$  then both  $LE$  and  $r_s$  are readily computable provided an effective model for  $r_a$  is used. The equality of  $T_e$  and  $T_s$  is the underlying assumption of the one-layer model. With this assumption, the moisture availability can be computed by defining  $E_p$  mathematically as the evapotranspiration which occurs when  $r_s$  is zero. Then, as defined previously,  $m_a(EB)$  is simply  $E/E_p$  where  $E$  is the ET obtained by equating the radiometric surface temperature ( $T_s$ ) with  $T_e$  and  $E_p$  is the zero resistance ET. From the above equation for ET it follows that:

$$m_a(EB) = \frac{r_a}{r_a + r_s} = \frac{1}{1 + \frac{r_s}{r_a}} \quad (19)$$

Computing this form of potential ET, as well as computing ET and  $T_e$  when one of  $r_s$  or  $m_a$  is specified rather than  $T_s$ , requires some care. The equations are nonlinear in that  $r_a$  is a function of  $T_e$  and can be numerically difficult to compute in situations of partial cover and unstable and drying meteorological conditions. However, with an appropriate numerical method, it is straightforward to derive an effective  $T_e$  (ie  $T_s$ ) corresponding to an input value for  $r_a$  or  $m_a$ . Alternatively, an effective  $r_s$  or  $m_a$  can be derived from an input  $T_s$ .

Finally, two special temperatures can be easily computed. These are the effective surface temperatures corresponding to fully wet conditions ( $r_s=0$ ) and fully dry conditions ( $r_s=\infty$ ) or, alternatively,  $m_a=1$  and  $m_a=0$ . The first is denoted  $T_0$  and the second  $T_\infty$  and their utility in our work will be discussed later. Obviously, if the model is adequate then the observed surface temperature should lie between these two extremes depending on the moisture availability.

## 5.2 Two-Layer REBM Model

The one-layer REBM provides a direct means for relating meteorological data, remotely sensed surface temperature and evapotranspiration through a single, composite 'surface resistance'. A disadvantage is that this surface resistance is the result of many factors from which any one, such as available soil moisture, is difficult to extract. Also, it has been found that in the presence of partial cover and drying conditions the model can perform very poorly.

A specific problem with the one-layer REBM has been discussed in Huband and Monteith (1986) and (using Lockyersleigh field data) by Kalma and Jupp (1990). This takes the form of a systematic discrepancy which occurs between the measured surface temperature and the estimate for  $T_e$  which is obtained when  $IE$  and  $H$  are obtained by Bowen Ratio measurements and the temperature estimated using the energy balance equations. In the latter case, the value for  $T_e$  which satisfies the observed flux measurements is known as the 'aerodynamic' temperature,  $T_{aer}$  and it should have been equal to  $T_s$  if the assumptions used in the one-layer REBM were correct. L'Homme *et al.* (1994) have also investigated this effect using Hapex data and examined methods by which it might be overcome.

The problem seems particularly severe in cases when sensible heat fluxes from the soil surface are high and de-couple from the mid-canopy interactions. The least complex model of the type outlined previously that provides a separation of the water loss through transpiration by plants and direct evaporation by soil and provides some explanation of the difference between aerodynamic temperature and the radiometric surface temperature is the Two-layer REBM. This is described in detail in Choudhury (1989). In this resistance formulation, the flux terms take the form:

$$\begin{aligned}
IE_v &= \frac{\mathbf{r} C_p (e_s(T_v) - e_e)}{\mathbf{g} (r_v + r_{vs})} & (20) \\
H_v &= \mathbf{r} C_p \frac{(T_v - T_e)}{r_v} \\
IE_g &= \frac{\mathbf{r} C_p (e_s(T_g) - e_e)}{\mathbf{g} (r_g + r_{gs})} \\
H_g &= \mathbf{r} C_p \frac{(T_g - T_e)}{r_g}
\end{aligned}$$

where:

$IE_v$  and  $H_v$  are latent and sensible heat fluxes between foliage and the mid-canopy air stream;

$IE_g$  and  $H_g$  are latent and sensible heat fluxes between ground and mid-canopy air stream;

$T_e$ ,  $T_v$  and  $T_g$  are the temperatures of the mid-canopy air-stream, the foliage and the ground respectively;

$e_e$  is the vapour pressure of the mid-canopy air-stream; and

$r_{vs}$  and  $r_{gs}$  are surface resistances to flux between an assumed saturated source and the surface for vegetation and the ground respectively.

The primary resistance terms  $r_a$ ,  $r_v$  and  $r_g$  have been computed as presented in Choudhury (1989). With these in place, the four basic conditions on a solution may then be written:

$$\begin{aligned}
\frac{1}{\mathbf{r} C_p} A_v &= \frac{1}{\mathbf{g}} \frac{(e_s(T_v) - e_e)}{r_v + r_{vs}} + \frac{(T_v - T_e)}{r_v} & (21) \\
\frac{1}{\mathbf{r} C_p} A_g &= \frac{1}{\mathbf{g}} \frac{(e_s(T_g) - e_e)}{r_g + r_{gs}} + \frac{(T_g - T_e)}{r_g} \\
\frac{(T_e - T_a)}{r_a} &= \frac{(T_v - T_e)}{r_v} + \frac{(T_g - T_e)}{r_g} \\
\frac{(e_e - e_a)}{r_a} &= \frac{(e_s(T_v) - e_e)}{r_v + r_{vs}} + \frac{(e_s(T_g) - e_e)}{r_g + r_{gs}}
\end{aligned}$$

where  $A_v$  and  $A_g$  are the partition of the total available energy ( $R_n - G$ ) between vegetation and soil. This can be done approximately in a similar way as was done for the one-layer case or more completely as discussed later.

These four equations provide constraints for the six unknowns  $e_e$ ,  $T_e$ ,  $T_g$ ,  $T_v$ ,  $r_{gs}$  and  $r_{vs}$  so that a solution is only possible when two extra conditions are given. These may be from a model for (or specification of)  $r_{gs}$  and  $r_{vs}$ , for example, or from mass balances and models for the relationships between root zone moisture, surface layer moisture and the two ‘moisture availability’ terms for vegetation and soil:

$$\begin{aligned}
m_{av} &= \mathbf{1}E_v / \mathbf{1}E_{vp} \\
m_{ag} &= \mathbf{1}E_g / \mathbf{1}E_{gp}
\end{aligned}
\tag{22}$$

where  $m_{av}$  is a moisture availability for the vegetation component and  $m_{ag}$  is a moisture availability for the soil surface.

These terms provide a means for the energy balance to integrate with water balances that separate evaporation and transpiration. In particular, a mathematical potential total ET ( $E_p$ ) and similar expressions for the soil evaporation ( $E_{gp}$ ) and transpiration ( $E_{vp}$ ) can be computed from these equations by setting  $r_{vs} = r_{gs} = 0$  which corresponds to no resistance to moisture available at both leaf and soil surfaces from the internal storages. In each of these cases, it is quite straightforward to derive estimates of the foliage ( $T_v$ ) and ground ( $T_g$ ) temperatures by application of a nonlinear solver. The equations and derivatives needed to do this are given in the Appendix. The Appendix also shows how estimates for surface temperature may be obtained for the extreme cases of fully wet ( $r_{vs} = r_{gs} = 0$ ) and fully dry ( $r_{vs} = r_{gs} = \infty$ ). These temperatures, denoted  $T_0$  and  $T_{\infty}$  should provide bounds within which the observed surface temperature will lie - depending on the moisture available for either or both of soil evaporation and canopy transpiration.

Of particular significance for this Report is the addition or derivation of a measurement on the system through remote sensing of the radiometric surface temperature ( $T_s$ ). This may (under general assumptions such as vertical view and relatively small differences between soil and vegetation emissivity) be approximated by the linear expression:

$$T_s = f_v T_v + (1 - f_v) T_g \tag{23}$$

where  $f_v$  is the fraction of vegetation cover which we are assuming in these Reports may be estimated from the remotely sensed data. If a measurement for  $T_s$  is provided, there remain five conditions and six unknowns resulting in an under-determined system of equations (short by one term) given only the remotely sensed data and reference meteorological data. Alternatively, if an integrated estimate of  $m_a$  such as:

$$m_a(EB) = \frac{\mathbf{1}E_v + \mathbf{1}E_g}{\mathbf{1}E_{vp} + \mathbf{1}E_{gp}} \tag{24}$$

were available (such as through the water balance model) then a complete solution is again short by one condition.

Separate estimates of foliage and background temperatures or separate estimates of ground evaporation and foliage transpiration could provide complete and determining sets of equations, but these are difficult to derive.

### 5.3 Constrained Two-Layer Models

There exist a number of ways in which the Two-layer REBM can be made soluble and provide a model with the convenience of the One-layer REBM or Penman-Monteith formula but still (in some cases) with the extra freedom and separation of vegetation and soil water loss that the Two-layer model provides. They each provide an extra condition which effectively reduces the Two-layer model to a modified one-layer model. Some constraints that have been investigated in this project (Jupp, 1990) include:

1. Observed temperature equal canopy temperature ( $T_s=T_e$ );
2. Canopy temperature equal foliage temperature ( $T_e=T_v$ );
3. Foliage temperature equal ground temperature ( $T_v=T_g$ );
4. Smith *et al.* (1988) condition ( $H_g=(1-\mathbf{a}_s)A_g$ );
5. Minimum power ( $P = r_v H_v^2 + r_g H_g^2 + r_a H^2$ );
6. Canopy Aerodynamic Resistance (L'Homme *et al.*, 1988);
7. Equal moisture availability ( $m_{av}=m_{ag}$ );

Only the One-layer REBM (which is equivalent to Case 1.) and the minimum Power (which is equivalent to Case 5. as described below) examples will be compared with data in this Report. The other Cases will be evaluated in a separate publication. In many examples, Cases 2., 4., 5. and 6. all behave similarly. But for the reasons illustrated in the following, the Case 5. seems to have greater robustness.

Norman *et al.* (1995) have also addressed this problem and provided a similar constraint to the Smith *et al.* (1988) condition but applied to the canopy so that ( $H_v=(1-\mathbf{a}_n)A_v$ ) where  $\mathbf{a}_n$  depends on canopy “dryness” just as the Smith *et al.* (1988)  $\mathbf{a}_s$  depends on soil “dryness”. It is not clear that the application of this assumption to the canopy is useful for partial canopies. The application to the soil does, however, seem to provide a very robust solution. L’Homme *et al.* (1994) investigated the difference between  $T_s$  and  $T_{aer}$  and proposed that the equations could be solved and the differences resolved with the addition of a constraint of the form:

$$T_g - T_v = a(T_s - T_a)^m \quad (25)$$

for suitable values for  $a$  and  $m$ . The Case 3. listed above was not a good choice in most examples and corresponds to  $a=0$ . Perhaps the more general equation introduced by L’Homme *et al.* (1994) can perform much better. These more recently published constraints should also be compared on an equal basis with the 7 constraints listed here.

The Case 5. ‘minimum power’ solution is an heuristic which seeks to choose a solution that minimises an energy type condition among possible solutions (Jupp, 1990). The condition chosen is an analogue of the variational principle which leads to Kirchhoff’s laws for electrical circuits and minimises the quantity P where:

$$P = r_v H_v^2 + r_g H_g^2 + r_a H^2 \quad (26)$$

By applying the minimum power principle to the under-specified system of equations without applying constraints, a solution is obtained in which:

$$\begin{aligned} H &= r C_p \frac{(T_e - T_a)}{r_a} \\ &= r C_p \frac{(T_s - T_a)}{r_a + r_a'} \end{aligned} \quad (27)$$

The solution can be obtained using either of the expressions:

$$r_a' = f_v^2 r_v + (1 - f_v)^2 r_g \quad (28)$$

or

$$T_e = \frac{r_a'}{r_a + r_a'} T_a + \frac{r_a}{r_a + r_a'} T_s \quad (29)$$

Either way, convenient solutions for evapotranspiration components (including  $m_a(EB)$ ) when  $T_s$  is given or  $T_s$  when  $m_a(EB)$  is given can be obtained by nonlinear equation solving using the equations and derivatives given in the Appendix. Note also that the last equation shows how  $T_e$  (i.e.  $T_{aer}$ ) and  $T_s$  can be different as discussed in Huband and Monteith (1986) and Kalma and Jupp (1990). However, the constraint also limits the flexibility of the solution so that some but not all of the observed effects are resolved when this is done.

The minimum power solution can be shown to be very close to the solution obtained by L'Homme *et al.* (1988) (Case 6.) when their method is applied to the two-layer lumped parameter case. Their solution seems to be a sufficient but not necessary one given their assumptions. The form of the minimum power solution also provides an explicit formula for the 'residual resistance' developed by Chen (1988) to explain discrepancies found in field data. Using general arguments, Chen (1988) concluded that an effective estimate for  $r_a'$  has the form:

$$r_a' = C \left| \frac{w_L}{u} \right|^{1/2} \quad (30)$$

where  $C$  is a constant,  $w_L$  is the effective leaf width and  $u$  is the wind speed in the mid-canopy area. For complete vegetation cover, the minimum power solution equates  $r_a'$  to  $r_v$  which (from Choudhury, 1989) has the same form. However, the advantage of the minimum power form is that an expression can be found when there is partial cover and it involves the canopy structure as well.

It can be shown that each of the constraints corresponds to some form of computable  $r_a'$  and allows our objectives of solving for the moisture availability when surface temperature is known and *vice versa* to be met.

Knowing the observed surface temperature and enforcing one of the listed constraints allows the evaporation to be computed with little extra computation than the one-layer model. The separate vegetation and ground temperatures can be computed as well as separate estimates for evaporation from the soil surface and transpiration from the

canopy. Using the mathematical form of  $E_p$  defined in the last section, the  $m_a(EB)$  can be computed and it is relatively straightforward to invert a value of  $m_a(EB)$  to provide an estimated surface temperature.

## 5.4 Available Energy

To complete the solution for either one or two layer model cases, some expressions are need for the available energy. In our work, two cases have been distinguished. The first is bare soil where the diurnal variations cannot be simply modelled by an empirical closing condition on G and the other is where there is a reasonable cover of vegetation.

### 5.4.1 Low cover or bare soil

When the vegetation cover is low, the diurnal cycle of surface temperature needs to be taken into account and the simple approximations for the available energy at the surface are not sufficient. In this case, heat conduction in the earth needs to be modelled. Many models have been proposed (e.g. Zhang, 1990, Wetzal *et al.*, 1984, Van de Griend *et al.*, 1985, Idso *et al.*, 1976, Cracknell and Xue, 1996a, Carlson *et al.*, 1981, Xue and Cracknell, 1995). In this research the model of Zhang (1990) is that which is implemented.

Thermal inertia is an internal factor which measures the way material temperatures change with the variations in external sources of heat, see Cracknell and Xue (1996b) for a review of the theory. It can be expressed as:

$$P = \sqrt{Irc} \quad (31)$$

where

P is thermal inertia of soil ( $J m^{-2} K^{-1} S^{1/2}$ );  
 $\lambda$  is heat conductivity of soil ( $J m^{-2} S^{-1} K^{-1}$ );  
 $\rho$  is density of soil ( $Kg m^{-3}$ );  
c is specific heat of soil ( $J Kg^{-1} K^{-1}$ ).

In particular, if the local region has a high thermal inertia then the temperature difference of the ground between day and night will be low relative to the diurnal change for material with a low thermal inertia. Since water increases the thermal inertia of a region this diurnal variation may be used to provide information about water content of the upper soil layers. However, since vegetation has a very low thermal inertia and resistance effects dominate in vegetated areas, the main opportunities for using thermal inertia are in semi-arid or bare conditions.

The equation of thermal transmission in soil is:

$$rc \frac{\partial T}{\partial t} = I \frac{\partial^2 T}{\partial z^2} \quad (32)$$

where

T is soil temperature (K);  
t is time (sec);  
z is depth of soil (m);

The boundary condition for this equation is simply:

$$G = -1 \frac{\partial T}{\partial z} \Big|_{z=0} = R_n - IE - H \quad (33)$$

where the terms are as defined for the one layer model previously with no vegetation cover. Pratt (1980), Price (1982) and others have provided convenient formulae for the thermal inertia when the boundary condition can be approximated in the form:

$$G = (1 - a) R_s - (A(t) + B T_s) \Big|_{z=0} \quad (34)$$

where:

**a** is albedo and  
 $R_s$  is the shortwave solar radiation

The time varying component  $A(t)$  can be constructed from meteorological station data using the interpolations discussed in Section 6.  $B$ , which can also be constructed from environmental data is assumed to remain constant.

If only the first term of the Fourier series for the temperature time series is evaluated and with various approximations which have been discussed recently by Xie (1991) it may be shown that:

$$P = \frac{-\sqrt{2\omega}B + \sqrt{2\omega^2 B^2 - 4\omega(B^2 - C^2)}}{2\omega} \quad (35)$$

with

$$C^2 = \left| \frac{(1 - a) R_s A_1 (\cos \omega t_{\max} - \cos \omega t_{\min})}{\Delta T_s} \right|^2 \quad (36)$$

In these expressions:

$\Delta T_s$  is the diurnal temperature difference  $T_{\max} - T_{\min}$   
 $T_{\max}$  is maximum surface temperature;  
 $T_{\min}$  is minimum surface temperature;  
 $A_1$  is amplitude of radiation Fourier series;  
 $t_{\max}$  is time at  $T_{\max}$ ;  
 $t_{\min}$  is time at  $T_{\min}$ ;  
 $\omega$  is rotation rate of earth.

NOAA AVHRR and meteorological data can be used to obtain an initial estimate for  $B$  and to estimate thermal inertia. This method was used by Zhang (1990) in the North

China Plain and some results of the work which make use of empirical relationships established between  $P$  and soil moisture will be provided in Part II.

#### 5.4.2 Vegetated case

When vegetation cover is present, as it will be in cropping systems apart from the period following fallowing, it is better to use the two layer model formulation with its separation of soil and vegetation temperatures. For day-time data, the energy balance can be closed by an assumption relating  $G$  to  $R_n$  as was done before. This approximation is best for the higher cover situations.

The available energy for the foliage ( $A_v$ ) and soil ( $A_g$ ) are partitions of the total net radiation such that:

$$\begin{aligned} A_v &= R_{nv} & (37) \\ A_g &= R_{ng} - G \\ &= (1 - G_f) R_{ng} \\ R_n &= R_{nv} + R_{ng} \end{aligned}$$

The main difference in the expression for the total net radiation compared with the expression introduced for the one layer model is in the longwave upwards term ( $R_{Lu}$ ). This has a reasonable approximation as:

$$\begin{aligned} R_{Lu} &= f_v \mathbf{e}_v \mathbf{s} T_v^4 + (1 - f_v) \mathbf{e}_g \mathbf{s} T_g^4 \\ &= \mathbf{e}_s \mathbf{s} T_s^4 \end{aligned} \quad (38)$$

where  $T_s$  is the composite measured surface temperature and  $\mathbf{e}_s$  is a composite surface emissivity. In this Report, we have made the further approximation, which is reasonable for the ranges of variation we find in the images, that:

$$\begin{aligned} T_s &= f_v T_v + (1 - f_v) T_g \\ \mathbf{e}_s &= f_v \mathbf{e}_v + (1 - f_v) \mathbf{e}_g \end{aligned} \quad (39)$$

The net radiation could be simply partitioned to provide a means for solving the two layer equations in the way that was used with the one-layer model by assuming:

$$\begin{aligned} R_{nv} &= f_v R_n \\ R_{ng} &= (1 - f_v) R_n \end{aligned} \quad (40)$$

where the subscript  $v$  generally denotes a vegetation component and  $g$  the soil or (ground) surface component.

However, despite the simplicity it provides for the mathematical solution, this would seem to involve a major departure from expressions that would be developed from a complete canopy model. It is possible to provide a formulation that is still simple to use (especially as this term is used in solution of nonlinear equations which need derivatives as well) based on a two-flow (Kubelka Munk) model. Assuming the

vegetation components have a shortwave albedo of  $\mathbf{a}_v$  and the soil surface has an albedo of  $\mathbf{a}_g$  then for the shortwave net radiation ( $R_{ns}$ ):

$$\begin{aligned}
R_{ns} &= (1 - \mathbf{a}_s) R_s & (41) \\
&= R_{nsv} + R_{nsg} \\
R_{nsv} &= (1 - [w_f(1 - f_v \mathbf{a}_g) + f_v \mathbf{a}_v]) R_s \\
R_{nsg} &= w_f(1 - \mathbf{a}_g) R_s \\
\mathbf{a}_s &= f_v \mathbf{a}_v + w_f(1 - f_v) \mathbf{a}_g \\
w_f &= \frac{1 - f_v}{1 - f_v \mathbf{a}_v \mathbf{a}_g}
\end{aligned}$$

If the vegetation and soil albedos are zero, this reduces to the simple model used for the one layer REBM case. For the longwave radiation the situation is complicated by the fact that vegetation and soil may have different temperatures and emissivities. Again using the simple two-flow formulation to enable convenient formation of derivatives we used:

$$\begin{aligned}
R_{nL} &= R_{Ld} - R_{Lu} & (42) \\
R_{nLg} &= R_{Lgd} - R_{Lgu} \\
R_{nLv} &= R_{nL} - R_{nLg} \\
R_{Lgd} &= \frac{(1 - f_v) R_{Ld} + f_v \mathbf{s} [e_v T_v^4 + (1 - e_v) T_g^4]}{1 - f_v(1 - e_v)(1 - e_g)} \\
R_{Lgu} &= e_g \mathbf{s} T_g^4 + (1 - e_g) R_{Lgd} \\
R_{Lu} &= (1 - f_v) R_{Lgu} + f_v (e_v \mathbf{s} T_v^4 + (1 - e_v) R_{Ld})
\end{aligned}$$

If the vegetation and soil emissivity are each 1.0 this does not reduce to the simple model used for the one layer case but if the vegetation and soil temperatures are also the same it does.

These models have provided useful results but should have more validation and comparison with others of similar complexity (Dickinson *et al.*, 1987, Dickinson, 1983). The main shortcoming is the lack of dependence of the surface albedo on sun angle. This can be done by separating the diffuse and direct terms and introducing a sun angle dependent soil albedo.

## 5.5 Performance with Data

Out of a variety of data sets which have been used to examine the models, two somewhat extreme examples will be used to illustrate the different capabilities of the approaches. The data sets are to be found in Choudhury *et al.* (1986) and Choudhury (1989) and comprise records of all relevant fluxes over an irrigated wheat field (Phoenix day 67) in the first case and a very hot, dry patchily covered area (in the Owens Valley) in the second. Figures 3 and 5 show the results of using the One-layer REBM (equivalent to Case 1 constrained two-layer solutions) and Figures 4 and 6 the minimum power constrained Two-layer model (Case 5 of the constrained two-layer solutions) for the two examples. The solid lines are the predicted fluxes and the points are the measured data. The line with both lines and symbols is an error estimate defined as:

$$A_d = (IE_{meas} - IE_{pred}) - (H_{meas} - H_{pred}) \quad (43)$$

that represents a term which explains the discrepancy by a quantity that does not alter the energy balance. Its most likely nature is an advective term - hence its notation although it can also be affected by differences between the modelled and actual ground heat flux components.

The two situations are very different. Over the irrigated wheat with high leaf area, the ET flux is very high. ET follows the pattern of net radiation over the day and the sensible heat flux actually becomes negative later in the day. The surface temperature is low and conditions are stable. In the Owens Valley data the sensible heat flux is very high and ET near constant and very small. Surface temperatures are high and the conditions unstable.

The graphs show how the constrained Two-layer model performs well compared with the One-layer REBM on the Owens Valley data with its partial cover and drying conditions. The One-layer model cannot cope with the unstable conditions and produces very large negative ET values! The results for the closed canopy wheat data are almost identical in each case and the systematic ‘advective’ error term is not changed. In common with other examples studied, there is a residual which does not seem to be a function of the disaggregation of the model into layers but is more likely the result of unaccounted advection and capacitance effects. Since these often balance over time and space scales the REBM does seem to produce a conservative and (with the constrained model modification discussed here) stable estimates for the ET flux attributable to the net radiation.

A more complete evaluation of the different forms of constraint and the remaining areas of inadequacy will be left to another publication. However, it has been clear from our studies that the minimum power solution is as robust as any of the models we have examined. Our selection has been based on the need to use the model with standard meteorological data providing model closure at a “reference” height above the canopy and to require as much as possible other observations that can be derived from remotely sensed data. This objective has been largely met with the constrained two-layer model provided we can estimate the closing meteorological conditions at the

location and time that the remotely sensed data were obtained. Achieving this is the subject of the next section.

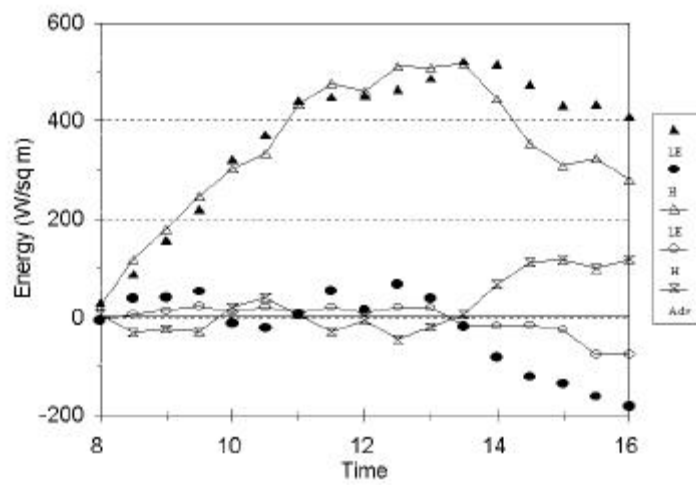


Figure 3. One-layer REBM for Crop Data for DOY 67 from Choudhury *et al.* (1986).

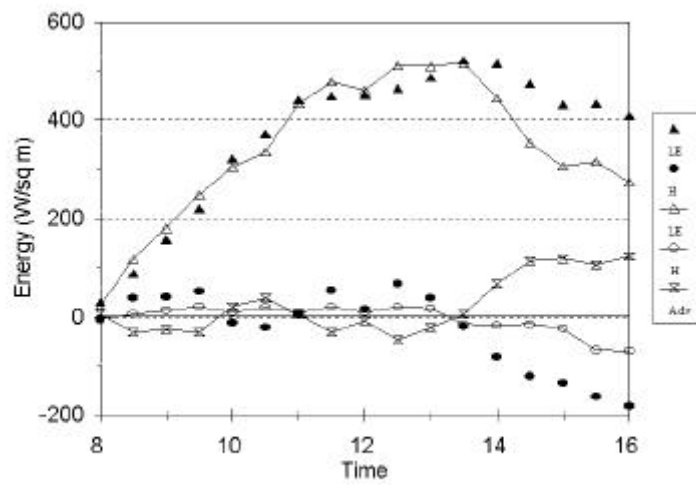


Figure 4. Minimum Power constrained Two-layer REBM for Crop Data for DOY 67 from Choudhury *et al.* (1986).

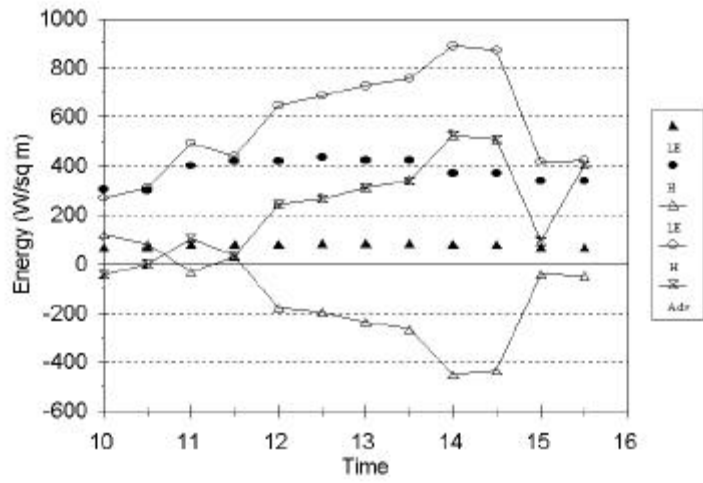


Figure 5. One-layer REBM for Owens Valley from 2 June 1986.

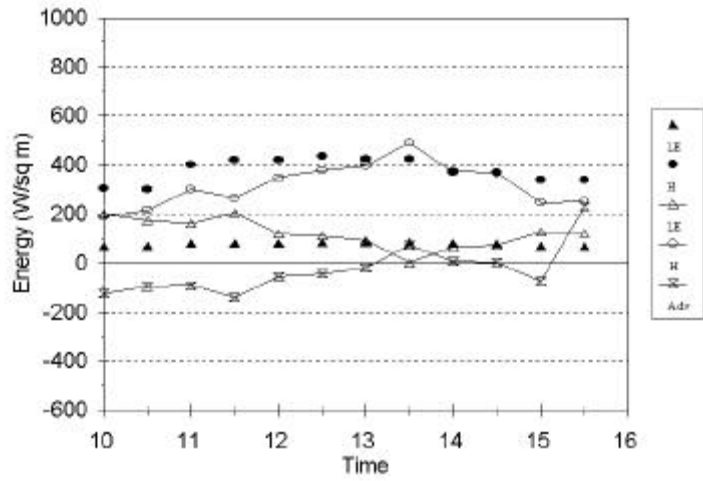


Figure 6. Minimum Power constrained Two-layer REBM for Owens Valley from 2 June 1986.



## **6 ESTIMATING METEOROLOGICAL DATA AT THE TIMES AND ON THE DATES OF AVHRR OVERPASSES FROM STANDARD DATA**

Provided effective models for the resistances and other terms are used, the energy balance methods should provide estimates for ET and other components of the energy balance if adequate meteorological data are available and if either of the surface temperature or the moisture availability is available. However, having detailed meteorological data over areas like the MDB and NCP is either a very difficult or very expensive and time consuming task to manage. We have therefore investigated how well meteorological data for the time of an AVHRR overpass can be estimated from readily available data. Minimally, we have assumed that a number of stations exist in an area which record minimum ( $T_{min}$ ) and maximum ( $T_{max}$ ) daily air temperature and rainfall ( $P$ ). If at least some stations record wind run or average wind speed it is taken as an advantage and at least one station should have recorded daily solar radiation for some period of time.

Such a general specification can be satisfied over large areas of the world. In many cases, even managing and validating such a restricted data set is a very difficult task and in others, while more extensive data sets are available, managing and validating the extra information is almost prohibitively expensive and time consuming. The methods we have tried were therefore aimed principally at estimating air temperature, Solar radiation and humidity with wind speed being provided only when wind run or averages have been recorded. The project received strong support from the authors of the MTCLIM package (Hungerford *et al.*, 1989) and had access to a modification of it due to R. Nemani (1991, *pers. comm.*) called HOURLY.

Validation of the temporal interpolation from daily meteorological data to hourly data has been undertaken for a number of sites where actual hourly data is available. Hourly air temperature and humidity data recorded during 1989 from the CSIRO experimental site at Lockyersleigh (Kalma *et al.*, 1987) was used for validation of those data. Daily global shortwave irradiance for several points within the MDB and NCP, collected by the Australian Bureau of Meteorology (AMB) and Chinese Bureau of Meteorology (CBM) respectively, were used to locally calibrate a simple model to estimate atmospheric transmittance. Global (direct and diffuse) shortwave irradiance data for 1989 collected by the ABM for Canberra were used for the investigations of the shortwave radiation environment on an hourly interval.

### **6.1 Air Temperature**

Knowing only  $T_{min}$  and  $T_{max}$  means that  $T_{air}$  at other times must be interpolated from the two extremes. A satisfactory method for the interpolation of  $T_{air}$  is the model proposed by Parton and Logan (1981) which uses a truncated sine wave to estimate daytime  $T_{air}$  and an exponential function to estimate night-time  $T_{air}$ . The Parton and Logan (1981) method was tested in our study areas using hourly  $T_{air}$  data recorded during 1989 from the CSIRO experimental site at Lockyersleigh (Kalma *et al.*, 1987). The Lockyersleigh data were recorded instantaneously every 10 minutes and averaged to hourly data. To test the temporal interpolation of  $T_{air}$  (and RH and  $e_a$ , refer to the

next section), we assumed that the data average for the hour would best represent the instantaneous data recorded at the 30 minute mark. To measure the performances we have used mean error (or bias), the Root Mean Square (RMS) deviation about the bias, and the linear regression statistics.  $T_{min}$  is the minimum measurement between 9am of the previous day and 8am of current day.  $T_{max}$  is the maximum between 9am the current day and 8am the next day. Using these times to define  $T_{min}$  and  $T_{max}$  means that the assumption that  $T_{min}$  occurs within a few of hours of sunrise and  $T_{max}$  occurs during daylight hours (Parton and Logan, 1981) are met more often.

Results for interpolated  $T_{air}$  showed good agreement between modelled and observed values for clear days. A plot showing the differences between actual and modelled  $T_{air}$  for Lockyersleigh for day-of-year (DOY) 40 to 49, 1989, is presented in Fig. 7 and the data cross-plotted in Fig. 8. For 1989, the statistics summarising the errors between the modelled and measured  $T_{air}$  has been reported for the AVHRR overpass times (13:30, 14:30 and 15:30) and for the TM overpass time (9:30) for all days. The statistics were also generated for the 162 days when no rainfall was recorded, as these are the days when remotely sensed data are more likely to be acquired. Table 1 shows that for non-rainy days the bias in temporally interpolating  $T_{air}$  for the times of the satellite overpass from the daily extremes of recorded  $T_{air}$  is within 0.2 °C. For non-rainy days at the times that AVHRR is acquired, the model performs well and explains 99% of the variance of measured  $T_{air}$ . The model did not perform as well at the time of TM data acquisition as early morning fog would suppress  $T_{air}$  increases after sunrise, this is not modelled by Parton and Logan (1981).

Table 1. Summary statistics between  $T_{air}$  interpolated from  $T_{min}$  and  $T_{max}$  and  $T_{air}$  measured, times and conditions indicated. Basic statistics for  $T_{air}$  measured are also provided.

	AVHRR Overpass Time 13:30, 14:30 and 15:30		TM Overpass Time 9:30	
	All Days	Non-rain Days	All Days	Non-rain Days
<b>MEASURED</b>				
Mean °C	16.570	18.110	13.751	14.512
STD °C	6.479	6.9349	6.022	6.468
Num of Obs	1095	486	365	162
<b>MODELLED</b>				
Bias °C	0.461	0.186	0.081	0.048
RMS deviation °C	1.021	0.693	1.571	1.655
Slope	0.985	0.989	0.972	0.961
Offset °C	0.709	0.375	0.469	0.614
$r^2$	0.975	0.990	0.934	0.935
Std Err Y Estimate °C	1.017	0.690	1.561	1.635
Num of Obs	1095	486	365	162

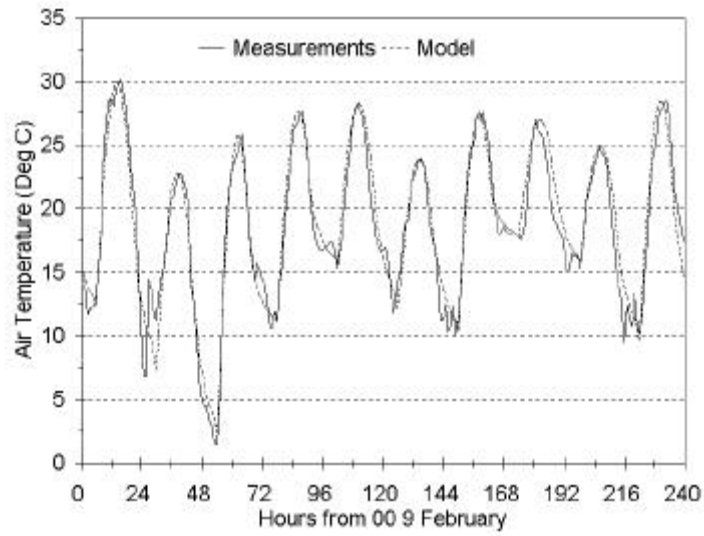


Figure 7. Measured and modelled hourly air temperatures for 9 - 18 February 1989, Lockyersleigh, Australia.

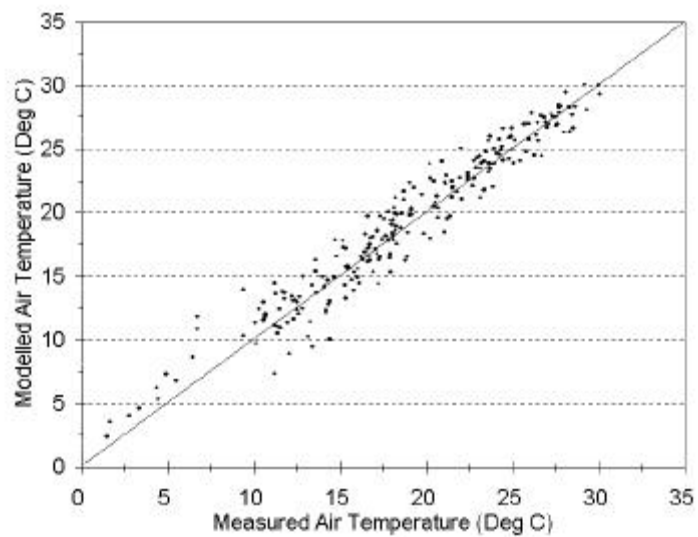


Figure 8. Crossplot of measured and modelled hourly air temperature for 9 - 18 February 1989, Lockyersleigh, Australia. The 1:1 line is shown.

## 6.2 Humidity / Vapour Pressure

### 6.2.1 Daytime humidity from daily meteorological data

Two assumptions are often made to construct daytime humidity variations when none were measured. The first is that  $T_{min}$  is also at dew point temperature ( $T_{dew}$ ) (see Dyer and Brown, 1977) so that dew just forms at the minimum. The second is that vapour pressure (or equivalently, dew point temperature or mixing ratio) remains constant during the day. That is:

$$e_a = e_s(T_{min}) \quad (44)$$
$$RH = 100 \frac{e_a}{e_s(T_a)}$$

where

$e_s(T)$  is saturated vapour pressure at temperature  $T$ ;  
 $e_a$  is vapour pressure at the reference height; and  
 $RH$  is the percent relative humidity.

In humid climates, this approximation has been reported as good but it has also been reported that it is not as good in arid areas (Bristow, 1992). Castellví *et al.* (1996) developed methods for estimating daily average relative humidity, however daily average dew point temperature is assumed to be known. Recently, Kimball *et al.* (1997), referred to here as K97, provided an alternative to the estimation of the  $T_{dew}$  calculated from readily available meteorological data. The empirical model, developed for 20 sites from continental USA and Alaska, uses  $T_{min}$  and  $T_{max}$ , daily  $ET_p$ , calculated by the Priestly-Taylor method (see K97 for full description of the method) and annual precipitation. These either constitute, or can be calculated from, the minimum data set,  $T_{min}$ ,  $T_{max}$  and  $P$ .

The difference between actual and modelled RH based upon  $T_{min} = T_{dew}$  for Lockyersleigh data over DOY 40 to 49, 1989, are presented in Fig. 9 and the data cross-plotted in Fig. 10. The bias and RMS deviation between the modelled and measured relative humidities for the AVHRR and TM overpass times, for the entire year and the days when no rain fell are given in Table 2. The K97 model was also used to estimate  $T_{dew}$  in the calculation of RH (Table 2). The results presented in Table 2 show that the bias in the estimation of RH at the time of satellite overpass is reduced when using the K97 approach to calculate  $T_{dew}$ . There was however, still considerable daily variation, illustrated by the RMS deviation.

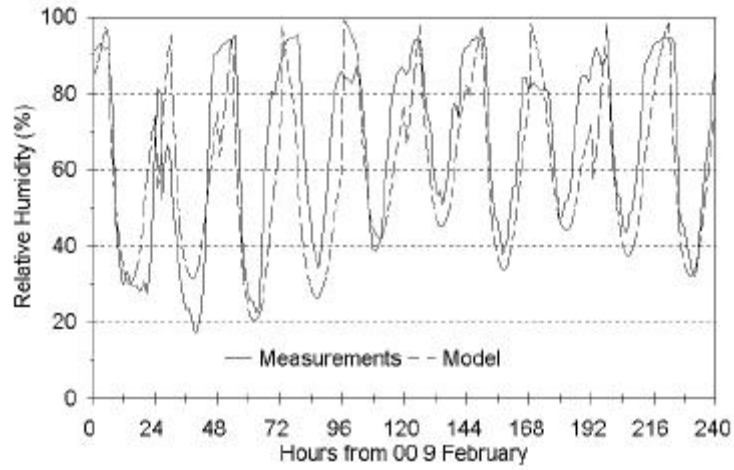


Figure 9. Measured and modelled hourly relative humidity for 9 - 18 February 1989, Lockyersleigh, Australia.

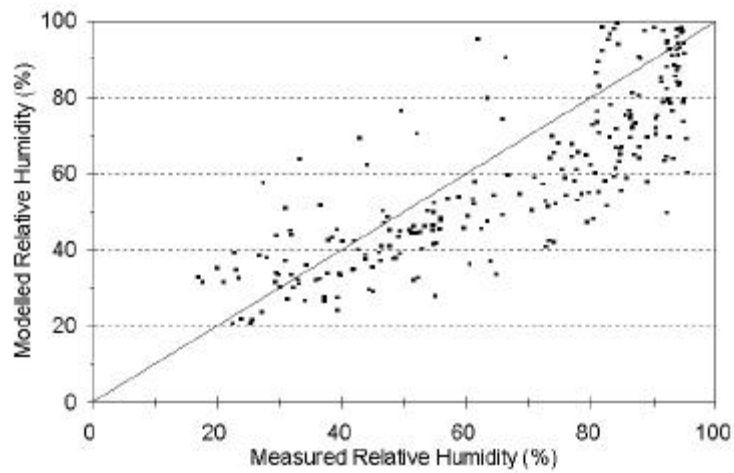


Figure 10. Crossplot of measured and modelled hourly relative humidity for 9 - 18 February 1989, Lockyersleigh, Australia. The 1:1 line is shown.

Table 2. Summary statistics between RH interpolated, methods indicated, and RH measured, times and conditions indicated. Basic statistics for RH measured are also provided.

	<b>AVHRR Overpass Time</b> <b>13:30, 14:30 and 15:30</b>		<b>TM Overpass Time</b> <b>9:30</b>	
	All Days	Non-rain Days	All Days	Non-rain Days
<b>MEASURED</b>				
Mean %	56.548	47.168	66.591	58.616
STD %	19.506	16.69	17.315	15.602
Num of Obs	1095	486	365	162
<b>MODELLED</b>				
$T_{min} = T_{dew}$				
Bias %	-6.713	-4.497	-6.266	-5.019
RMS deviation %	12.268	11.140	12.731	11.645
Slope	0.665	0.639	0.651	0.670
Offset %	12.126	12.393	16.904	14.193
$r^2$	0.560	0.536	0.494	0.482
Std Err Y Estimate %	10.446	9.522	11.249	10.523
Num of Obs	1090	483	363	161
<b>K97</b>				
Bias %	-1.959	0.895	-0.289	1.910
RMS deviation %	12.087	11.349	11.850	11.179
Slope	0.606	0.569	0.568	0.574
Offset %	20.208	21.053	28.392	26.758
$r^2$	0.605	0.506	0.522	0.475
Std Err Y Estimate %	9.423	9.013	9.272	9.131
Num of Obs	1090	483	363	161

## 6.2.2 Interpolating vapour pressure

Vapour pressure ( $e_a$ ) is a measure of partial pressure of water vapour in air which is not dominated by  $T_{air}$  like RH but is rather related to the mass of water vapour to the mass of dry air for a given volume (or the mixing ratio). Obviously, the results obtained by the model presented by K97 are encouraging. The basis of the model is that there is an underlying relationship between  $T_{max}-T_{min}$  and  $e_a$ . To understand the bias in estimating  $e_a$  we have divided daily average vapour pressure ( $e_{a,day}$ ) by vapour pressure at the time of minimum air temperature ( $e_{a,Tmin}$ ). The result presented (Fig. 11 and Table 3) show a positive correlation between these variables. The term EF, introduced by K97, the ratio of daily Priestly-Taylor  $ET_p$  divided by annual precipitation, was also plotted against  $e_{a,day} / e_{a,Tmin}$  (Fig. 12). The result for Lockyersleigh 1989 shows that EF and  $e_{a,day} / e_{a,Tmin}$  are correlated (19%) to a lesser extent than  $T_{max}-T_{min}$  and  $e_{a,day} / e_{a,Tmin}$  (35%) (Table 3). The standard error of the Y estimate is also reduced when using  $T_{max}-T_{min}$  compared to EF.

Fig. 13 and Table 3 reveal that it may possible to develop an empirical model to estimate  $T_{dew}$  based on  $T_{max}-T_{min}$ . This has some advantages over K97 as it removes

dependence on having at least a year of data to calculate annual precipitation, allowing short time series of data to be used. There appears to be an opportunity to develop a non-linear function between  $T_{max}-T_{min}$  and  $T_{dew}$  which has similar form to the relationship developed by Bristow and Campbell (1984) between  $T_{max}-T_{min}$  and daily total atmospheric transmittance (discussed in the next section). It would be best if  $T_{dew}$  was estimated using EF and  $T_{max}-T_{min}$  with the data set developed by K97 and differences presented.

Table 3. Summary Statistics for the background issues to K97.

<b>X variable</b>	$T_{max} - T_{min}$	<b>EF</b>	$T_{max} - T_{min}$
<b>Y variable</b>	$e_{a,day} / e_{a,Tmin}$	$e_{a,day} / e_{a,Tmin}$	<b>EF</b>
Bias	9.836	-1.2401	11.0766
RMS deviation	5.514	0.1567	5.6034
Slope	0.0166	21.4859	0.00045
Offset	1.0597	1.1573	-0.00105
$r^2$	0.3483	0.1846	0.6649
Std Err Y Estimate	0.1276	0.1427	0.00183
Num of Obs	345	345	345

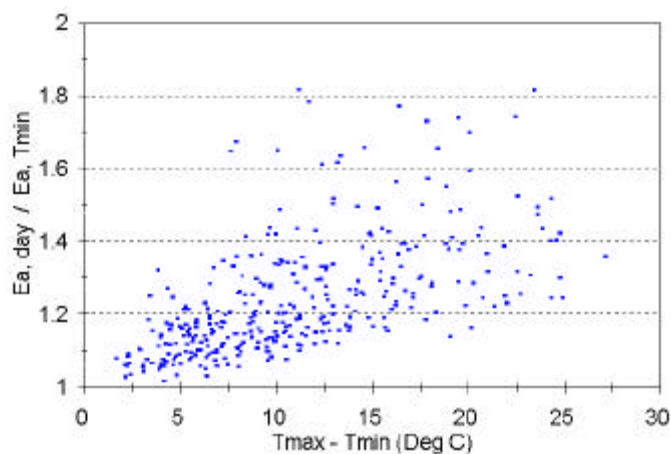


Figure 11. Plot of  $T_{max} - T_{min}$  versus  $e_{a, day} / e_{a,Tmin}$  for 1989, Lockyersleigh, Australia.

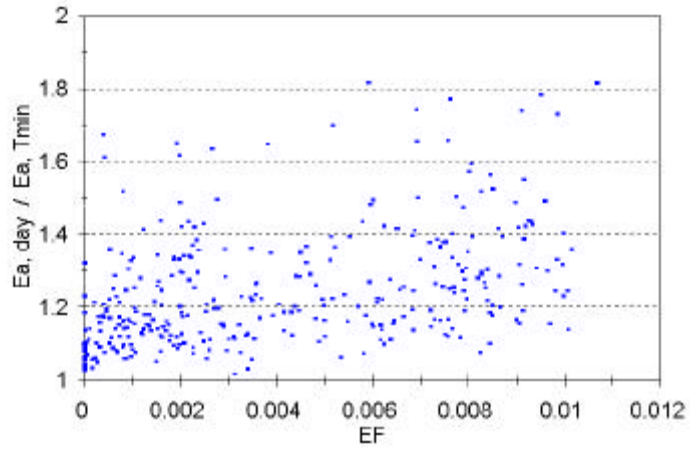


Figure 12. Plot of EF versus  $e_{a, day} / e_{a, Tmin}$  for 1989, Lockyersleigh, Australia.

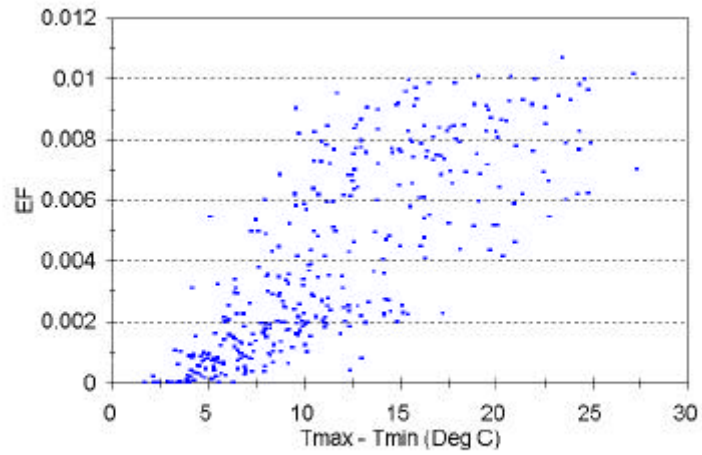


Figure 13. Plot of EF versus  $T_{max} - T_{min}$  for 1989, Lockyersleigh, Australia.

The time series trace from the Lockyersleigh data for DOY 40 to 49 of 1989 of measured  $e_a$  and the implied ‘constant’ value, when  $T_{dew} = T_{min}$ , are compared in Fig. 14 and cross-plotted in Fig. 15. There is clearly a wide variation on many days. This is referred to as  $T_{dew} = T_{min}$  ‘constant’, in the following. Figure 14 suggests that an improvement may be obtained if the vapour pressures were linearly interpolated from the assumed time of  $T_{min}$ . This is referred to as  $T_{dew} = T_{min}$  ‘interpolation’, in the following. Comparing  $T_{dew} = T_{min}$  ‘constant’ with  $T_{dew} = T_{min}$  ‘interpolation’ illustrates that there is little or no improvement in the bias of the estimates with only minimal improvement in the RMSD by applying the linear interpolation to attempt to account for some of the daily variation at the times of both AVHRR and TM overpasses (Table 4).

$T_{dew}$  was also estimated using the empirical model developed by K97. They assume that the vapour pressure is constant over the day, this is referred to as K97 ‘constant’ in Table 4. Results presented show that the K97 ‘constant’ model greatly reduces the bias in the estimate while the RMS increases compared to  $T_{dew} = T_{min}$  ‘constant’. The percentage of variation ( $r^2$ ) explained by the K97 ‘constant’ compared to the  $T_{dew} = T_{min}$  ‘constant’ model is also slightly reduced. The obvious improvements in the reduction of the bias introduced by the K97 model to estimate  $T_{dew}$  appear to be offset by the increase in RMSD and decrease in  $r^2$ .

Using the K97 model and linear interpolation of  $e_a$  between the time of  $T_{min}$  reduces the variance in the difference between measured and estimated  $e_a$ . This is illustrated in a lowering of the bias and RMS deviation for K97 ‘Interpolation’ against K97 ‘Constant’. Including the interpolation of  $e_a$  between the time of  $T_{min}$  results in a 10% improvement in explaining the variance at the time of AVHRR overpass for non-rainy days and a 5% improvement for TM data for non-rainy days (Table 4). The K97 ‘Interpolation’ method for AVHRR and TM acquisition times on non-rain days has the smallest bias and RMSD, the highest ability to explain variance, and the slope closest to 1 of the four methods (Table 4). This linear interpolation improvement to the method proposed by K97 to estimate  $T_{dew}$  needs to be assessed with longer time periods of data available from more locations and warrants further investigation.

Table 4. Summary Statistics for Vapour Pressure Estimation for Lockyersleigh 1989.

	<b>AVHRR Overpass Time</b> <b>13:30, 14:30 and 15:30</b>		<b>TM Overpass Time</b> <b>9:30</b>	
	All Days	Non-rain Days	All Days	Non-rain Days
<b>MEASURED</b>				
Mean hPa	9.867	8.886	9.953	9.141
STD hPa	8.152	9.178	8.726	9.116
Num of Obs	1095	486	365	162
<b>MODELLED</b>				
<b><math>T_{dew} = T_{min}</math> 'constant'</b>				
Bias hPa	-0.821	-0.730	-1.009	-0.987
RMS deviation hPa	2.282	2.390	1.929	1.860
Slope	0.747	0.688	0.846	0.821
Offset hPa	1.804	2.254	0.611	0.771
$r^2$	0.604	0.556	0.691	0.694
Std Err Y Estimate hPa	2.105	2.130	1.862	1.768
Num of Obs	1090	483	363	161
<b><math>T_{dew} = T_{min}</math> 'interpolation'</b>				
Bias hPa	-0.818	-0.701	-1.021	-0.976
RMS deviation hPa	2.212	2.317	1.850	1.791
Slope	0.739	0.683	0.841	0.818
Offset hPa	1.891	2.334	0.651	0.805
$r^2$	0.620	0.574	0.709	0.712
Std Err Y Estimate hPa	2.016	2.039	1.776	1.691
Num of Obs	1087	480	362	160
<b>K97 'Constant'</b>				
Bias hPa	0.260	0.594	0.070	0.337
RMS deviation hPa	2.510	2.735	2.012	2.020
Slope	0.777	0.744	0.918	0.940
Offset hPa	2.554	3.036	0.941	0.923
$r^2$	0.563	0.498	0.696	0.697
Std Err Y Estimate hPa	2.390	2.588	1.994	2.011
Num of Obs	1090	483	363	161
<b>K97 'Interpolation'</b>				
Bias hPa	0.118	0.435	-0.048	0.164
RMS deviation hPa	2.197	2.314	1.826	1.765
Slope	0.773	0.755	0.900	0.911
Offset hPa	2.475	2.781	1.018	1.032
$r^2$	0.633	0.597	0.731	0.743
Std Err Y Estimate hPa	2.049	2.152	1.795	1.741
Num of Obs	1087	480	362	160

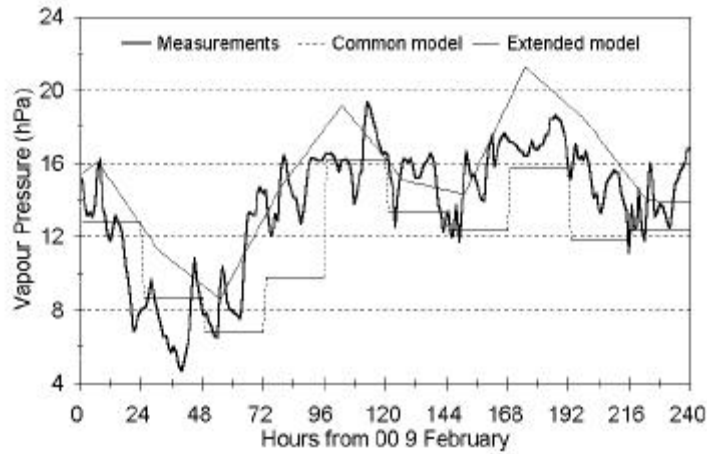


Figure 14. Measured and modelled hourly  $e_a$  for 9 - 18 February 1989, Lockyersleigh, Australia.

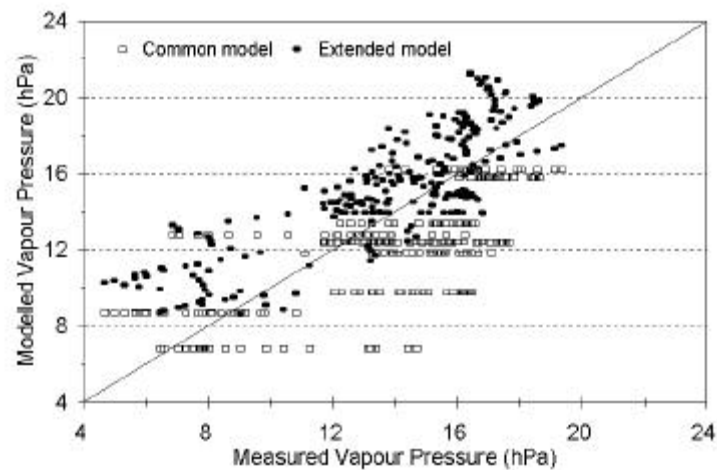


Figure 15. Crossplot of measured and modelled hourly  $e_a$  for 9 - 18 February 1989, Lockyersleigh, Australia. The 1:1 line is shown.

The model which K97 has developed could also be refined for different climatic regions, based on a classification similar to Köppen (1931). The regions, and the corresponding empirical model which is used for a particular station for a particular year can then be determined to allow spatial and interannual variability in climatic data to be incorporated in the estimation of dew point. The disadvantage of introducing this complexity is that spatial discontinuities (artificial boundaries) in regional (or continental) vapour pressure fields between classes may be introduced. This could offset the perceived improvement by estimating vapour pressure within each region. This requires further investigation.

## 6.3 Solar Radiation

### 6.3.1 A simple daily model

Shortwave solar radiation ( $S$ ) is a key input to the energy balance model, however, there are few stations in the MDB and NCP which record such solar radiation data. To utilise the limited data available we first tested an algorithm described in Hungerford *et al.* (1989) to distribute solar irradiance over a day based on the daily total atmospheric transmittance ( $T_t$ ). This relies on measurement of  $T_t$  and was performed at Canberra over 1989. Total and diffuse sky radiation were collected on a half hourly basis, direct solar radiation was calculated as the residual. The measured  $T_t$  is derived by dividing daily total solar radiation by the daily exoatmospheric irradiance, or integrated solar constant, with allowance for changes in the sun-earth distance over the year and passage of the sun over the day.

The first step taken was to model the time trace of the daily solar radiation assuming a constant atmosphere with effective beam transmittance ( $t$ ) and a model for the radiation components between sunrise and sunset as (Hungerford *et al.*, 1989):

$$\begin{aligned} R_s &= t^{m/2} \cos \mathbf{q}_s E'_0 \\ &= E_{dir} + E_{diff} \\ &= t^m \cos \mathbf{q}_s E'_0 + t^{m/2} (1 - t^{m/2}) \cos \mathbf{q}_s E'_0 \end{aligned} \quad (45)$$

where:

- $R_s$  is the total shortwave irradiance at the time of day ( $Wm^{-2}$ )
- $t$  is the effective beam transmittance
- $m$  is the airmass or transmission path length (using Kaasten's formula)
- $\cos \mathbf{q}_s$  is the cosine of the solar zenith angle
- $E'_0$  is the exoatmospheric normal solar irradiance modified for the sun-earth distance
- $E_{dir}$  is the direct solar irradiance
- $E_{diff}$  is the diffuse solar irradiance

By solving for  $t$  from  $T_t$  for each day it is possible to provide a disaggregated model that is consistent with the daily total solar radiation. That is,  $t$  is the solution to the nonlinear equation:

$$T_t = \frac{S_{day}}{E'_{0,day}} = \frac{\int_{s_{rise}}^{s_{set}} t^{m/2} \cos \mathbf{q}_s(s) ds}{\int_{s_{rise}}^{s_{set}} \cos \mathbf{q}_s(s) ds} \quad (46)$$

where the sun rise and set times ( $s_{rise}$ ,  $s_{set}$ ) and the sun zenith angle ( $\mathbf{q}_s(s)$ , on which  $m$  depends) as functions of time of day ( $s$ ) will depend on season and location.

In this notation, the daily exoatmospheric irradiance, which also depends on season and location, is:

$$E'_{0,day} = E'_0 \int_{s_{rise}}^{s_{set}} \cos q_s(s) ds \quad (47)$$

This model has sometimes been used by equating  $t$  with  $T_t$ . However, the significant differences between  $T_t$  and  $t$  are shown in Fig. 16. Once  $t$  is estimated then the trace of  $S$  during the day can be obtained from the above model. This expanded solar model based on Hungerford *et al.* (1989) is referred to here as ESM\_H.

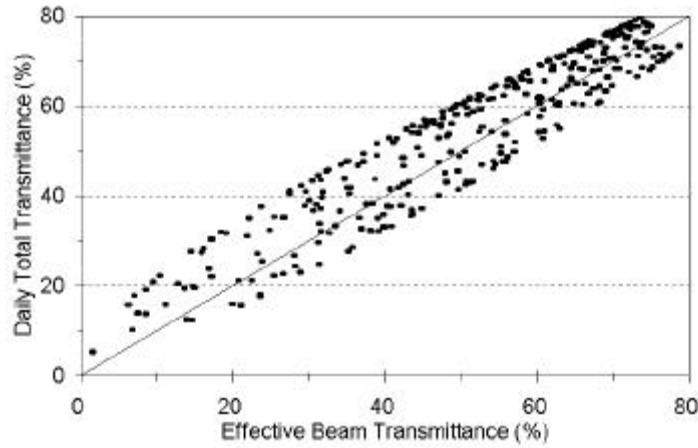


Figure 16. Plot of effective beam transmittance ( $t$ ) and total daily transmittance ( $T_t$ ), Canberra, 1989, Australia. The 1:1 line is shown.

Despite the simplicity of the ESM\_H, it works well on most days and best on the clearest days. Table 5 reports the bias, RMS deviation and linear regression statistics between the modelled (using the ESM\_H &  $T_t$  from measurements) and measured instantaneous radiative fluxes (total, diffuse and direct). Results for total radiation show that the bias is less than  $25 \text{ Wm}^{-2}$ , with a RMSD of approximately  $100 \text{ Wm}^{-2}$  and an  $r^2$  greater than 80% for both AVHRR and TM overpass times (Table 5). The ESM\_H model distributes the total solar radiation over the day well. The ratio of the RMSD/Mean of the measured data are approximately 20% for both times for non-rain days. The direct component of the total radiation is modelled better than the diffuse sky component. For example at the time of AVHRR data acquisition for all days, the direct component is modelled with an  $r^2$  of 82% whereas the diffuse sky radiation is modelled with an  $r^2$  of 45% (Table 5).

Table 5. Summary Statistics for the differences between total, diffuse and direct solar radiation modelled (using the ESM\_H &  $T_i$  from measurements) and ABM data for the times of the AVHRR and TM overpasses for all days and for days when no rain was recorded, Canberra, Australia, 1989.

Solar Radiation Type	AVHRR Overpass Time 13:30, 14:30 and 15:30		TM Overpass Time 9:30	
	All Days	Non-rain Days	All Days	Non-rain Days
<b>MEASURED Total</b>				
Mean $Wm^{-2}$	458.732	513.624	477.621	533.652
STD $Wm^{-2}$	271.907	271.948	253.051	239.427
Num of Obs	1065	681	355	227
<b>MODELLED</b>				
<b>Total</b>				
Bias $Wm^{-2}$	20.137	23.337	3.494	4.294
RMS deviation $Wm^{-2}$	107.977	103.465	105.411	101.584
Slope	0.942	0.962	0.933	0.9107
Offset $Wm^{-2}$	7.687	-3.061	28.545	43.728
$r^2$	0.845	0.857	0.831	0.828
Std Err Y Estimate $Wm^{-2}$	106.871	102.993	104.120	99.314
Number of Obs	1065	681	355	227
<b>Diffuse Sky</b>				
Bias $Wm^{-2}$	7.923	14.318	2.354	12.041
RMS deviation $Wm^{-2}$	65.626	65.290	83.507	82.287
Slope	0.920	1.168	0.900	1.172
Offset $Wm^{-2}$	5.146	-43.736	13.975	-42.336
$r^2$	0.447	0.515	0.264	0.321
Std Err Y Estimate $Wm^{-2}$	65.353	64.586	83.351	81.872
Number of Obs	510	333	170	111
<b>Direct</b>				
Bias $Wm^{-2}$	2.364	1.652	-6.051	-16.510
RMS deviation $Wm^{-2}$	115.987	123.205	135.944	145.682
Slope	1.071	1.058	1.093	1.085
Offset $Wm^{-2}$	-25.186	-22.584	-23.442	-13.993
$r^2$	0.826	0.779	0.744	0.682
Std Err Y Estimate $Wm^{-2}$	111.723	122.559	134.550	144.726
Number of Obs	463	315	155	104

### 6.3.2 The Bristow-Campbell model for daily total transmittance

Few stations within the MDB and NCP measure solar radiation data which allow measured  $T_i$  to be derived. However, BC84 present a method to estimate  $T_i$  as a function of  $\Delta T$ , which is modified by some simple empirical rules if there has been rain on the current day or during previous days (BC84). The basic model is that the  $T_i$  can be estimated as:

$$T_i = AT_c (1 - e^{-b \Delta T_c}) \quad (48)$$

The term  $AT_c$  is a 'clear air' transmittance which is the asymptote for wide diurnal variation and which was assumed to depend on elevation according to the simple lapse model:

$$AT_c(z) = AT_c(0) + 0.00001 * z \quad (49)$$

where  $z$  is elevation in m.

The original coefficients presented in BC84 were obtained using long term North American data. However, significant differences were found between the measured and modelled total solar radiation using the empirical coefficients ( $AT_c(0)$ ,  $b$  and  $c$ ) determined in North America compared with those computed for Australia and China. The usefulness of the formula increased significantly when it was calibrated for local conditions. The data for this analysis, centred on MDB and NCP, were obtained from the Australian Bureau of Meteorology and Chinese Bureau of Meteorology, respectively. The sites used and period of recording in each agricultural region are listed in Table 6.

Table 6. Station Locations and periods of available data.

Station	Identification	Lat	Long	Elev (m)	Start	Finish
<b>Australia</b>						
Canberra	70014	-35.31	149.20	571	19840126	19891231
Condobolin	50052	-33.06	147.23	195	19840601	19870930
Hamilton	90103	-37.43	142.16	205	19830601	19880630
Longreach	36031	-23.43	144.28	192	19840101	19881231
Mildura	76031	-34.23	142.08	51	19830601	19880629
Orange	63231	-33.38	149.13	948	19820901	19870331
Wagga Wagga	72150	-35.16	147.46	221	19930601	19880629
<b>China</b>						
Anyang	53898	36.12	114.36	76	19900101	19901231
Beijing	54511	39.93	116.28	55	19900101	19910630
Gushi	58208	32.16	115.67	10	19900101	19910531
Hefei	58321	31.86	117.23	19	19900101	19901231
Jinan	54823	36.68	116.98	12	19900101	19910430
Tianjin	54527	39.10	117.16	5	19900101	19910630
Zhengzhou	57083	34.72	113.65	111	19900101	19910531
Zhumadian	57290	33.00	114.01	83	19900101	19901231

Local calibration was performed by minimising the cumulative squared difference between measured  $T_i$  and BC84 modelled  $T_i$ . The 3 BC84 variables ( $AT_c(0)$ ,  $b$  and  $c$ ) were transformed to  $AT_c(0)'$ ,  $b'$  and  $c'$  using the following:

$$AT_c(0)' = \ln[AT_c(0) / (1 - AT_c(0))] \quad (50)$$

$$b' = \ln(b); \text{ and}$$

$$c' = \ln(c).$$

The optimisation was performed, by allowing  $AT_c(0)$ ,  $b'$  and  $c'$  to vary, using a Newtonian search method. Results from the minimisation of the function to provide the best fit  $AT_c(0)$ ,  $b$  and  $c$  coefficients are given in Table 7. Several initial conditions of the transformed coefficients were tested to ensure that the values reported were the local minima, over the range of possibilities attempted.

The solar radiation environment was modelled using the new locally calibrated BC84 coefficients. Being able to locally calibrate BC84 means that there is an improvement from 5% to over 30% for some stations (Table 7). The improvement is calculated as cumulative locally calibrated BC84 total solar radiation minus cumulative BC84 US coefficients total solar radiation divided by the actual cumulative measured total solar radiation, expressed as a percentage.

The results highlight the importance of being able to regionally or locally calibrate  $T_i$ . An example of the difference that local calibration provides is presented in Fig. 17, which shows the improvement in the relationship between modified  $\Delta T$  and  $T_i$  measured and modelled that it affords. There are obviously also major regional differences between the three continents indicated by these results. To investigate if altitude was playing any part in this, the pooled BC84 coefficients from the two countries were plotted against elevation (see Fig. 18, 19 and 20) and it seems that there is still a residual elevation relationship. However, this does not explain the major regional differences between the three continents.

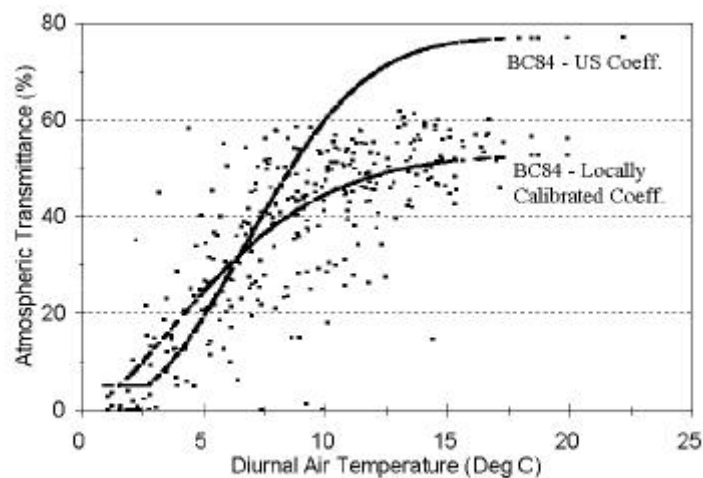


Figure 17. Crossplot of measured daily atmospheric transmittance, BC84 with US coefficients, BC84 locally calibrated coefficients against diurnal air temperature (modulated for rainfall) for Jan 1990 to May 1991 Anyang, China.

Locally calibrating the BC84 coefficients clearly improves the estimates of total solar radiation. However, in doing this, some questionable values of  $AT_c(0)$  were calculated for Condobolin, Hamilton and Orange (see Table 7). The two stations Hamilton and

Condobolin, also appear to be outliers in the plots showing the residual effects of altitude, Fig. 18, 19 and 20.

Table 7. Locally Calibrated BC84  $AT_c(0)$ , b and c coefficients and the % improvement in using a locally calibrated BC84 model for the cumulative total daily solar radiation.

Station	$AT_c(0)$	b	c	Improvement (%)
<b>Australia</b>				
Canberra	0.772	0.132	0.975	5.27
Condobolin	0.945	0.221	0.581	9.68
Hamilton	0.989	0.218	0.613	12.0
Longreach	0.793	0.062	1.341	4.9
Mildura	0.752	0.105	1.112	7.4
Orange	0.960	0.276	0.468	8.3
Wagga Wagga	0.730	0.080	1.199	11.7
<b>China</b>				
Anyang	0.529	0.049	1.577	27.7
Beijing	0.639	0.030	1.737	8.4
Gushi	0.657	0.040	1.749	9.4
Hefei	0.605	0.018	1.969	14.8
Jinan	0.508	0.018	2.275	11.7
Tianjin	0.555	0.011	2.519	6.7
Zhengzhou	0.636	0.036	1.557	19.7
Zhumadian	0.513	0.039	1.692	31.8

Local calibration requires that total solar radiation measurements are locally collected using routinely calibrated equipment. Table 8 shows the frequency distribution of the calculated atmospheric transmittance for the Australian sites. This shows that Condobolin, Hamilton and Orange all have some days where the recorded atmospheric transmittance is greater than 90%. A clear sky daily total atmospheric transmittance of more than 85% would be unusual, even for the clear skies of Australia. We have therefore assumed some form of calibration drift accounts for their unusual nature.

Table 8. Frequency distribution of daily atmospheric transmittance (%).

Station	Frequency of days with calculated atmospheric transmittance (%)				
	> 95	95-90	90-85	85-80	< 80
Canberra	0	0	0	4	1956
Condobolin	2	1	0	13	1151
Hamilton	1	5	20	106	1697
Longreach	0	0	0	41	1637
Mildura	0	0	0	0	1856
Orange	0	5	17	34	1102
Wagga Wagga	0	0	0	0	1856

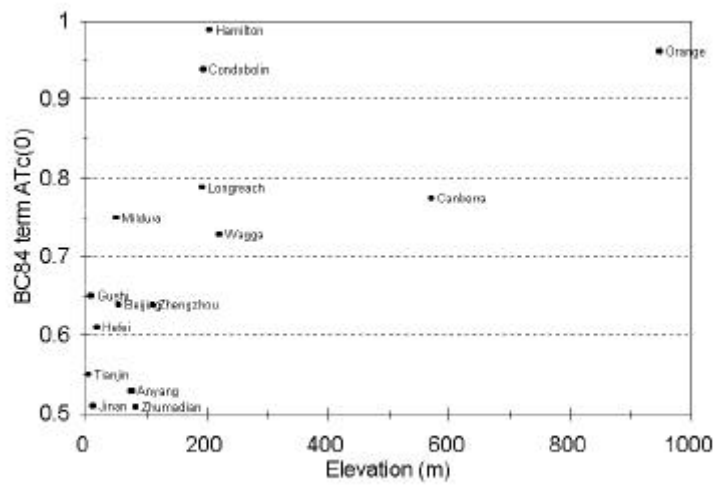


Figure 18. BC84 model term ATc(0) for China and Australian sites against elevation.

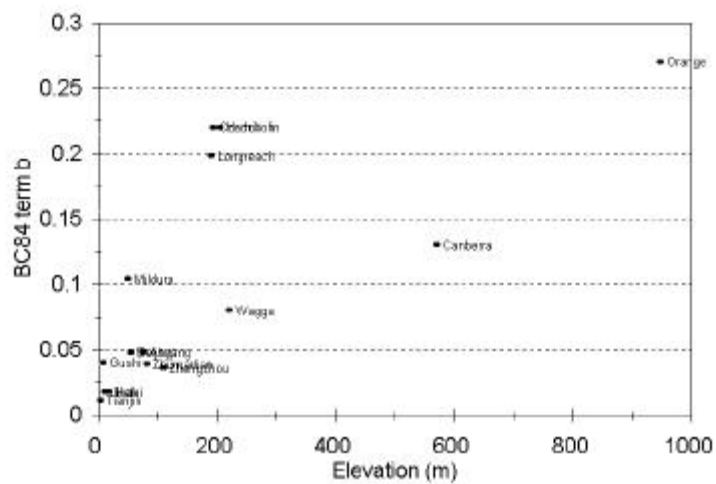


Figure 19. BC84 model term b for China and Australian sites against elevation.

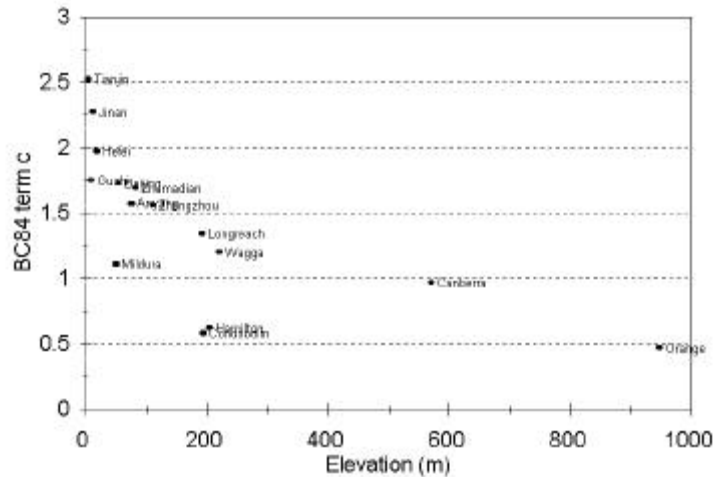


Figure 20. BC84 model term c for China and Australian sites against elevation.

Longreach appears to be an outlier in BC84 coefficient b (Fig. 19). Longreach is located in an arid region and dust probably plays an important role in atmospheric transmittance in this environment. BC84 is based on the assumption that atmospheric water content (measured by diurnal air temperature differences) is the main controller of atmospheric transmittance. The other BC84 coefficients ( $AT_c(0)$  and c) for Longreach seem reliable, Fig. 18 and 20, respectively, as does the frequency data presented in Table 8.

The BC84 locally calibrated coefficients for Orange are doubtful. However, to properly test the optimisation of the BC84 model coefficients for Orange, an analysis needs to be performed using data from stations with similar, or greater, altitudes than Orange (1000m). These data would need to be obtained from countries other than Australia so that it is unlikely we can determine unequivocally if Orange is an outlier in this Australian relationship.

For Australia, if the data from Condobolin, Hamilton and Orange are ignored, the solar radiation model ( $T_i$  calculated by locally calibrated BC84) is able to explain more than 80% of the variance in total incoming daily solar radiation. For the Chinese stations 57 to 80% of the measured total daily incoming solar radiation is explained by the locally calibrated models (Table 9).

Table 9. Linear regression summary statistics between locally calibrated BC84 modelled daily total solar radiation and measured total solar radiation. Only for days when no rain was recorded.

Station	Offset (Wm <sup>-2</sup> )	Slope	r <sup>2</sup>	Std Err Y Estimate (Wm <sup>-2</sup> )
<b>Australia</b>				
Canberra	3762.797	0.804	0.859	2701.456
Condobolin	3507.437	0.772	0.839	2653.376
Hamilton	5358.193	0.750	0.784	3663.060
Longreach	3456.351	0.849	0.839	2222.735
Mildura	4302.110	0.791	0.820	3092.967
Orange	7112.606	0.626	0.647	3330.702
Wagga Wagga	3354.059	0.841	0.830	3012.974
<b>China</b>				
Anyang	3293.473	0.728	0.729	2547.673
Beijing	3487.411	0.722	0.797	2694.270
Gushi	5079.427	0.659	0.771	2893.706
Hefei	3875.942	0.687	0.638	3193.410
Jinan	4267.231	0.637	0.571	3181.378
Tianjin	3364.817	0.750	0.774	2682.663
Zhengzhou	3769.475	0.729	0.738	2897.794
Zhumadian	4251.992	0.673	0.692	2748.765

Pooling the radiation data for Australia, excluding Condobolin, Hamilton and Orange, we optimised the BC84 coefficients by minimising the cumulative squared difference between measured  $T_t$  and BC84  $T_t$ . The 3 BC84 variables were transformed in a similar manner to that described above. The regional coefficients for the MDB are  $AT_c(0) = 0.8073$ ,  $b = 0.1747$  and  $c = 0.8493$ . The BC84 modelled regional coefficients for the North China Plain, using the same optimisation approach, are  $AT_c(0) = 0.5750$ ,  $b = 0.0324$  and  $c = 1.8036$ . In these regional models, the BC84 model coefficients were optimised for all days and not just for days when no rain fell. This was done as the solar radiation models are used both to link with remotely sensed data and also to drive the estimates of daily  $ET_p$  for use in water balance modelling.

The capacity of the BC84 model to estimate  $T_t$  is obviously not perfect. It is clear that the transmittance is being attributed to a single atmospheric effect whereas both dust and water vapour can act very differently to affect  $DT$  and  $T_t$ . There are obviously major transmittance differences between Australia and China as well. It is likely the higher haze levels in the heavily populated and industrial city areas of China where solar radiation was collected is one cause. That is, away from these populated areas  $T_t$  may be much higher.

### 6.3.3 Estimation of solar radiation at the times of overpasses

Comparing the results from Table 5 (using the  $ESM_H$  and  $T_t$  from measurements) and from Table 10 (using the  $ESM_H$  &  $T_t$  calculated by BC84) allows the relative effects of measuring or modelling  $T_t$  on the estimation of the solar radiation at the times of overpasses to be investigated. The BC84 coefficients used in Table 10 were the regional MDB coefficients, and not those for Canberra. This comparison reveals that the BC84 model reduces the amount of variance that can be explained between

modelled and measured solar radiation at the times of AVHRR and TM data acquisition. For example, for total radiation at the times of AVHRR data acquisition for non-rain days this figure is 85.7% when  $T_i$  is measured (Table 5) and becomes 69.7% when  $T_i$  is modelled using the BC84 model (Table 10). There is also a slight increase in the bias and RMSD statistics presented for all types of radiation, times of remotely sensed data acquisition and rain conditions. Fig. 21 shows the differences between the actual and modelled (using the ESM\_H and  $T_i$  calculated by BC84) total shortwave radiation for DOY 40 to 49 at Canberra and Fig. 22 shows the comparison as a cross-plot.

Table 10. Summary Statistics for the differences between total, diffuse and direct solar radiation modelled (using the ESM\_H &  $T_i$  calculated by BC84) and Abm data for the times of the AVHRR and TM overpasses for all days and for days when no rain was recorded, Canberra, Australia, 1989.

Solar Radiation Type	AVHRR Overpass Time 13:30, 14:30 and 15:30		TM Overpass Time 9:30	
	All Days	Non-rain Days	All Days	Non-rain Days
<b>Measured Total</b>				
Mean $Wm^{-2}$	458.732	513.624	477.621	533.652
STD $Wm^{-2}$	271.907	271.948	253.051	239.427
Num of Obs	1065	681	355	227
<b>MODELLED</b>				
<b>Total</b>				
Bias $Wm^{-2}$	52.886	43.477	36.597	24.263
RMS deviation $Wm^{-2}$	154.036	149.835	142.866	131.087
Slope	0.972	0.990	1.033	1.0251
Offset $Wm^{-2}$	-38.462	-37.669	-53.673	-38.304
$r^2$	0.680	0.697	0.682	0.701
Std Err Y Estimate $Wm^{-2}$	153.898	149.816	142.708	130.994
Number of Obs	1065	681	355	227
<b>Diffuse Sky</b>				
Bias $Wm^{-2}$	27.167	24.672	23.157	23.724
RMS deviation $Wm^{-2}$	74.846	76.677	88.933	92.359
Slope	0.887	1.080	0.886	0.912
Offset $Wm^{-2}$	-6.652	-39.450	-2.213	-7.147
$r^2$	0.288	0.318	0.161	0.137
Std Err Y Estimate $Wm^{-2}$	74.124	76.580	89.021	92.291
Number of Obs	510	333	170	111
<b>Direct</b>				
Bias $Wm^{-2}$	12.022	12.484	2.099	-10.0322
RMS deviation $Wm^{-2}$	187.691	186.942	192.924	198.543
Slope	1.0853	1.027	1.224	1.156
Offset $Wm^{-2}$	40.190	-22.479	-74.482	-46.888
$r^2$	0.554	0.486	0.491	0.409
Std Err Y Estimate $Wm^{-2}$	179.057	186.881	189.876	197.299
Number of Obs	463	315	155	104

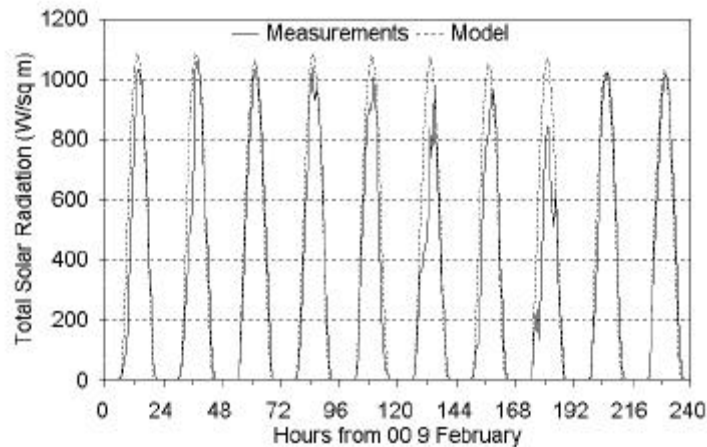


Figure 21. Measured and modelled total solar radiation for 9 - 18 February 1989, Canberra, Australia.

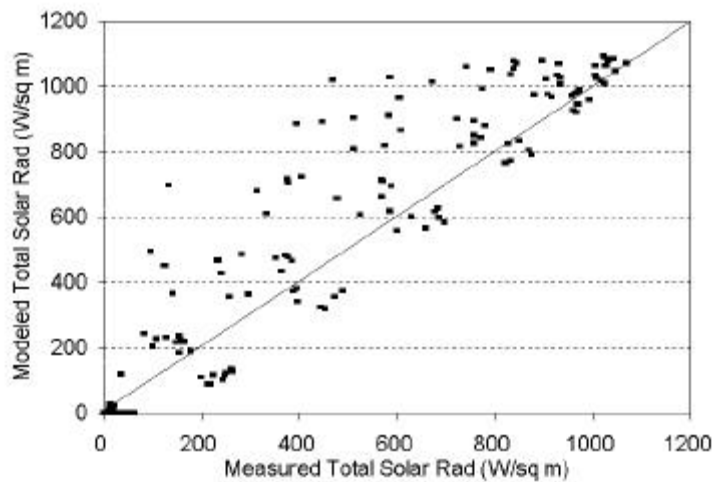


Figure 22. Crossplot of measured and modelled total solar radiation for 9-18 February 1989, Canberra, Australia. The 1:1 line is shown.

For days when no rain fell for total radiation the ratio of the RMSD modelled (using the  $ESM_H$  and  $T_i$  calculated by BC84) divided by the mean of measured data are 29% and 24% for AVHRR times and TM times, respectively (Table 10). These values are similar to the relative error of daily solar radiation estimated from a model using air temperature and rainfall measurements (Bindi and Miglietta, 1991). While these errors appear large it should be noted that cloudy days when no rain fell will be included in this analysis. BC84 has no ability to handle cloudy days when no rain fell.

Detailed error analysis reveals that the modelled estimate is within  $\pm 50 \text{ Wm}^{-2}$  of the measured for at least 50% of the cases for both times with the  $T_i$  being measured, this figure reduced to 25% when  $T_i$  is estimated from BC84 (Table 11). Using BC84 model

to estimate  $T_i$  for both times meant that in over 60% of the cases the model was within  $\pm 100 \text{ Wm}^{-2}$  of the measurements (Table 11). The relative error, expressed as a percentage of the measured total radiation, was greater than 75% of the number of cases for both times and both methods of obtaining  $T_i$  (Table 11). This analysis included cloudy days when no rain fell and when the errors, both absolute and relative (see Fig. 23 and 24 respectively) were highest. Days during which no rain fell and had a high amount of cloud cover are included in this error analysis.

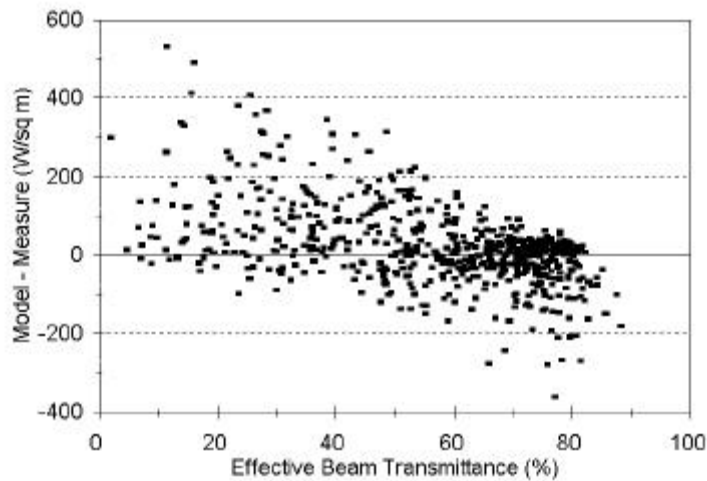


Figure 23. Absolute error versus instantaneous effective beam transmittance ( $t$ ) at AVHRR times for non-rain days, 1989, Canberra, Australia.

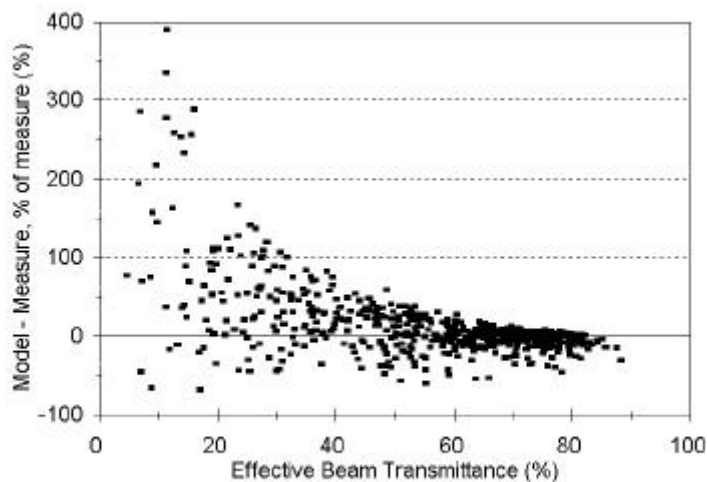


Figure 24. Relative error versus instantaneous effective beam transmittance ( $t$ ) at AVHRR times for non-rain days, 1989, Canberra, Australia.

Table 11. Frequency Distribution of the error of total solar radiation; model - measured ( $\text{Wm}^{-2}$ ) and model - measure, expressed as a percentage of the measured total solar radiation. The number in parentheses are the percentage of the 681 AVHRR

timed (13:30, 14:30 and 15:30) observations and 227 TM timed (9:30) observations that falls within each class. This analysis is only for days when no rain fell.

	<b><math>T_t</math> from measurements</b>		<b><math>T_t</math> from BC84</b>	
	<i>Model – Measure</i> ( $\text{Wm}^{-2}$ )	<i>Model – Measure</i> <i>Measure</i> (%)	<i>Model – Measure</i> ( $\text{Wm}^{-2}$ )	<i>Model – Measure</i> <i>Measure</i> (%)
<b>AVHRR Times</b>				
> 400	4 (0.59)	1 (0.15)	22 (3.23 )	8 (1.17)
300 to 400	13 (1.91)	2 (0.29)	27 (3.96 )	9 (1.32)
200 to 300	21 (3.08)	8 (1.17)	48 (7.05 )	14 (2.06)
100 to 200	78 (11.45)	22 (3.23)	98 (14.39 )	47 (6.9)
50 to 100	69 (10.13)	43 (6.31)	69 (10.13 )	68 (9.99)
0 to 50	222 (32.6)	331 (48.6)	64 (9.4 )	182 (26.73)
-50 to 0	156 (22.91)	268 (39.35)	158 (23.2 )	353 (51.84)
-100 to -50	59 (8.66)	6 (0.88)	128 (18.8 )	0 (0)
< -100	59 (8.66)	0 (0)	67 (9.84 )	0 (0)
<b>TM Times</b>				
> 400	1 (0.44)	0 (0)	2 (0.88 )	0 (0)
300 to 400	2 (0.88)	0 (0)	10 (4.41 )	0 (0)
200 to 300	7 (3.08)	0 (0)	15 (6.61 )	5 (2.2)
100 to 200	20 (8.81)	3 (1.32)	32 (14.1 )	11 (4.85)
50 to 100	18 (7.93)	11 (4.85)	21 (9.25 )	20 (8.81)
0 to 50	63 (27.75)	97 (42.73)	16 (7.05 )	60 (26.42)
-50 to 0	64 (28.19)	113 (49.78)	43 (18.94 )	131 (57.71)
-100 to -50	23 (10.13)	3 (1.32)	66 (29.07 )	0 (0)
< -100	29 (12.78)	0 (0)	22 (9.69 )	0 (0)

Table 12 shows the instantaneous atmospheric transmittance associated with non rain days and rain days at the times of AVHRR data acquisition for Canberra, 1989. This shows that nearly 70% of the cases when no rain fell in the 24 hour period had an instantaneous atmospheric transmittance greater than 50%. The instantaneous atmospheric transmittance was distributed evenly over the classes for the rainy day cases. The value of 50% instantaneous atmospheric transmittance was chosen as a filter to distinguish times when high cloud cover may have been associated with the observation of the solar radiation on days when no rain was recorded (Table 12 and Fig. 23 and 24). For non rainy days only cases with an instantaneous atmospheric transmittance greater than 50% were included in the total radiation error analysis presented in Table 13. This shows that the ratio of the RMSD modelled (using the ESM\_H &  $T_t$  calculated by BC84) divided by the mean of measured data are 13.3% and 12.7% for AVHRR times and TM times, respectively (Table 13). The value of this ratio when  $T_t$  was obtained by measurement are slightly lower. The ability of the ESM\_H &  $T_t$  calculated by BC84 model to estimate instantaneous total solar radiation appear acceptable at both the AVHRR and TM overpasses times when conditions (no rain in the day and instantaneous atmospheric transmittance greater than 50%) are likely that remotely sensed data would be acquired. This is especially the case considering that total solar radiation is modelled only using the variables  $T_{min}$ ,  $T_{max}$  and  $P$ .

Table 12. Frequency Distributions of the atmospheric transmittance at AVHRR timed (13:30, 14:30 and 15:30) observations for non raindays (681 observations) and rain days (363 observations). The number in parentheses is the percentage that falls within each class.

Atmospheric Transmittance (%)	Non Rain Days	Rainy Days
0 to 10	11 (1.62)	13 (3.58)
10 to 20	35 (5.14)	54 (14.88)
20 to 30	42 (6.17)	50 (13.77)
30 to 40	61 (8.96)	36 (9.92)
40 to 50	66 (9.69)	48 (13.22)
50 to 60	84 (12.33)	42 (11.57)
60 to 70	120 (17.62)	48 (13.22)
70 to 80	211 (30.98)	62 (17.08)
80 to 90	51 (7.49)	10 (2.75)
90 to 100	0 (0)	0 (0)

Table 13. Summary Statistics for the differences between total solar radiation modelled and Abm data for the times of the AVHRR and TM overpasses for times when no rain was recorded on the day and the instantaneous atmospheric transmittance was greater than 50%.

	AVHRR Overpass Time 13:30, 14:30 and 15:30	TM Overpass Time 9:30
<b>MEASURED</b>		
Mean $Wm^{-2}$	639.467	645.405
STD $Wm^{-2}$	223.155	184.858
Num of Obs	466	159
<b>MODELLED</b>		
<b><math>T_i</math> from measurements</b>		
Bias $Wm^{-2}$	-8.773	-25.497
RMS deviation $Wm^{-2}$	76.212	77.322
Slope	0.904	0.823
Offset $Wm^{-2}$	69.479	135.420
$r^2$	0.893	0.865
Std Err Y Estimate $Wm^{-2}$	72.826	67.860
Number of Obs	466	159
<b><math>T_i</math> from BC84</b>		
Bias $Wm^{-2}$	-27.122	-36.531
RMS deviation $Wm^{-2}$	84.907	81.955
Slope	0.819	1.093
Offset $Wm^{-2}$	90.628	-89.323
$r^2$	0.749	0.657
Std Err Y Estimate $Wm^{-2}$	105.770	137.967
Number of Obs	466	159

The reduction in accuracy by using the BC84 method to estimate  $T_i$ , rather than relying on solar radiation measurements of total solar radiation to derive a measured  $T_i$ , is far outweighed by the number of meteorological stations that can be linked with thermal remote sensing. For example, in the MDB the number of Australian Bureau of

Meteorology stations which record daily air temperature extremes and rainfall continuously from 1980 until the present is 63. If solar radiation were required this would reduce to 7. This has implications for understanding and handling the spatial variation of the soil moisture effects apparent in remotely sensed data for the entire MDB.

To further investigate the relative effects of the ESM\_H model and the BC84 model we calculated an effective beam transmittance contained within both combinations: (i) ESM\_H and  $T_i$  from measurements; and (ii) ESM\_H and  $T_i$  from BC84. We obtained one estimate of  $t$  by inverting the measured  $T_i$  and the second estimate of  $t$  was inverted from the BC84 estimate of  $T_i$  (Fig. 25). The scatter illustrates the limitations of the BC84 model even when it is locally calibrated. Fig. 26, a plot of measured and modelled hourly solar radiation, shows that BC84 distributes solar radiation well during the day. In this case, the total daily solar radiation values were identical and the scatter is due to within-day variations away from the BC84 model. Clearly, the spread is greater at times when  $T_i$  is low and smaller on the clearer days when we cloud-free remotely sensed data to be acquired.

### 6.3.4 Estimation of diffuse fraction

Although the diffuse sky radiation model has not been used extensively, it is interesting to compare it by plotting modelled and measured hourly fraction diffuse sky radiation (Fig. 27). The cluster of points in the low fraction diffuse sky radiation area are clear day data and the simple model obviously overestimates fraction diffuse sky radiation and diffuse sky radiation on clear days. However, on cloudy days the reverse is true. The BC84 model balances between clear and cloudy cases but is not good in either case. Bristow *et al.* (1985) provide methods to separate total daily solar radiation into the direct radiation and diffuse sky radiation components.

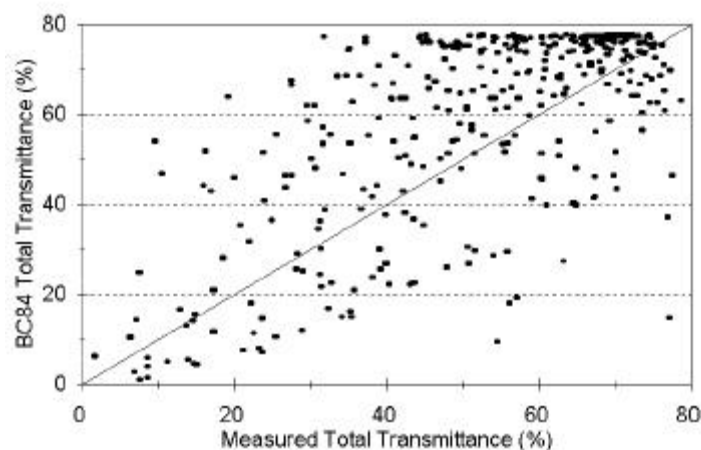


Figure 25. Crossplot of measured  $T_i$  versus BC84 modelled  $T_i$  for 1989, Canberra, Australia. The 1:1 line is shown.

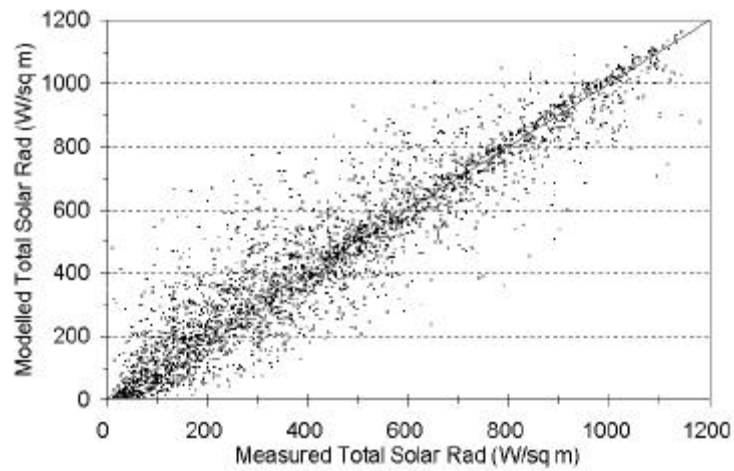


Figure 26. Crossplot of Measured and Modelled Hourly Total Solar Radiation for 1989, Canberra, Australia. The 1:1 line is shown.

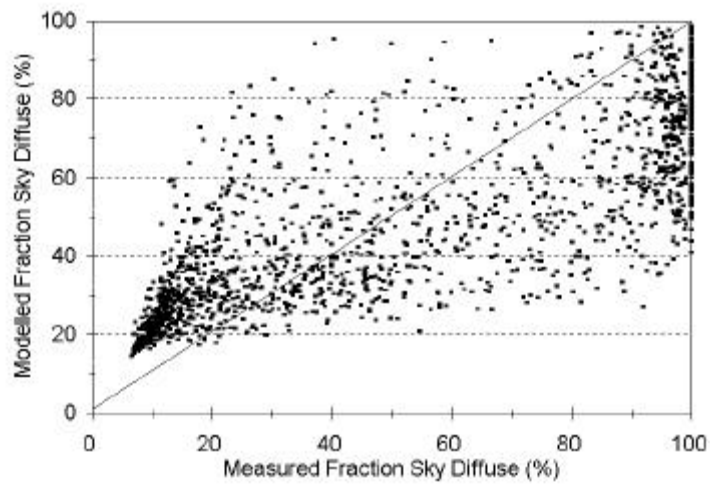


Figure 27. Crossplot of Measured and Modelled Hourly Fraction Diffuse Sky Radiation, expressed as a % of the total solar radiation, for 1989, Canberra, Australia. The 1:1 line is shown.

## 6.4 Wind Speed

Wind speed ( $u$ ) is one of the least easily estimated and least available parameters needed for REBM. Wind speed affects the daily and instantaneous estimates of  $ET_p$  and  $ET_a$ . The moisture availability ( $m_a$ ), the ratio of  $ET_a$  over  $ET_p$ , is also influenced by wind speed. The relationship between wind speed and evapotranspiration in the model used here is outlined in previous sections describing the REBM.

### 6.4.1 Influence of wind speed on daily $ET_p$ calculations

Daily wind run ( $\text{km day}^{-1}$ ) is recorded at 21 stations within the MDB. Average day-time wind speed ( $\text{m s}^{-1}$ ) was calculated, taking day/night differences into account (Smith *et al.*, 1991). This is termed varying wind speed in the following discussions. Basic descriptive statistics for the average day-time wind speed show that setting a constant wind speed of  $2 \text{ ms}^{-1}$  for those stations where daily wind run is not recorded (or days when wind run is not recorded at the stations which usually record it) is appropriate (Table 14).

Table 14. Basic statistics of average day-time wind speed in the MDB, Australia.

Station	ID Num	Days	Mode $\text{ms}^{-1}$	Median $\text{ms}^{-1}$	Mean $\text{ms}^{-1}$	Std Dev $\text{ms}^{-1}$
Applethorpe	41175	5128	0	1.29	1.52	1.18
Charleville	44021	6169	2.51	2.6	2.73	1.11
Lake Victoria	47016	5713	0	1.92	2.42	2.07
Cobar	48027	6032	1.83	2.54	2.71	1.22
Condobolin	50052	6111	1.74	2.34	2.61	1.47
Trangie	51049	5583	0	2.43	2.77	2.05
Moree	53048	5553	0.8	1.51	1.65	0.89
Pindari Dam	54104	6206	1.05	1.25	1.37	0.71
Tamworth	55054	4642	0	1.95	2.03	1.37
Bathurst	63005	6113	0.85	1.39	1.56	0.96
Cowra	63023	5122	0.99	1.26	1.51	0.97
Canberra	70014	6092	2.06	2.37	2.9	1.96
Khancoban	72060	5527	0.69	1.12	1.26	0.7
Wagga Wagga	72150	6201	2.17	2.51	2.76	1.4
Burrinjuck Dam	73007	6179	0.46	0.85	0.99	0.63
Temora	73038	3084	0	0	1	1.27
Mildura	76031	6191	3.33	3.25	3.48	1.7
Longerenong	79028	4735	0	1.57	1.7	1.29
Tatura	81049	6075	0.89	1.82	2.09	1.35
Rutherglen	82039	6118	1.6	1.89	2.18	1.35
Lake Eildon	88023	6186	0	0.77	0.82	0.56

To analyse the sensitivity of using a constant wind speed on daily estimates of  $ET_p$  we have calculated the difference in daily  $ET_p$  when wind speed varied, denoted  $ET_{p,u\_vary}$ , and when wind speed was set to the constant of  $2 \text{ ms}^{-1}$ , denoted  $ET_{p,u\_const}$ , for the 21 stations. Table 15 shows the differences in daily  $ET_p$  for the 21 sites in the MDB. For

all stations, except Lake Victoria and Mildura, the difference in the estimate of daily  $ET_p$  was less than  $\pm 0.5$  mm per day for at least 70 % of the cases (Table 15).

Table 15. Frequency distributions of the differences of daily  $ET_{p,u\_vary}$  minus daily  $ET_{p,u\_const}$ , expressed as a percentage of the total number of days for each station. The units for each class is  $mm\ day^{-1}$ .

Station	Ranges of daily $ET_p$ values, units for each class are $mm\ day^{-1}$									
	< -1	-1..-0.5	-0.5..0	0..0.5	0.5..1	1..1.5	1.5..2	2..2.5	2.5..3	> 3
Applethorpe	0	0.39	64.29	32.27	2.54	0.31	0.12	0.04	0.02	0.02
Charleville	0	0.13	28.11	42.41	19.45	7.6	1.54	0.55	0.13	0.08
Lake Victoria	2.07	9.7	35.76	25.36	12.9	7.6	3.76	1.86	0.65	0.35
Cobar	0.03	0.56	29.71	47.15	16.05	4.74	1.26	0.35	0.08	0.07
Condobolin	0	0.25	39.8	37.42	13.94	5.33	1.91	0.75	0.21	0.38
Trangie	0	0.5	33.46	35.68	15.44	6.88	3.31	1.67	0.59	2.47
Moree	0	1.4	69.24	24.53	3.89	0.72	0.16	0.04	0	0.02
Pindari Dam	0.03	1.43	80.7	16.26	1.45	0.13	0	0	0	0
Tamworth	0	0.3	35.44	42.16	14.82	4.52	1.98	0.41	0.22	0.15
Bathurst	0.31	2.11	72.03	23.72	1.34	0.26	0.1	0.05	0.07	0.02
Cowra	0.02	1.89	76.16	18.76	2.32	0.55	0.18	0.1	0	0.02
Canberra	0	0.1	40.74	33.42	15.94	6.09	2.36	0.92	0.23	0.2
Khancoban	0	1.77	87.75	9.72	0.6	0.05	0.05	0	0.02	0.04
Wagga Wagga	0	0.08	34.78	39.06	15.38	7.05	2.39	0.74	0.27	0.24
Burrinjuck Dam	0.1	4.9	88.22	6.47	0.28	0.02	0.02	0	0	0
Temora	0	0.52	60.54	27.27	6.81	2.92	0.75	0.55	0.16	0.49
Mildura	0	0.34	20.89	35.26	22.66	11.71	5.39	2.29	0.95	0.5
Longerenong	0	2.68	47.18	37.28	9.17	2.47	0.61	0.19	0.06	0.36
Tatura	0.03	4.02	51.95	31.9	8.33	2.4	0.94	0.26	0.07	0.1
Rutherglen	0.18	1.65	52.09	31.64	9.04	3.33	1.27	0.42	0.18	0.18
Lake Eildon	2.67	11.38	83.2	2.68	0.06	0	0	0	0	0

However, for all stations which recorded wind run, plots of  $ET_{p,u\_vary}$  minus  $ET_{p,u\_const}$  show a seasonal trend as shown in Fig. 28. The REBM sensitivity to wind speed therefore requires that some estimate be obtained for the study areas. This would be, at best, interpolated daily wind run, or an interpolated long term average for each month or season. The small numbers of meteorological stations within each broad agricultural region recording wind run means using interpolated long term average wind run is the more accessible solution. Currently, there are opportunities developing to integrate general circulation model outputs of near surface wind speed with remotely sensed data. This topic requires further investigation.

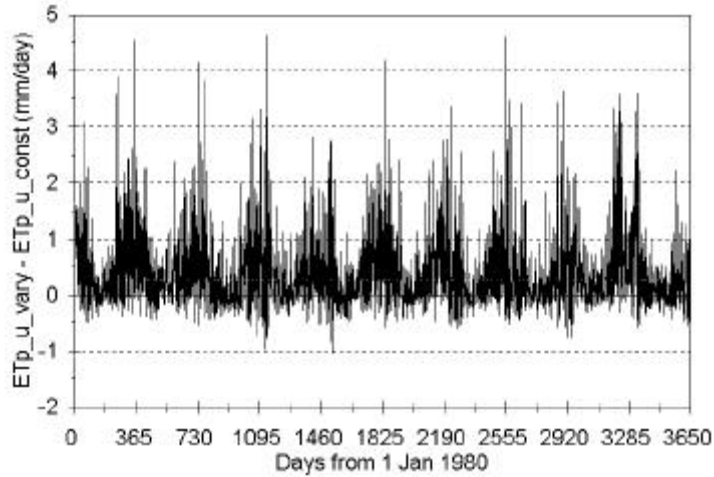


Figure 28. Time series plot of daily  $ET_{p,u,vary}$  minus daily  $ET_{p,u,const}$  for 10 years (1980-1989), Mildura, Australia.

#### 6.4.2 Influence of wind speed on instantaneous $ET_a$ , $ET_p$ and $m_a$ calculations

For the 21 MDB stations the effects of wind speed on the model based calculations of instantaneous  $ET_a$ ,  $ET_p$  and  $m_a$  were analysed. Daily meteorological data has been related to thermal remotely sensed estimates of surface temperature at these stations. The remotely sensed data was acquired by the AVHRR sensor onboard the NOAA-9 and NOAA-11 satellites. The data archive consists of 96 AVHRR single overpass daytime images from June 1986 until January 1994, these are recorded at a near-monthly time gap. Extensive preprocessing including rectification, validating the rectification accuracy (McVicar and Mashford, 1993), visual cloud clearing, salt and pepper removal, and thermal radiometric corrections (Jupp, 1989) have been applied to the entire data archive. In the meteorological data base, wind run is not recorded at every station each day (Table 14). This means that there is a variable number of observations, less than the potential 96, when both valid AVHRR data were acquired and meteorological data were recorded (Table 16). For these times / days, the REBM has been run and differences in instantaneous  $ET_a$ ,  $ET_p$  and  $m_a$  using varying wind speed and the constant wind speed have been calculated.

The mean and median of the difference between REBM  $ET_{a,u,vary}$  minus REBM  $ET_{a,u,const}$  confirms that  $2 \text{ ms}^{-1}$  is a reasonable constant when wind run data are not recorded (Table 16). However, for some sites at particular times there is large variation in these estimates, this is indicated by the std deviation, maximum and minimum values presented in Table 16. The smallest minimum difference for the instantaneous  $ET_a$  flux is for Lake Victoria,  $-252.98 \text{ Wm}^{-2}$ , when the Abm wind speed was  $0.0 \text{ ms}^{-1}$ . The largest maximum difference was found at Trangie with  $164.68 \text{ Wm}^{-2}$  with a Abm measured wind speed of  $12.02 \text{ ms}^{-1}$ . The minimum difference between REBM  $ET_{p,u,vary}$  minus REBM  $ET_{p,u,const}$  is for Lake Victoria of  $-166.71 \text{ Wm}^{-2}$ , again when the Abm wind speed was  $0.0 \text{ ms}^{-1}$ . The maximum difference of  $773.54 \text{ Wm}^{-2}$  was recorded at Trangie when the wind speed was  $14.07 \text{ ms}^{-1}$  (Table 17). Comparing the summary

statistics of Table 16 with those in Table 17 shows that the REBM  $ET_p$  is more sensitive than REBM  $ET_a$  with respect to variable wind speed.

Table 16. Summary statistics of instantaneous REBM  $ET_{a,u\_vary}$  minus instantaneous REBM  $ET_{a,u\_const}$ .

Station	Number	Median $Wm^{-2}$	Mean $Wm^{-2}$	Std Dev $Wm^{-2}$	Min $Wm^{-2}$	Max $Wm^{-2}$
Applethorpe	13	2.44	2.25	7.5	-13.31	10.3
Charleville	41	-10.07	-13.06	21.37	-79.31	51.67
Lake Victoria	49	4.85	-3.63	58.55	-252.98	123.33
Cobar	56	-4.75	-9.46	24.7	-114.48	21.44
Condobolin	53	0.39	-8.74	42.56	-168.38	40.46
Trangie	39	-2.95	-22.49	59.71	-227.55	164.68
Moree	35	8.43	9.73	14.3	-41.65	40.1
Pindari Dam	20	12.85	11.96	11.42	-18.28	32.08
Tamworth	22	-3.51	-21.42	36.6	-89.45	21.91
Bathurst	27	8.43	11.26	15.59	-15.25	43.01
Cowra	37	14.74	19.38	21.74	-25.63	72.77
Canberra	27	-2.09	-1.24	19.64	-68.98	39.95
Khancoban	31	6.96	7.17	10.61	-24.73	28.42
Wagga Wagga	49	-2.21	-14.99	35.74	-123.58	33.99
Burrinjuck Dam	32	2.75	0.36	11.71	-34.65	15.16
Temora	35	1.24	-7.4	37.98	-162.87	27.68
Mildura	67	-5.57	-18.38	35.42	-132.82	36.54
Longerenong	37	-0.17	-4.63	36.59	-133.79	65.83
Tatura	47	3.26	2.09	22.45	-127.64	40.89
Rutherglen	46	9.16	10.42	19.6	-38.38	59.29
Lake Eildon	30	-4.38	-3.22	17.34	-44.79	38.5

Table 17. Summary statistics of instantaneous REBM  $ET_{p,u\_vary}$  minus instantaneous REBM  $ET_{p,u\_const}$ .

Station	Number	Median Wm <sup>-2</sup>	Mean Wm <sup>-2</sup>	Std Dev Wm <sup>-2</sup>	Min Wm <sup>-2</sup>	Max Wm <sup>-2</sup>
Applethorpe	13	-24.28	-19.76	32.3	-62.8	77.49
Charleville	41	26.35	30.47	41.79	-78.31	121.52
Lake Victoria	49	-32.53	-20.78	70.21	-166.71	236.89
Cobar	56	13.91	14.17	34.91	-51.87	127.86
Condobolin	53	-8.85	9.25	61.17	-64.01	188.99
Trangie	39	30.53	92.04	186.36	-51.87	773.54
Moree	35	-26.76	-27.56	22.43	-63.9	47.25
Pindari Dam	20	-40.18	-33.66	20.77	-60.1	19.49
Tamworth	22	20.16	21.29	44.32	-41.14	97.88
Bathurst	27	-30.22	-25.72	21.84	-59.66	27.37
Cowra	37	-39.69	-38.89	12.43	-60.95	-1.24
Canberra	27	-11.03	8.05	61.13	-55.06	178.32
Khancoban	31	-39.93	-40.01	13.16	-56.77	13.88
Wagga Wagga	49	21.57	32.85	71.19	-45	304.42
Burrinjuck Dam	32	-39.16	-37.32	19.49	-68.05	10.95
Temora	35	-29.6	-2.64	72.69	-56.07	341.27
Mildura	67	22.75	36.23	72.76	-70.99	320.34
Longerenong	37	-4.57	0.45	45.92	-63.94	94.58
Tatura	47	-35.97	-20.81	43.14	-67.13	132.54
Rutherglen	46	-39.79	-23.21	39.46	-73.29	86.14
Lake Eildon	30	-48.34	-46.46	13.55	-69.24	-19.6

Fig. 29 shows the differences between instantaneous REBM  $ET_{p,u\_vary}$  minus instantaneous REBM  $ET_{p,u\_const}$  as a function of wind speed for Cobar. The relationship between instantaneous REBM  $ET_p$  and wind speed has a strong positive correlation, indicating that increasing wind speed results in increased estimates of instantaneous REBM  $ET_p$ , all other conditions being unchanged. The relationship between instantaneous REBM  $ET_{a,u\_vary}$  minus instantaneous REBM  $ET_{a,u\_const}$  and wind speed shows a negative (but not linear) correlation. The effect of these two opposing directions of correlation is shown in Fig. 30 as a strong negative correlation between instantaneous REBM  $m_{a,u\_vary}$  minus instantaneous REBM  $m_{a,u\_const}$  and wind speed for Cobar.

The reason for these opposing effects is that in the model we are using,  $T_s$  is measured and staying the same but  $u$  is varying independently of the other parameters. Hence,  $ET_p$  (which does not use  $T_s$ ) increases because of the increased aerodynamic term (ventilation). However,  $ET_a$  shows a negative correlation, as the input AVHRR  $T_s$  is fixed, consequently this constraint within the REBM means that there is an increase in the surface resistance, which results in a decrease in the modelled  $ET_a$ . This model behaviour induces a large change in the estimated  $m_a$ .

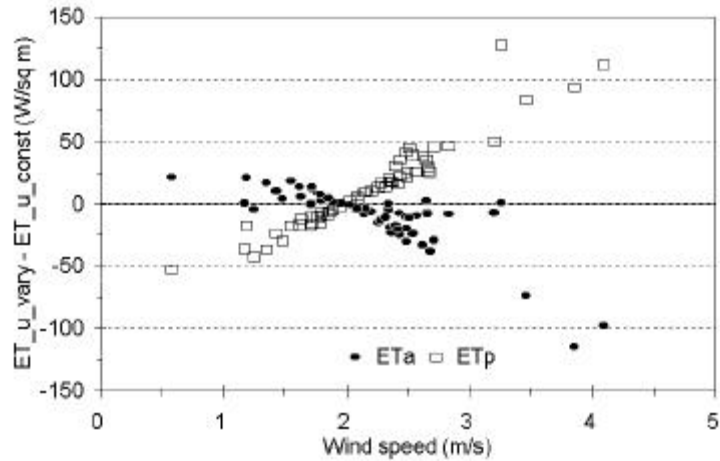


Figure 29. Plots of instantaneous REBM  $ET_{p\_u\_vary}$  minus instantaneous REBM  $ET_{p\_u\_const}$  and instantaneous REBM  $ET_{a\_u\_vary}$  minus instantaneous REBM  $ET_{a\_u\_const}$  against wind speed for Cobar, Australia.

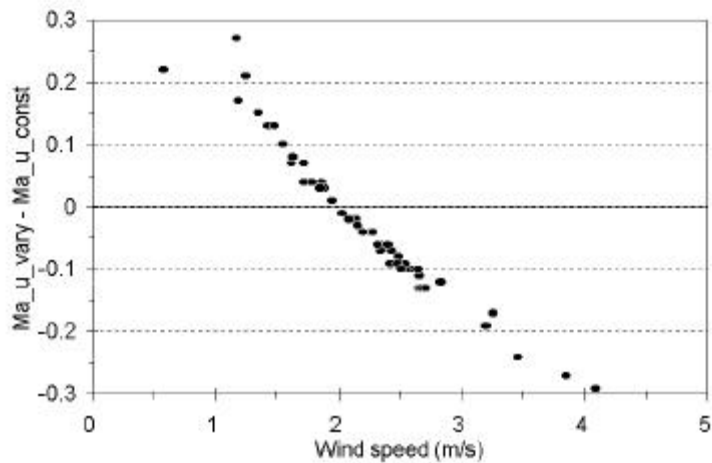


Figure 30. Plot of instantaneous REBM  $m_{a\_u\_vary}$  minus instantaneous REBM  $m_{a\_u\_const}$  against wind speed.

Table 18 shows that the mean difference in instantaneous REBM  $m_a$  is within  $\pm 0.1$  of a  $m_a$  unit for 11 of the 21 stations and within  $\pm 0.15$  of a  $m_a$  unit for 16 of the 21 stations. However, the standard deviation is greater than or equal to 0.15 of a  $m_a$  unit for a 15 of the 21 stations.

Table 18. Summary statistics of instantaneous REBM  $m_{a\_u\_vary}$  minus instantaneous REBM  $m_{a\_u\_const}$ .

Station	Number	Median	Mean	Std Dev	Min	Max
Applethorpe	13	0.1	0.11	0.15	-0.24	0.41
Charleville	41	-0.08	-0.07	0.12	-0.27	0.31
Lake Victoria	49	0.12	0.06	0.28	-0.82	0.55
Cobar	56	-0.04	-0.03	0.11	-0.29	0.27
Condobolin	53	0.05	0.03	0.18	-0.38	0.46
Trangie	39	-0.09	-0.09	0.24	-0.72	0.4
Moree	35	0.11	0.15	0.15	-0.12	0.71
Pindari Dam	20	0.2	0.17	0.12	-0.06	0.36
Tamworth	22	-0.06	-0.04	0.16	-0.26	0.26
Bathurst	27	0.14	0.15	0.14	-0.09	0.4
Cowra	37	0.22	0.24	0.15	0.01	0.77
Canberra	27	0.04	0.07	0.26	-0.38	0.57
Khancoban	31	0.23	0.23	0.14	0	0.53
Wagga Wagga	49	-0.09	-0.05	0.18	-0.47	0.34
Burrinjuck Dam	32	0.14	0.21	0.16	-0.04	0.64
Temora	35	0.1	0.06	0.17	-0.53	0.28
Mildura	67	-0.06	-0.05	0.2	-0.43	0.66
Longerenong	37	0.02	0.04	0.19	-0.31	0.56
Tatura	47	0.11	0.12	0.17	-0.4	0.47
Rutherglen	46	0.16	0.15	0.19	-0.18	0.61
Lake Eildon	30	0.15	0.18	0.12	0.03	0.6

Frequency distributions of the instantaneous REBM  $m_{a\_u\_vary}$  minus instantaneous REBM  $m_{a\_u\_const}$  are shown in Table 19. The results illustrate that wind speed has a major influence on the value of the instantaneous calculated REBM  $m_a$ . This influence in the difference in REBM  $m_a$  varies from 62% of data being in the range of  $\pm 0.1$  of a  $m_a$  unit for Cobar to only 13% of the data being in the range  $\pm 0.1$  of a  $m_a$  unit for Cowra.

Table 19. Frequency distributions of the difference of instantaneous REBM  $m_{a\_u\_vary}$  minus instantaneous REBM  $m_{a\_u\_const}$ , expressed as a % of the total number of days for each station.

Station	Percentage of total number of days where the difference of instantaneous REBM $m_{a\_u\_vary}$ minus instantaneous REBM $m_{a\_u\_const}$ is in the range $m_a$ listed.										
	#	< -0.2	-0.2	-0.15	-0.1	-0.05	0	0.05	0.1	0.15	> 0.2
		0.2	-0.15	-0.1	-0.05	0	0.05	0.1	0.15	0.2	
Applethorpe	13	7.69	0	0	0	0	15.38	23.08	30.77	0	23.08
Charleville	41	14.63	12.2	14.63	19.51	19.51	4.88	7.32	4.88	0	2.44
Lake Victoria	49	12.24	6.12	4.08	6.12	6.12	6.12	6.12	8.16	10.2	34.69
Cobar	56	5.36	3.57	12.5	26.79	14.29	17.86	5.36	5.36	3.57	5.36
Condobolin	53	9.43	5.66	3.77	3.77	22.64	1.89	22.64	3.77	5.66	20.75
Trangie	39	30.77	15.38	0	10.26	12.82	2.56	7.69	5.13	2.56	12.82
Moree	35	0	0	2.86	0	5.71	11.43	28.57	5.71	11.43	34.29
Pindari Dam	20	0	0	0	5	5	5	20	5	15	45
Tamworth	22	27.27	4.55	9.09	9.09	13.64	9.09	0	13.64	9.09	4.55
Bathurst	27	0	0	0	3.7	14.81	11.11	7.41	18.52	11.11	33.33
Cowra	37	0	0	0	0	0	8.11	5.41	10.81	18.92	56.76
Canberra	27	18.52	0	11.11	14.81	3.7	3.7	0	7.41	11.11	29.63
Khancoban	31	0	0	0	0	3.23	0	16.13	19.35	3.23	58.06
Wagga Wagga	49	14.29	10.2	12.24	8.16	10.2	10.2	8.16	8.16	4.08	14.29
Burrinjuck Dam	32	0	0	0	0	6.25	6.25	9.38	31.25	3.13	43.75
Temora	35	8.57	5.71	0	5.71	5.71	5.71	14.29	20	22.86	11.43
Mildura	67	20.9	8.96	5.97	16.42	11.94	13.43	5.97	2.99	5.97	7.46
Longerenong	37	10.81	5.41	10.81	8.11	13.51	8.11	5.41	8.11	10.81	18.92
Tatura	47	4.26	2.13	4.26	2.13	10.64	4.26	19.15	10.64	10.64	31.91
Rutherglen	46	0	2.17	10.87	4.35	6.52	8.7	8.7	6.52	8.7	43.48
Lake Eildon	30	0	0	0	0	0	3.33	26.67	20	20	30

### 6.4.3 Influence of wind speed when inverting $T_s$ from the REBM when $m_a$ is known

It is also possible, using the simple REBM, to assume that  $m_a$  is known and to estimate  $T_s$ . In this case, the variations in  $u$  result in variations of the estimated surface temperature, when  $m_a$  is fixed. Results for this analysis show a negative correlation with wind speed (Fig. 31). An increase in wind speed, greater than the default of  $2 \text{ ms}^{-1}$ , results in the estimate of aerodynamic resistance decreasing, which in turn causes a decrease in REBM-inverted  $T_s$ . Table 20 reports the frequency distribution of this for all 21 sites in the MDB.

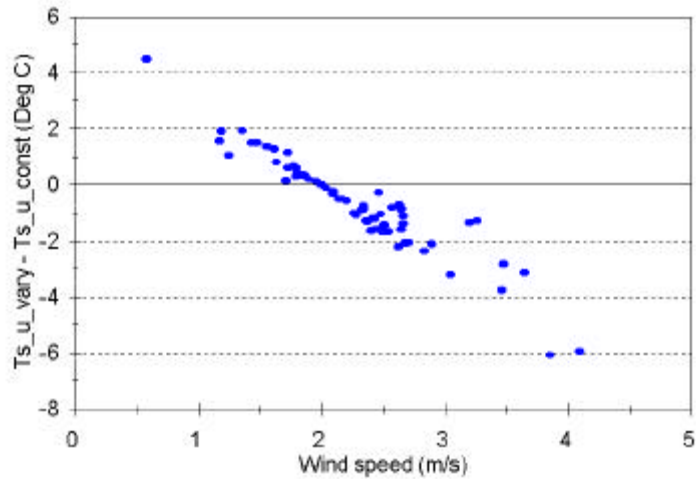


Figure 31. Plot of  $T_{s\_u\_vary}$  minus REBM  $T_{s\_u\_const}$ , both inverted through the REBM when  $m_a$  was known, versus wind speed for Cobar, Australia.

Table 20. Frequency distributions of the difference of instantaneous REBM  $T_{s\_u\_vary}$  minus instantaneous REBM  $T_{s\_u\_const}$ , expressed as a % of the total number of days for each station.

Station	Percentage of total number of days where the difference of instantaneous REBM $T_{s\_u\_vary}$ minus instantaneous REBM $T_{s\_u\_const}$ is in the range of $T_s$ ( $^{\circ}$ C) listed.								
	#	< -4	-4	-2	-1	0	1	2	> 4
			-2	-1	0	1	2	4	
Applethorpe	13	0	7.69	0	0	23.08	30.77	23.08	15.38
Charleville	48	6.25	25	22.92	22.92	12.5	2.08	6.25	2.08
Lake Victoria	53	11.32	7.55	3.77	7.55	3.77	9.43	18.87	37.74
Cobar	65	3.08	13.85	27.69	21.54	18.46	13.85	0	1.54
Condobolin	55	10.91	12.73	3.64	20	12.73	18.18	16.36	5.45
Trangie	45	24.44	15.56	11.11	20	8.89	8.89	11.11	0
Moree	39	0	2.56	0	12.82	20.51	20.51	28.21	15.38
Pindari Dam	25	0	0	12	8	16	16	32	16
Tamworth	26	19.23	15.38	11.54	19.23	7.69	15.38	11.54	0
Bathurst	28	0	0	7.14	7.14	21.43	10.71	39.29	14.29
Cowra	39	0	0	0	0	5.13	7.69	66.67	20.51
Canberra	31	6.45	12.9	22.58	3.23	12.9	6.45	22.58	12.9
Khancoban	32	0	0	0	3.13	3.13	18.75	65.63	9.38
Wagga Wagga	54	11.11	18.52	3.7	18.52	22.22	7.41	18.52	0
Burrinjuck Dam	36	2.78	0	0	5.56	11.11	8.33	61.11	11.11
Temora	36	11.11	0	5.56	8.33	11.11	25	36.11	2.78
Mildura	74	24.32	14.86	13.51	13.51	14.86	9.46	9.46	0
Longerenong	41	12.2	9.76	17.07	12.2	7.32	12.2	7.32	21.95
Tatura	49	6.12	4.08	2.04	10.2	6.12	12.24	36.73	22.45
Rutherglen	49	0	6.12	8.16	12.24	8.16	16.33	28.57	20.41
Lake Eildon	30	0	0	0	0	0	13.33	53.33	33.33

The findings in relation to instantaneous  $ET_a$ ,  $ET_p$  and  $m_a$  estimates coupled with those presented for daily  $ET_p$  estimates indicate that some indication of “windiness” needs to be available to support the REBM. Instantaneous wind speed at the time of the remotely sensed data acquisition, are only available at a few research station locations and usually only for a period of detailed experimental data collection. At 21 of 63 Australian Bureau of Meteorology operated stations in the MDB, daily wind run is available, the data used in this analysis. For the other 42 locations it appears using interpolated surfaces of long term monthly average daily wind run (Hutchinson *et al.*, 1984), from which instantaneous wind speed at the time of the satellite overpass can be calculated, may be more relevant than using the constant value of  $2 \text{ ms}^{-1}$ . Most of the MDB and NCP are greater than 45 kilometres inland from the coast, which is the distance that is affected by the coastal sea breezes (Hutchinson *pers. comm.* 1998), and hence distance from the coast is not required as a covariate for the wind run interpolation.

Some understanding of the sensitivities of disaggregation of long term average monthly values to average daily wind run must be addressed. It would also be useful to examine what influence the gustiness of instantaneous wind speed, which is integrated into the daily wind run statistic, has on the instantaneous REBM estimates of  $ET_a$ ,  $ET_p$  and  $m_a$  at the time of the remotely sensed data acquisition. Leuning (Leuning, 1998) has addressed this issue using hourly-mean meteorological data obtained near Wagga Wagga for the 1991 wheat growing season. Leuning (1998) notes that using a sinusoidal function for estimating wind speed does not achieve adequate results, however, the alternative provided assumes that the time of maximum wind speed is available (Leuning *et al.*, 1995, Leuning, 1998). This parameter is rarely available and was not available for any of the Australian Bureau of Meteorology operated sites. This issues of disaggregating long term wind run averages and disaggregating the gustiness of wind speed integrated into the daily wind run measurement both warrant further investigation.

## 6.5 Daily Potential Evaporation

It is important that the estimates for terms common to the water and energy balance be consistently defined. Differences in the calculation of  $E_p$ , in particular, between the water balance model and the Resistance Energy Balance Model (REBM) will impact on the calculation of the moisture availability and make equating the two difficult or impossible. A simple potential ET formula (Choudhury *et al.*, 1987), originally used in the simple water balance model was compared with a REBM daily estimate of  $E_p$  obtained by integrating numerically over each day using meteorological and interpolated solar radiation with the constrained Two-layer model with  $r_{sv}=r_{sg}=0$ . This measure of daily  $E_p$  was fully consistent with the energy balance equations used to interpret the AVHRR data.

Integrating the REBM over each day was computationally demanding. To overcome this we used the well known relationship proposed by Jackson *et al.* (1983) and extended by Xie (1991) that  $E_p$  at solar noon can be scaled to a daily value by multiplying it by the ratio of daily solar irradiance over solar irradiance at solar noon.

The result differed only marginally from full integration. In this way this apparently complex definition of  $E_p$  became quite easy to compute.

For 10 years at Cobar, it was established quickly that significant differences in the results due to differing  $E_p$  estimation can be observed. The differences for the water balance model are illustrated in Fig. 32 for Anyang in the NCP. By using a consistent formulation for  $E_p$  in both the Water Balance and REBM we therefore reduced a major cause of variation between the two estimates of  $m_a$  which was perturbing the model calibration.

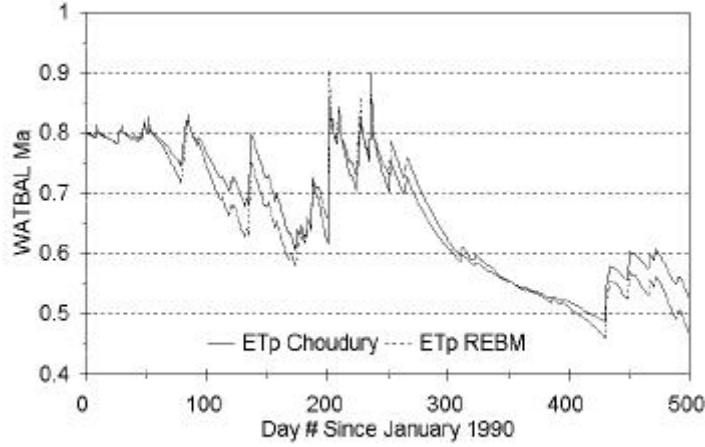


Figure 32. WATBAL moisture availability using the Choudhury and Resistance Energy Balance Model estimates of  $ET_p$ .

For the AVHRR ‘Timeslice’ products, the consistency with the water balance model was less critical and both the daily  $E_d$  and  $E_{pd}$  were produced using the Jackson and Xie formula from estimates of  $E$  and  $E_p$  at the time of the overpass. In China, the solar radiation was estimated from the same radiative transfer model as was used to correct the AVHRR data, meteorological data were interpolated from meteorological station data for the nearest time to the overpass and the formula used for  $E_p$  was the linearised Penman formula (Frere and Popov, 1979):

$$E_p = \frac{\Delta R_{nd} + 0.26 \mathbf{g} (e_a - e_d) [1 + f(u)]}{\Delta + \mathbf{g}} \quad (51)$$

where:

- $\Delta$  is slope of the saturated vapour pressure-temperature relation;
- $e_a$  is the saturated vapour pressure at the reference temperature;
- $e_d$  is the vapour pressure of the air at dewpoint;
- $f(u)$  is function of wind speed:

$$f(u) = \begin{cases} 0.54 u_2 & T_{\max} - T_{\min} \leq 12^\circ C \\ [0.54 + 0.07(T_{\max} - T_{\min} - 12)] u_2 & T_{\min} > 5^\circ C \text{ and } 12^\circ C \leq T_{\max} - T_{\min} \leq 17^\circ C \\ 0.89 u_2 & T_{\max} - T_{\min} \geq 17^\circ C \end{cases} \quad (52)$$

where:

$T_{\max}$  is maximum air temperature ( $^\circ C$ );  
 $T_{\min}$  is minimum air temperature ( $^\circ C$ ); and  
 $u_2$  is the wind speed at 2 metres ( $msec^{-1}$ ).

Since the Penman formula was based on a dense cover of short green vegetation, it is normally modified for a growing crop. In this case, the correction used was:

$$E_p[wheat] = 1.914 + 1.013 E_p \quad (53)$$

for winter wheat in the North China Plain (Liu *et al.*, 1991).

Use of this linearised formula and (more importantly) the correction for growing crops produced some differences between it and the integrated (nonlinear) REBM estimate but these made no essential difference to the Timeslice product classes described in Part II.

## 6.6 Application to Yucheng Data

Yucheng field station is an experimental station on the NCP in Shandong, China which is run by Chinese Academy of Sciences (CAS), Institute of Geography and in which CAS Institute of Remote Sensing Applications has been involved with data collection and research. The station is fully equipped with instrumentation including a large weighing lysimeter. Energy balance, micro-meteorological and surface temperature data were available for 13 days from 29 March to 2 June 1992. The dates were 29<sup>th</sup> March, 3<sup>rd</sup>, 8<sup>th</sup>, 13<sup>th</sup>, 18<sup>th</sup>, 23<sup>rd</sup> April 3<sup>rd</sup>, 8<sup>th</sup>, 13<sup>th</sup>, 18<sup>th</sup>, 23<sup>rd</sup> 29<sup>th</sup> May and 2<sup>nd</sup> June. On these days, surface and air temperatures, components of the energy balance, wind speed and relative humidity were measured hourly. Crop height and cover were also recorded on these days and evapotranspiration was estimated using a number of methods including Bowen-ratio and lysimeter data. Rain fell on the 8<sup>th</sup> April and 13<sup>th</sup> May. Daily meteorological data ( $T_{\min}$ ,  $T_{\max}$ ,  $P$  and  $u$ ) were available from the 27<sup>th</sup> March until the 3<sup>rd</sup> June 1992. This data set allowed the influence of estimating meteorological parameters on calculations of REBM  $ET_a$  and net radiation ( $R_n$ ), both discussed later, to be analysed.

### 6.6.1 Modelling of individual terms and $ET_a$

Firstly, the differences between estimates and measurements for  $T_{air}$ ,  $S$ , and  $RH$  at Yucheng (Table 21) are documented. The errors in estimating both  $T_{air}$  (compare Table 21 with Table 1) and  $S$  (compare Table 21 with Table 10 Total) are similar to the data presented in the previous sections.  $RH$  was estimated using the  $T_{\min} = T_{dew}$  'constant'

method as K97 could not be used as the length of recording period was less than one year. For RH at Yucheng, RMS deviation was similar with the validation data set (compare Table 21 with Table 2), however, the RH model was only able to explain 14.1% (Table 21) of the observed variance at Yucheng compared with the lowest value of 48.2% (TM time, non-rain days Table 2) for Lockyersleigh. Wind speed was estimated to be  $2 \text{ ms}^{-1}$ , it ranged from 0.226 to  $6.425 \text{ ms}^{-1}$ .

Table 21. Summary Statistics for variable estimation for the Yucheng data set.

<b>X variable</b> <b>Y variable</b> Units	<b><math>T_{air}</math> measured</b> <b><math>T_{air}</math> modelled</b> °C	<b>S measured</b> <b>S modelled</b> $\text{Wm}^{-2}$	<b>RH measured</b> <b>RH modelled</b> %
<b>MEASURED</b>			
Mean	21.085	526.686	50.619
STD	5.662	266.378	17.007
<b>MODELLED</b>			
Bias	-0.602	51.372	-3.930
RMS deviation	1.204	94.670	16.677
Slope	0.935	0.881	40.420
Offset	1.980	11.138	0.279
$r^2$	0.9552	0.874	0.150
Std Err Y Estimate	1.146	89.235	11.305
Num of Obs	137	137	137

REBM  $ET_a$  was estimated for two situations. Firstly,  $ET_a$  was estimated when  $T_s$ , cover and height were measured with  $T_{air}$ , RH and S being estimated and the default wind speed ( $2 \text{ ms}^{-1}$ ) used. Secondly,  $ET_a$  was estimated when all parameters were measured. The two model estimates of  $ET_a$  are crossplotted in Fig 33 and show some scatter about the 1:1 line. However, the differences are smaller when the flux is larger. The bias, RMSD and  $r^2$  between the two  $ET_a$  model estimates were  $-13.94 \text{ Wm}^{-2}$ ,  $71.4 \text{ Wm}^{-2}$  and 0.759, respectively at AVHRR times on days when no rain fell, see Table 22.

Table 22. Shows the summary statistics for  $ET_{a\_all\_known}$  versus  $ET_{a\_Ts,cover,ht\_known}$  AVHRR times and TM times are only for days when no rain fell.

	<b>All Data</b>	<b>AVHRR Times</b> <b>13, 14, 15, and 16</b>	<b>TM Times</b> <b>9 and 10</b>
Bias	-3.405	-13.940	-8.209
RMS deviation	93.285	71.417	116.909
Slope	0.900	0.879	0.486
Offset	32.984	54.110	189.429
$r^2$	0.769	0.759	0.563
Std Err Y Estimate	91.414	69.373	74.911
Num of Obs	137	39	22

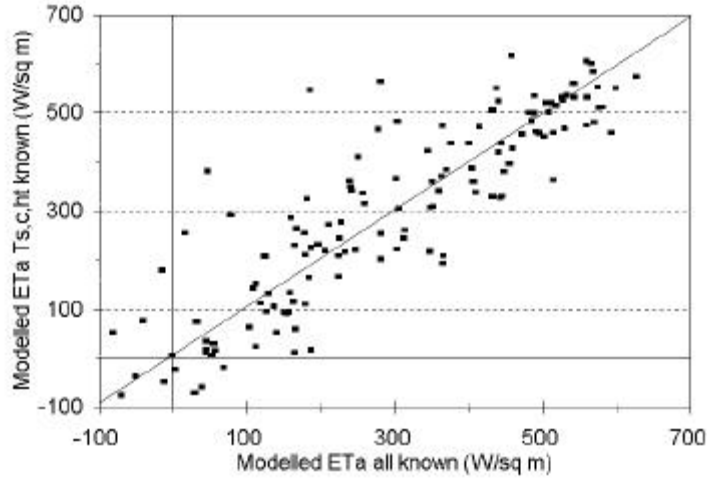


Figure 33. Plot of modelled  $ET_{a\_all\_known}$  versus modelled  $ET_{a\_Ts,cover,ht\_known}$  for selected days Yucheng, China. The 1:1 line is shown.

### 6.6.2 Comparing modelled $ET_a$ with measured $ET_a$

Model estimates of  $ET_a$  for the two cases: [1.] when meteorological variables are estimated and [2.] when meteorological variables were measured, were compared with the field measurements of  $ET_a$ . The summary statistics are listed in Table 23. These were crossplotted as shown in Fig 34 and Fig. 35, respectively which show that  $ET_a$  may be over estimated in the middle of the day, when the values are highest.

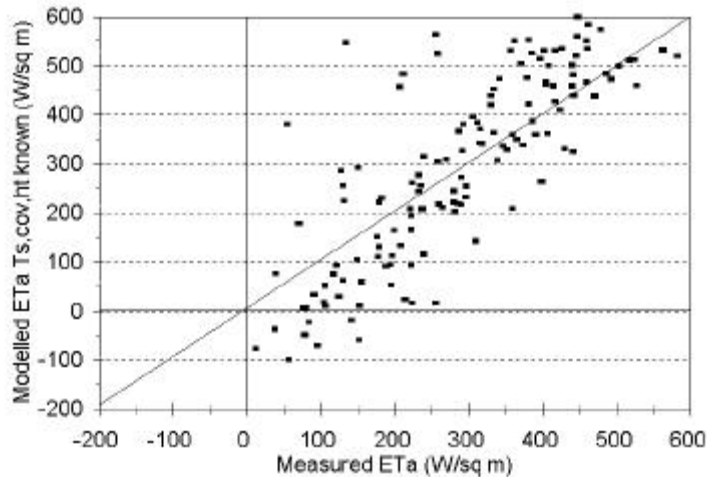


Figure 34. Crossplot of measured  $ET_a$  against modelled  $ET_a$ , with  $T_s$ , cover and height measured and other variables estimated, selected days, 1992, Yucheng, China. The 1:1 line is shown.

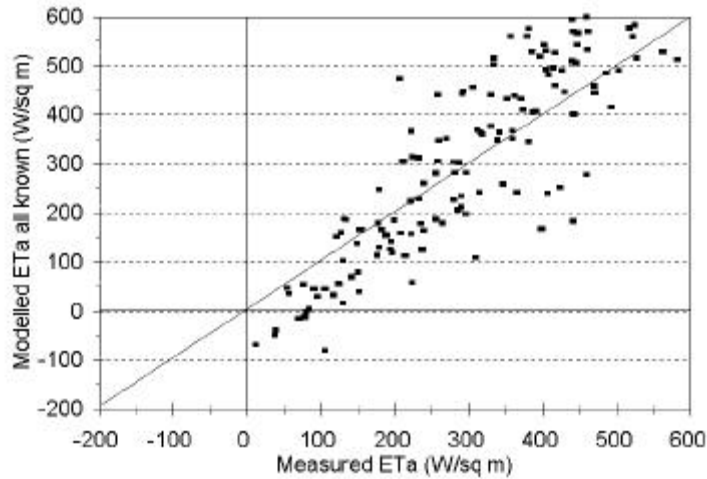


Figure 35. Crossplot of measured  $ET_a$  against modelled  $ET_a$  with surface temperature, air temperature, relative humidity, total solar radiation, wind speed, cover and height all measured, selected days, 1992, Yucheng, China. The 1:1 line is shown.

There is a range of some  $400 \text{ Wm}^{-2}$  in modelled instantaneous  $ET_a$  over a large range of measured  $ET_a$  values for both cases shown in Figure 34 and Figure 35. This range of modelled instantaneous  $ET_a$  is similar to results presented for the validation data sets for HAPEX-MOBILY, FIFE IFC2 and FIFE IFC3 using a combination equation (Raupach *et al.*, 1997). The range was smaller for other validation data sets (Cabauw and OASIS), but the actual value of  $ET_a$  did not exceed  $400 \text{ Wm}^{-2}$  in these data sets (Raupach *et al.*, 1997). Zhang *et al.* (1995) show a similar range of modelled instantaneous  $ET_a$  presented for the HAPEX-MOBILY validation data set. No statistical measure of divergence from the mean was provided in these references.

There are no obvious improvements when using all measured data, compared with using estimated variables, in the REBM estimates of instantaneous  $ET_a$  (Table 23) compared with the field data. This means that the variance between REBM estimated  $ET_a$  and  $ET_a$  measured independently at Yucheng is mainly due to the difficulty in modelling instantaneous  $ET_a$  and/or the uncertainties of field measurement of ET and not due to the methods used here to estimate the required variables used as input to the REBM. From Table 23 the ratio of RMSD (when all variables are measured) divided by the mean of the observed data is 33.23%, 27.42% and 30.3% for all data, AVHRR times (when no rain fell) and TM times (when no rain fell), respectively.

Similar values have been found for a grass-dominated site (38.69%, Kendall) and a shrub-dominated site (29.71% Lucky Hills) (Flerchinger *et al.*, 1998; Flerchinger pers. comm. 1998) and for a site in Owens valley (Kustas *et al.*, 1989). Kustas *et al.* (1990) showed that the instantaneous root mean square error for  $ET_a$  from several fields was over  $100 \text{ W m}^{-2}$  in all cases. In all of these experiments (Raupach *et al.*, 1997, Zhang *et al.*, 1995, Flerchinger *et al.*, 1998, Kustas *et al.*, 1989, Kustas *et al.*, 1990) detailed measurements of meteorological variables were made during the day. When estimating

instantaneous  $ET_a$  using variables estimated from daily extremes, the results for Yucheng are of a similar magnitude. This means that using estimated variables from daily extremes does not worsen the accuracy of estimating instantaneous  $ET_a$ .

Table 23. Summary Statistics between modelled  $ET_a$  and measured  $ET_a$  when variables are either estimated or measured. The AVHRR and TM data are only for the days when no rain fell.

	All data	AVHRR Time 13, 14, 15 and 16	TM Time 9 and 10
<b>MEASURED</b>			
Mean $Wm^{-2}$	290.602	354.416	291.170
STD $Wm^{-2}$	133.626	93.860	111.997
Num of Obs	137	39	22
<b>MODELLED</b>			
<b><math>T_s</math>, cover, height = measured <math>T_{air}</math>, RH &amp; S interpolated Default (<math>2\ ms^{-1}</math>) Wind speed.</b>			
Bias $Wm^{-2}$	-8.075	9.138	-69.932
RMS deviation $Wm^{-2}$	111.494	94.572	89.822
Slope	1.167	1.124	0.690
Offset $Wm^{-2}$	-40.360	-52.927	160.116
$r^2$	0.671	0.558	0.465
Std Err Y Estimate $Wm^{-2}$	109.2465	93.858	82.853
Num of Obs	137	39	22
<b><math>T_s</math>, cover, height = measured <math>T_{air}</math>, RH &amp; S measured Wind speed measured</b>			
Bias $Wm^{-2}$	-4.670	23.078	-61.723
RMS deviation $Wm^{-2}$	96.578	97.165	88.239
Slope	1.203	1.075	1.407
Offset $Wm^{-2}$	54.350	49.757	56.883
$r^2$	0.751	0.520	0.813
Std Err Y Estimate $Wm^{-2}$	92.686	96.908	75.531
Num of Obs	137	39	22

### 6.6.3 Modelling Net Radiation

The sensitivity of estimating meteorological variables on the model estimate of  $R_n$  was performed at Yucheng. Firstly,  $R_n$  was estimated when  $T_s = T_{air}$  with  $T_{air}$ , RH and S being estimated, constants were used for wind speed ( $2\ ms^{-1}$ ), cover (70 %) and crop height (20 cm) (Fig. 36). Secondly,  $R_n$  was estimated when  $T_s$ , cover and height were measured with all parameters estimated as above. (Fig. 37). Finally,  $R_n$  was estimated when all variable were measured (Fig. 38). Table 24 shows the regression statistics for Fig. 36, 37, 38. This analysis was also performed at times when AVHRR and TM data would be captured, the plots for these particular times have not been presented. In all

cases, providing more measured data to the model of  $R_n$  slightly increases the accuracy of the model. This is to be expected. For AVHRR times, when only  $T_s$  was measured the bias and RMS deviation both increase by  $30 \text{ Wm}^{-2}$ , compared to the case when all variables are measured (Table 24). There is a similar decrease when only  $T_s$  was measured at the time of TM data acquisition.

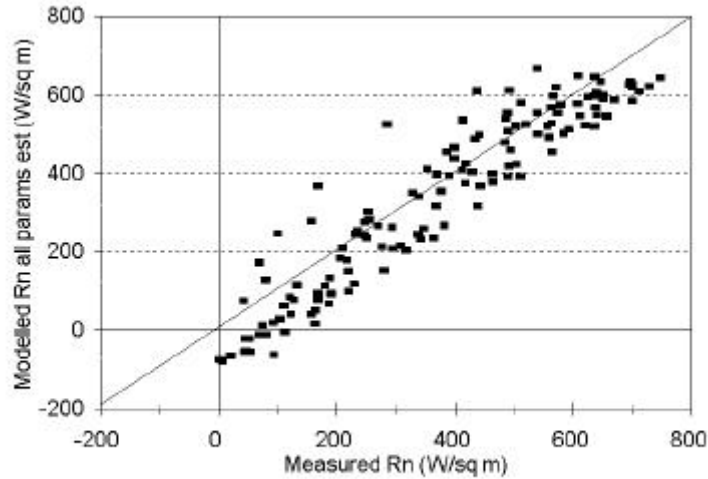


Figure 36. Crossplot of measured  $R_n$  against modelled  $R_n$ , with  $T_s = T_{air}$ , other variables estimated, selected days, 1992, Yucheng, China. The 1:1 line is shown.

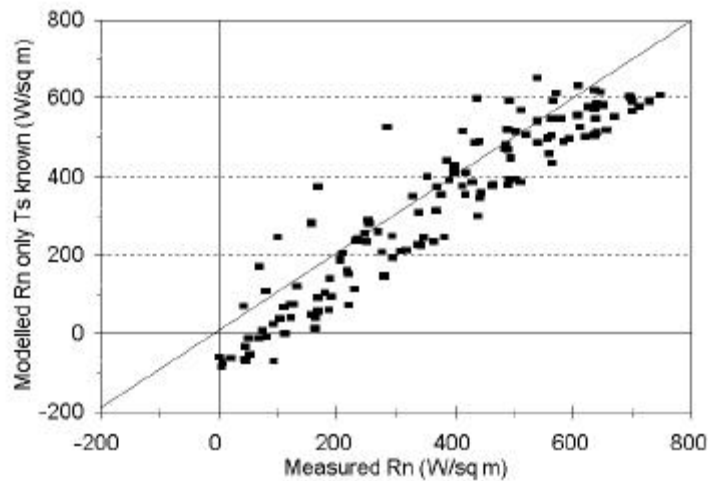


Figure 37. Crossplot of measured  $R_n$  against modelled  $R_n$ , with  $T_s$  measured, other variables estimated, selected days, 1992, Yucheng, China. The 1:1 line is shown.

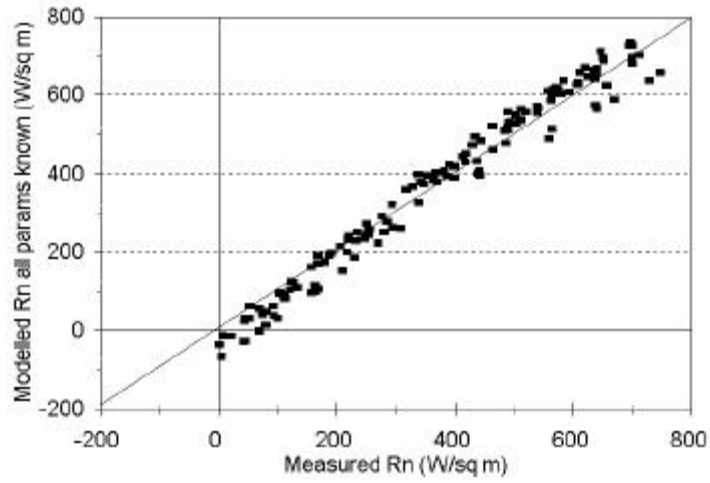


Figure 38. Crossplot of measured  $R_n$  against modelled  $R_n$  with  $T_s$ ,  $T_{air}$ , RH, S,  $u$ , cover and height all measured, selected days, 1992, Yucheng, China. The 1:1 line is shown.

Table 24. Summary Statistics between modelled  $R_n$  and measured  $R_n$  when variables are either estimated or measured. The AVHRR and TM data are only for the days when no rain fell.

	All data	AVHRR Time 13, 14, 15 and 16	TM Time 9 and 10
<b>MEASURED</b>			
Mean $Wm^{-2}$	373.194	426.393	434.423
STD $Wm^{-2}$	207.902	154.972	156.128
Num of Obs	137	39	22
<b>MODELLED</b>			
<b><math>T_s = T_{air}</math></b>			
<b><math>T_{air}</math>, RH &amp; S interpolated</b>			
<b>Wind, ht, cover assumed</b>			
Bias $Wm^{-2}$	36.481	18.723	36.833
RMS deviation $Wm^{-2}$	73.459	64.089	85.547
Slope	1.395	1.235	0.789
Offset $Wm^{-2}$	-68.719	-30.09	168.79
$r^2$	0.701	0.512	0.575
Std Err Y Estimate $Wm^{-2}$	119.46	111.45	75.744
Num of Obs	137	39	22
<b><math>T_s</math>, cover, height = measured</b>			
<b><math>T_{air}</math>, RH &amp; S interpolated</b>			
<b>Default (<math>2\ ms^{-1}</math>) Wind speed.</b>			
Bias $Wm^{-2}$	32.002	17.455	30.104
RMS deviation $Wm^{-2}$	76.360	65.777	90.112
Slope	0.992	0.940	0.609
Offset $Wm^{-2}$	29.0925	7.960	139.610
$r^2$	0.8795	0.834	0.673
Std Err Y Estimate $Wm^{-2}$	76.343	65.125	66.332
Num of Obs	137	39	22
<b><math>T_s</math>, cover, height = measured</b>			
<b><math>T_{air}</math>, RH &amp; S measured</b>			
<b>Wind speed measured</b>			
Bias $Wm^{-2}$	-0.090	0.8803	-15.296
RMS deviation $Wm^{-2}$	38.365	36.506	39.296
Slope	1.071	1.029	1.150
Offset $Wm^{-2}$	-26.500	13.385	-50.009
$r^2$	0.975	0.951	0.970
Std Err Y Estimate $Wm^{-2}$	35.390	36.222	31.517
Num of Obs	137	39	22

The energy balance model we have used allows the effective surface temperature to be inverted if the  $m_a$  is known (see Section 6.4.3). For Yucheng  $m_a$  could be derived using the measured  $ET_a$  and an estimate of  $ET_p$  consistent with the REBM. Fig. 39 shows a

comparison between the effective surface temperature inverted from  $m_a$  using the REBM with the measured (radiometric) surface temperature.  $T_{air}$ , RH, S,  $u$ , cover and crop height were measured. Apart from some points with inconsistent data the two estimates are close and support the modelling proposed in this Report.

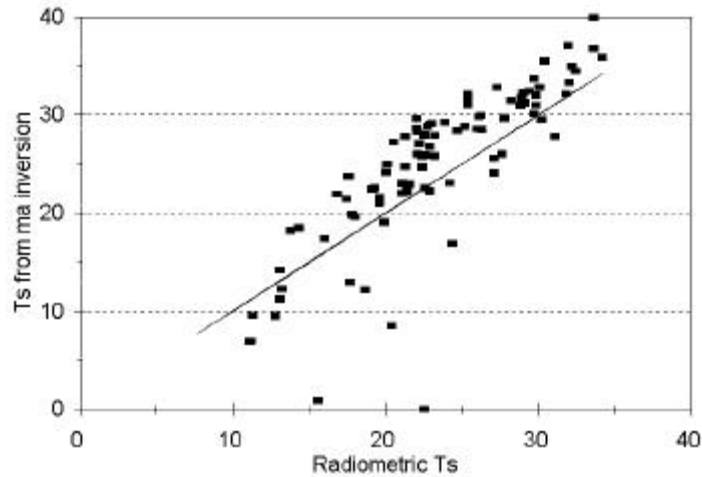


Figure 39. Crossplot of measured radiometric  $T_s$  with  $T_s$  from the inversion of the  $m_a$ .  $ET_a$  was calculated from lysimeter data and  $ET_p$  has been calculated solar radiation measurements. All other variables were measured, selected days, 1992, Yucheng, China.

The loss of accuracy when estimating meteorological variables for the REBM estimates of  $ET_a$  and  $R_n$  has been quantified. When modelling  $ET_a$  estimating meteorological variables has little impact on the accuracy of the model (Table 23). The sensitivity to estimating  $R_n$  when only  $T_s$  is measured and other meteorological variables were estimated has been documented (Table 24). If it were specified that all variables needed to solve the REBM has to be measured at the time of remotely sensed data acquisition then there would be few stations which could meet this criteria. Only needing stations which record at least daily  $T_{max}$ ,  $T_{min}$  and  $P$  means that more stations to be linked with regional remotely sensed data over the MDB and NCP. We expect that this would be true for other regions of the world.

## **7 INTEGRATING THE METHODS AT AVHRR OVERPASS TIMES**

The primary tools we have discussed as a means to use remotely sensed data in water balance studies are generally adequate for the kind of days on which clear overpasses are available provided adequate meteorological data are available. Under these conditions, mapping remotely sensed surface temperatures to spatially varying actual evapotranspiration is a reasonably well posed action. However, the provision of the meteorological data presents a problem in most cases. The airborne scanner study by Jupp and Kalma (1989) showed how surface temperature variations were adequate to extrapolate energy balance components from meteorological data sites unless (for example) air temperature varied significantly between the pixel of interest and its estimate derived from nearby base station(s).

Nevertheless, if topographic and other regional effects are modelled into the variation in meteorological data (Hungerford *et al.*, 1989) and if effective spatial interpolation is used, the effects of such variations may be reduced to a minimum. It is useful in this context to note that water balance modelling based only on GIS modelling and not using remotely sensed data faces similar limitations. How this was approached in the application of these tools will be addressed in Part II (Tian *et al.*, 1998). In that paper, the issues of image data processing from satellite observations to surface temperature will also be addressed as well as the opportunities the remotely sensed data provide for other parameters such as cover (or leaf area index, LAI) and albedo to be provided from the visible and near infrared channels of the AVHRR.

For now, it is useful to outline the different ways the tools can be put to use assuming these processing and data interpolation issues have been addressed. The uses can be looked at from the direction of the remotely sensed data and from the direction of the water balance data.

### **7.1 Image based Products**

Since the components of the evaporation can be calculated, it is possible to estimate on a pixel to pixel basis the quantities described previously:

$$m_a(EB) = \frac{IE}{IE_p} \quad (54)$$

and

$$CWSI = 1 - \frac{E_d}{E_{pd}} \quad (55)$$

These can be made into images to form a ‘gappy’ series of images estimating moisture availability or converted to soil moisture measurements when empirical relationships between soil moisture levels and moisture availability are available. The results of this approach and its success in mapping regional drought stress will be given in Part II.

It is often convenient for practical applications to average the results over management regions, such as counties which also provides a more stable result. The Timeslice products produced for the NCP and discussed in Part II use this approach. However, the pixel level spatial variation is also an interesting property and in order to provide

image showing variation at the pixel level it has been found useful to make use of an approximation to  $m_a$  presented by Jackson *et al.* (1983) in which it was noted that:

$$m_a(EB) \approx NDTI \quad (56)$$

$$= \frac{T_\infty - T_s}{T_\infty - T_0}$$

where  $T_\infty$  is the surface temperature which would theoretically occur if there was no available water - modelled as infinite surface resistances, and  $T_0$  is the temperature that would theoretically occur for fully available moisture - modelled as zero resistance and is the temperature corresponding to potential ET as used in this Report.

The term NDTI (or Normalised Difference Temperature Index) jointly developed by Jupp *et al.* (1992) and McVicar *et al.* (1992) who used this definition to map AVHRR surface temperatures to a spatially varying index of  $m_a$ . The two bounding temperatures can be derived by meteorological and GIS data based modelling and the AVHRR surface temperature is unchanged in the calculation. The variations demonstrated by the NDTI will also be shown in Part II.

## 7.2 Calibrating the Water Balance

The images produced in this way form useful tools for monitoring drought and to display its spatial variation either at the image pixel scale or by region. If consistent relationships can be established between the moisture availability and soil water content these data can be calibrated to soil moisture. In the case of fallow or bare areas, thermal inertia can be used instead of the CWSI or NDTI which assume at least partial vegetation cover. The problem they have is that the time series will be gappy, will not occur for predictable times and may even be quite sparse in some years. In addition, only a fraction of the meteorological data are used.

In this situation, an alternative can be investigated in which remotely sensed data are used to calibrate a traditional water balance that uses all of the meteorological data. Our work has investigated:

1. Whether the temperature effectively modelled from the water balance by its computation of  $m_a(WB)$  and the AVHRR based surface temperature can be made consistent or
2. Whether the  $m_a(WB)$  and  $m_a(EB)$  can be made consistent.

Such a consistency can provide calibration for the water balance model which can then estimate the water balances spatially over time as before but with parameters taking account of the remotely sensed information. At the time of overpasses, the remotely sensed data will still be available to provide spatial distributions and boundaries. The feasibility of this equation is investigated using Chinese and Australian data in Part II.

## **8 CONCLUSIONS**

In this first Part of two pieces of work, we have shown how relatively simple methods exist which can use the limited information normally available from AVHRR and meteorological data to map the evaporation at a regional scale in a way that can be related to moisture stress and be related directly to concepts and components of water balance approaches to regional soil moisture and moisture deficits. These water balance methods are currently used to infer drought but have problems in that they are generally aspatial and difficult to calibrate.

Modelling the surface temperatures at the time of an overpass requires estimates of air temperature, humidity, wind speed and incident solar radiation for specific times of the day. At best, such data are normally available on a daily basis at local meteorological stations. Solar radiation is rarely measured at all. Bringing the water and energy balances onto a consistent footing also requires the definition and use of common components, such as  $E_p$ , to be consistent. A set of methods have been described which seem to accomplish the task as well as the limited data allow. A good test of the success of this approach is the way in which the energy balance components have been shown to be estimated based only on available meteorological data and surface temperature.

We have shown how these tools could be integrated either to provide a number of 'Timeslice' views of the spatial extent of moisture availability or be integrated with the water balance models as calibrating information. The validation of the Timeslice approach and the feasibility of the water balance approach will be addressed in Part II using data from China and Australia. While the tools described are relatively simple and, given more ancillary data, many improvements are possible, it seems that they can both operate within the normal limits of data and provide adequate answers.

## **9 ACKNOWLEDGMENTS**

Research has been supported in Australia by CSIRO, the Land and Water Resources Research Development Commission (LWRRDC) and the Australian Centre for International Agricultural Research (ACIAR). In China the work is supported by the State Science and Technology Commission of China, the Chinese Academy of Sciences and the Natural Science Foundation of China. The international collaboration and exchanges have also been supported by the Australia/China Joint Science and Technology Commission and the CSIRO/CAS Cooperative Agreement, Visits Program. Thanks to Isabelle Balzer, Guy Byrne, James Davidson, Li Lingtao, Kate Mashford, Elizabeth McDonald and Nicole Williams who, at various times, helped maintain the MDB AVHRR archive. Rama Nemani of University of Montana helped greatly with provision of the HOURLY code and help with its development. Haralds Alksnis and Jetse Kalma provided help and data from the CSIRO Division of Water Resources Lockyersleigh experimental site. Drs Tom Hatton and Dean Graetz reviewed drafts of the report and made many helpful and valuable suggestions which improved this report. David Parkin designed the cover graphics and Susan Campbell improved the tables. The photo used in the cover is from the Dean Graetz collection. Thanks to any others that we may have over looked.



## **10 REFERENCES**

- Bindi, M. and Miglietta, F. (1991). Estimating daily global radiation from air temperature and rainfall measurements. *Climate Research*, **1**, 117-124.
- Bristow, K.L. (1992). Prediction of mean vapor density from daily minimum air temperature. *Agricultural and Forest Meteorology*, **59**, 309-317.
- Bristow, K.L. and Campbell, G.S. (1984). On the Relationship Between Incoming Solar Radiation and Daily Maximum and Minimum Temperature. *Agricultural and Forest Meteorology*, **31**, 159-166.
- Bristow, K.L., Campbell, G.S. and Saxton, K.E. (1985). An equation for separating daily solar radiation into direct and diffuse components. *Agricultural and Forest Meteorology*, **35**, 123-131.
- Brutsaert, W.H. (1975). On a derivable formula for longwave radiation from clear skies. *Water Resources Research*, **11**, 742-744.
- Carlson, T.N., Dodd, J.K., Benjamin, S.G. and Cooper, J.N. (1981). Satellite Estimation of the Surface Energy Balance, Moisture Availability and Thermal Inertia. *Journal of Applied Meteorology*, **20**, 67-87.
- Castellvi, F., Perez, P.J., Villar, J.M. and Rosell, J.I. (1996). Analysis of methods for estimating vapor pressure deficits and relative humidity. *Agricultural and Forest Meteorology*, **82**, 29-45.
- Chen, J. (1988). An important shortcoming and improvement of evapotranspiration models used in Remote Sensing. *Science Bulletin (China)*, **16**, 454-457.
- Choudhury, B.J. (1989). Estimating Evaporation and Carbon Assimilation Using Infrared Temperature Data: Vistas in Modelling. In *Theory and Applications of Optical Remote Sensing*(Ed, Asrar, G.) John Wiley and Sons, New York, pp. 628-690.
- Choudhury, B.J., Owe, M., Goward, S.N., Golus, R.E., Ormsby, J.P., Chang, A.T.C. and Wang, J.R. (1987). Quantifying Spatial and Temporal Variabilities of Microwave Brightness Temperature over the U.S. Southern Great Plains. *International Journal of Remote Sensing*, **8**, 177-192.
- Choudhury, B.J., Reginato, R.J. and Idso, S.B. (1986). An Analysis of Infrared Temperature Observation over Wheat and Calculation of Latent Heat Flux. *Agricultural and Forest Meteorology*, **37**, 75-88.
- Cracknell, A.P. and Xue, Y. (1996a). Estimation of ground heat flux using AVHRR data and an advanced thermal inertia model (SoA-TI model). *International Journal of Remote Sensing*, **17**, 637-642.

- Cracknell, A.P. and Xue, Y. (1996b). Thermal inertia determination from space - a tutorial review. *International Journal of Remote Sensing*, **17**, 431-461.
- Dickinson, R.E. (1983). Land surface processes and climate - Surface albedos and energy balance. *Advances in Geophysics*, **25**, 305-353.
- Dickinson, R.E., Sellers, P.J. and Kimes, D.S. (1987). Albedos of Homogeneous Semi-infinite canopies: Comparison of Two-stream Analytical and Numerical Solutions. *Journal of Geophysical Research*, **92**, 4282-4286.
- Dyer, J.A. and Brown, D.M. (1977). A climatic simulator for field-drying hay. *Agricultural Meteorology*, **18**, 37-48.
- Flerchinger, G.N., Kustas, W.P. and Wertz, M.A. (1998). Simulating Surface Energy Fluxes from Radiometric Surface Temperatures for Two Arid Vegetation Communities Using the SHAW Model. *Journal of Applied Meteorology*, **37**, 449-460.
- Frere, M. and Popov, G.F. (1979). Agrometeorological Crop Monitoring and forecasting. FAO, Rome.
- Huband, N.D.S. and Monteith, J.L. (1986). Radiative surface temperature and energy balance of a wheat canopy. *Boundary-Layer Meteorology*, **36**, 1-17.
- Hungerford, R.D., Nemani, R.R., Running, S.W. and Coughlin, J.C. (1989). MTCLIM: A mountain microclimate simulation model. USDA Forest Service, pp. 52.
- Hutchinson, M.F., Kalma, J.D. and Johnson, M.E. (1984). Monthly Estimates of Wind Speed and Wind Run for Australia. *Journal of Climatology*, **4**, 311-324.
- Idso, S.B., Jackson, R.D. and Reginato, R.J. (1976). Compensating for Environmental Variability in the Thermal Inertia Approach to Remote Sensing of Soil Moisture. *Journal of Applied Meteorology*, **15**, 811-817.
- Jackson, R.D. (1982). Soil Moisture Inferences from Thermal Infra-red Measurements of Vegetation Temperatures. *IEEE Transactions on Geoscience and Remote Sensing*, **GE-20**, 282-286.
- Jackson, R.D., Hatfield, J.L., Reginato, R.J., Idso, S.B. and Pinter Jr., P.J. (1983). Estimation of Daily Evapotranspiration from One Time-of-Day Measurements. *Agricultural Water Management*, **7**, 351-362.
- Jackson, R.D., Idso, S.B., Reginato, R.J. and Pinter Jr., P.J. (1981). Canopy temperature as a crop water stress indicator. *Water Resources Research*, **17**, 1133-1138.
- Jupp, D.L.B. (1989). Processing AVHRR Data with microBRIAN - Part 1 Background. MPA Communications, Melbourne, Australia, pp. 17.

- Jupp, D.L.B. (1990). Constrained two-layer models for estimating evapotranspiration. In *Proceedings of the 11th Asian Conference on Remote Sensing* Guangzhou, China, November, 1990, pp. B.4.1-B.4.6.
- Jupp, D.L.B. and Kalma, J.D. (1989). Distributing Evapotranspiration in a Catchment Using Airborne Remote Sensing. *Asian-Pacific Remote Sensing Journal*, **2**, 13-25.
- Jupp, D.L.B., McVicar, T.R., Walker, J., Held, A.A., Kalma, J.D. and McDonald, E.R. (1992). Remote sensing of change in components of the regional water balance of the Murray Darling Basin using satellite imaged and spatially registered environmental data. Final Report to the LWRRDC Project CWA6. CSIRO Division of Water Resources, Canberra.
- Jupp, D.L.B., Walker, J., Kalma, J.D. and McVicar, T.R. (1990). Using Thermal Remote Sensing to Monitor Land Degradation and Salinization in the Murray-Darling Basin of Australia. In *Twenty-Third International Symposium on Remote Sensing of the Environment, April 18-25* Bangkok, Thailand, pp. 1011-1021.
- Kalma, J.D. (1989). A comparison of expressions for the aerodynamic resistance to sensible heat transfer. CSIRO Division of Water Resources, Canberra, ACT, pp. 17.
- Kalma, J.D., Alksnis, H., Daniel, P. and Laughlin, G.P. (1987). The Regional Evaporation Project: Instrumentation and Field Measurements. CSIRO Division of Water Resources, Canberra, ACT, pp. 44.
- Kalma, J.D. and Jupp, D.L.B. (1990). Estimating evaporation from pasture using infrared thermometry: evaluation of a one-layer resistance model. *Agricultural and Forest Meteorology*, **51**, 223-246.
- Kimball, J.S., Running, S.W. and Nemani, R.R. (1997). An improved method for estimating surface humidity from daily minimum temperature. *Agricultural and Forest Meteorology*, **85**, 87-98.
- Köppen, W. (1931). *The Climates of the Earth*, DeGruyter, Berlin.
- Kustas, W.P., Choudhury, B.J., Moran, M.S., Reginato, R.J., Jackson, R.D., Gay, L.W. and Weaver, H.L. (1989). Determination of Sensible Heat Flux Over Sparse Canopy Using Thermal Infrared Data. *Agricultural and Forest Meteorology*, **44**, 197-216.
- Kustas, W.P., Moran, M.S., Jackson, R.D., Gay, L.W., Duell, L.F.W., Kunkel, K.E. and Matthias, A.D. (1990). Instantaneous and Daily Values of the Surface Energy Balance over Agricultural Fields Using Remote Sensing and a Reference Field in an Arid Environment. *Remote Sensing of Environment*, **32**, 125-141.

- Leuning, R. (1998). Averaging times and the Penman-Monteith equation. *Journal of Hydrology*, (in prep.).
- Leuning, R., Kelliher, F.M., DePury, D.G.G. and Schulze, E.-D. (1995). Leaf nitrogen, photosynthesis, conductance and transpiration: scaling from leaves to canopies. *Plant Cell and Environment*, **18**, 1183-1200.
- L'Homme, J.-P., Katerji, N., Perrier, A. and Bertolini, J.-M. (1988). Radiative surface temperature and convective flux calculation over crop canopies. *Boundary-Layer Meteorology*, **43**, 383-392.
- L'Homme, J.-P., Monteny, B. and Amadou, M. (1994). Estimating sensible heat flux from radiometric temperature over sparse millet. *Agricultural and Forest Meteorology*, **68**, 77-91.
- Liu, C., Hong, J. and Jin, H. (1991). Calculation of Field Evapotranspiration, Evapotranspiration of the Field-Measurement and Calculation. *Meteorology Press (Chinese)*, 134-142.
- Manabe, S. (1969). Climate and Ocean Circulation: I, The atmospheric circulation and the hydrology of the earth's surface. *Monthly Weather Review*, **97**, 739-805.
- McVicar, T.R. and Jupp, D.L.B. (1998). The current and potential operational uses of remote sensing to aid decisions on Drought Exceptional Circumstances in Australia: A Review. *Agricultural Systems*, **57**, 399- 468.
- McVicar, T.R., Jupp, D.L.B., Reece, P.H. and Williams, N.A. (1996a). Relating LANDSAT TM vegetation indices to in situ leaf area index measurements. CSIRO, Division of Water Resources, Canberra, ACT, pp. 80.
- McVicar, T.R., Jupp, D.L.B., Walker, J. and Tian, G. (1991). Remote Sensing with Physical Models of Soil Moisture Status to Monitor Land Degradation and Drought. In *Proceedings of the 12th Asian Conference on Remote Sensing* Singapore, pp. A.1.2.1- A.1.2.6.
- McVicar, T.R., Jupp, D.L.B. and Williams, N.A. (1996b). Relating AVHRR vegetation indices to LANDSAT TM leaf area index estimates. CSIRO, Division of Water Resources, Canberra, ACT, pp. 33.
- McVicar, T.R., Jupp, D.L.B., Yang, X. and Tian, G. (1992). Linking Regional Water Balance Models with Remote Sensing. In *Proceedings of the 13th Asian Conference on Remote Sensing* Ulaanbaatar, Mongolia, pp. B.6.1-B.6.6.
- McVicar, T.R. and Mashford, K.E. (1993). Establishment of Control Points for Accurate Co-Registration of AVHRR Data for the Murray Darling Basin. CSIRO Division of Water Resources, Canberra, ACT, pp. 72.

- McVicar, T.R., Tian, G., Jupp, D.L.B. and Li, F. (1993). Soil moisture and drought monitoring using remote sensing. In *Proceedings of the 14th Asian Conference on Remote Sensing* Tehran, Iran, pp. A.5.1 - A.5.6.
- McVicar, T.R., Walker, J., Jupp, D.L.B., Pierce, L.L., Byrne, G.T. and Dallwitz, R. (1996c). Relating AVHRR vegetation indices to in situ leaf area index. CSIRO, Division of Water Resources, Canberra, ACT, pp. 54.
- Monteith, J.L. (1981). Evaporation and Surface Temperature. *Quarterly Journal of Meteorological Society*, **107**, 1-27.
- Monteith, J.L. and Unsworth, M.H. (1990). *Principles of Environmental Physics*, Edward Arnold, London.
- Nemani, R.R. and Running, S.W. (1989). Testing a Theoretical Climate-Soil-Leaf Area Hydrologic Equilibrium of Forests Using Satellite Data and Ecosystem Simulation. *Agricultural and Forest Meteorology*, **44**, 245-260.
- Norman, J.M., Kustas, W.P. and Humes, K.S. (1995). Source approach for estimating soil and vegetation energy fluxes in observations of directional radiometric surface temperature. *Agricultural and Forest Meteorology*, **77**, 263-293.
- Parton, W.J. and Logan, J.A. (1981). A model for diurnal variation in soil and air temperature. *Agricultural and Forest Meteorology*, **23**, 205-216.
- Pratt, D.A., Foster, S.J. and Ellyett, C.D. (1980). A Calibration Procedure for Fourier Series Thermal Inertia Models. *Photogrammetric Engineering and Remote Sensing*, **46**, 529-538.
- Price, J.C. (1982). On the Use of Satellite Data to Infer Surface Fluxes at Meteorological Scales. *Journal of Applied Meteorology*, **21**, 1111-1122.
- Raupach, M.R., Finkele, K. and Zhang, L. (1997). SCAM: A Soil-Canopy-Atmosphere Model: Description and Comparisons with Field Data. CSIRO Centre for Environmental Mechanics, Canberra, ACT, pp. 81.
- Smith, M., Allen, R., Monteith, J.L., Perrier, A., Santos Pereira, L. and Segeren, A. (1991). Expert Consultation on Procedures for Revision of FAO Guidelines for Prediction of Crop Water Requirements. FAO Land and Water Development Division, Rome, Italy, pp. 54.
- Smith, R.C.G., Barrs, H.D. and Fischer, R.A. (1988). Inferring stomatal resistance of sparse crops from infrared measurements of foliage temperature. *Agricultural and Forest Meteorology*, **42**, 183-198.
- Tian, G. (1991). Methods for monitoring soil moisture using remote sensing. *Remote Sensing of Environment (China)*, **6**, 89-98.

- Tian, G. (1993). Estimation of Evapotranspiration and Soil moisture and Drought Monitoring using Remote Sensing in North China Plain. In Space and Environment, Special Plenary Session. In *International Astronautical Federation, 44th IAF Congress Graz, Austria*, pp. 23-31.
- Tian, G., Jupp, D.L.B., Qin, Y., McVicar, T.R. and Li, F. (1998). Monitoring Soil Moisture and Drought Using AVHRR Satellite Data II: Applications. CSIRO Earth Observation Centre, Canberra, ACT.
- Tian, G., Li, F., Sui, H. and Zheng, K. (1989). Estimating of evapotranspiration and soil moisture using NOAA-AVHRR image and ground based meteorological data. In *Proceedings of the 10th Asian Conference on Remote Sensing Kuala Lumpur, Malaysia*.
- Van de Griend, A.A., Camillo, P.J. and Gurney, R.J. (1985). Discrimination of Soil Physical Parameters, Thermal Inertia and Soil Moisture from Diurnal Surface Temperature Fluctuations. *Water Resources Research*, **21**, 997-1009.
- Wetzel, P.J., Atlas, D. and Woodward, R.H. (1984). Determining Soil Moisture from Geosynchronous Satellite Infrared Data: A Feasibility Study. *Journal of Climate and Applied Meteorology*, **23**, 375-391.
- White, D.H. (1990). A Study of the Feasibility of Using Simulation Models and Mathematical Programs as Aids to Drought Monitoring and Management. Bureau of Rural Resources, Canberra.
- Xie, X. (1991). Estimation of Daily Evapotranspiration (ET) From One-time-of-day Remotely Sensed Canopy Temperature. *Remote Sensing of Environment (China)*, **6**, 253-260.
- Xue, Y. and Cracknell, A.P. (1995). Advanced thermal inertia modelling. *International Journal of Remote Sensing*, **16**, 431-446.
- Yang, X. and Tian, G. (1991). A remote sensing model for wheat drought monitoring. In *Proceedings of the 12th Asian Conference on Remote Sensing, SEAMEO Singapore*.
- Zhang, L., Lemeur, R. and Goutorbe, J.P. (1995). A one-layer resistance model for estimating regional evapotranspiration using remote sensing data. *Agricultural and Forest Meteorology*, **77**, 241-261.
- Zhang, R. (1990). Improved thermal inertia model and remote sensing of soil moisture. *Geographical Research (China)*, **9**, 101-112.

## **11 APPENDIX: SOLUTION OF THE TWO LAYER ENERGY BALANCE EQUATIONS WHEN RESISTANCES ARE GIVEN**

### **11.1 Basic Equations**

The surface temperature, atmospheric emissivity, surface emissivity, net radiation, soil heat flux and available energy components for vegetation and soil are taken to be:

$$\begin{aligned}
 T_s &= f_v T_v + (1 - f_v) T_g \\
 e_a &= 1.24 (e_a / T_a)^{1/7} \\
 e &= f_v e_v + (1 - f_v) e_g \\
 R_n &= (1 - a) R_s + \epsilon \sigma (e_a T_a^4 - T_s^4) \\
 G &= G_f R_{ng} \\
 A_v &= R_{nv} \\
 A_g &= R_{ng} - G \\
 &= (1 - G_f) R_{ng}
 \end{aligned}$$

where:

$f_v$  is the fraction of vegetation cover;  
 $\alpha$  is the composite albedo of the surface  
 $a_v$  and  $a_g$  are the albedos of the vegetation and soil components  
 $R_s$  is the shortwave solar irradiance  
 $\epsilon$  is the composite surface emissivity  
 $e_v$  and  $e_g$  are the emissivities of the vegetation and soil components  
 $\sigma$  is the Stefan-Boltzmann constant  
 $e_a$  is the effective atmospheric emissivity  
 $T_a$  is air temperature at reference height, and  
 $T_s$  is the surface temperature.

The net radiation terms  $R_{nv}$  and  $R_{ng}$  are obtained from expressions or approximations to radiative transfer in the surface layer and are functions of the reflectivities and temperatures of the soil and vegetation components.

### **11.2 Defining Equations**

The energy balance components are defined and must balance as in the following equations and table:

$$\begin{aligned}
 IE &= (R_n - G) - H \\
 H &= rC_p \frac{(T_0 - T_a)}{r_a} \\
 IE &= \frac{rC_p}{g} \frac{(e_0 - e_a)}{r_a}
 \end{aligned}$$

where  $T_0$  and  $e_0$  are the air temperature and vapour pressure at the mid-canopy airstream point of the lumped model.

The soil and vegetation components must balance as in the following Table:

$IE_v$	$IE_g$	$IE$
$H_v$	$H_g$	$H$
$A_v$	$A_g$	$R_n - G$

That is, the marginals are sums of the four main terms:

$$\begin{aligned}
 IE_v + IE_g &= IE \\
 H_v + H_g &= H \\
 IE_v + H_v &= A_v \\
 IE_g + H_g &= A_g \\
 IE + H &= A_v + A_g = R_n - G
 \end{aligned}$$

where:

$IE_v$  and  $H_v$  are latent and sensible heat fluxes between foliage and the mid-canopy air stream;

$IE_g$  and  $H_g$  are latent and sensible heat fluxes between ground and mid-canopy air stream;

The system is resolved using resistance models for the latent and sensible heat terms in the form:

$$\begin{aligned}
 IE_v &= \frac{\mathbf{r} C_p}{\mathbf{g}} \frac{(e_s(T_v) - e_e)}{r_v + r_{vs}} \\
 H_v &= \mathbf{r} C_p \frac{(T_v - T_e)}{r_v} \\
 IE_g &= \frac{\mathbf{r} C_p}{\mathbf{g}} \frac{(e_s(T_g) - e_e)}{r_g + r_{gs}} \\
 H_g &= \mathbf{r} C_p \frac{(T_g - T_e)}{r_g}
 \end{aligned}$$

where:

$e_s(T)$  is saturated vapour pressure at temperature  $T$ ;

$e_a$  is vapour pressure at the reference height;

$\mathbf{r} C_p$  is the volumetric heat capacity of air;

$\gamma$  is the psychrometric constant;

$T_e$ ,  $T_v$  and  $T_g$  are the temperatures of the mid-canopy air-stream, the foliage and the ground respectively;

$e_e$  is the vapour pressure of the mid-canopy air-stream; and

$r_{vs}$  and  $r_{gs}$  are surface resistances to flux between an assumed saturated source and the surface for vegetation and the ground respectively.

The primary resistance terms  $r_a$ ,  $r_v$  and  $r_g$  may be computed as presented in Choudhury (1989).

The complete set of equations expressing these balances is:

$$A_v = \frac{\mathbf{r}C_p}{\mathbf{g}} \frac{(e_s(T_v) - e_0)}{r_v + r_{vs}} + \mathbf{r}C_p \frac{(T_v - T_0)}{r_v}$$

$$A_g = \frac{\mathbf{r}C_p}{\mathbf{g}} \frac{(e_s(T_g) - e_0)}{r_g + r_{gs}} + \mathbf{r}C_p \frac{(T_g - T_0)}{r_g}$$

where:

$$T_0 = c_1 T_a + c_2 T_v + c_3 T_g$$

$$e_0 = c_1 e_a + c_2 e_v + c_3 e_g$$

$$= c'_1 e_a + c'_2 e_s(T_v) + c'_3 e_s(T_g)$$

and

$$c_1 = \frac{1/r_a}{1/r_a + 1/r_v + 1/r_g}$$

$$c_2 = \frac{1/r_v}{1/r_a + 1/r_v + 1/r_g}$$

$$c_3 = \frac{1/r_g}{1/r_a + 1/r_v + 1/r_g}$$

$$c'_1 = \frac{1/r_a}{1/r_a + 1/(r_v + r_{vs}) + 1/(r_g + r_{gs})}$$

$$c'_2 = \frac{1/(r_v + r_{vs})}{1/r_a + 1/(r_v + r_{vs}) + 1/(r_g + r_{gs})}$$

$$c'_3 = \frac{1/(r_g + r_{gs})}{1/r_a + 1/(r_v + r_{vs}) + 1/(r_g + r_{gs})}$$

By substituting the expressions for  $T_0$  and  $e_0$  into the first two equations, two equations are obtained in four unknowns:  $[T_v, T_g, r_{sv}, r_{sg}]$ . Hence, two more independent conditions must be known to resolve the equations.

### 11.3 Solution when resistances are known

If the surface resistances are given, the nonlinear equations can, in principle, be solved. A difficulty is that  $r_a$  depends on  $T_0$  which introduces a nonlinearity that must be handled with care.

With substitution, the equations can be written in the form:

$$\mathbf{A} \begin{pmatrix} e_s(T_v) \\ e_s(T_g) \end{pmatrix} + \mathbf{B} \begin{pmatrix} T_v \\ T_g \end{pmatrix} - \mathbf{d} = \mathbf{0}$$

Where for the matrix **A**:

$$a_{11} = \frac{(1 - c'_2)}{\mathbf{g}(r_v + r_{vs})}$$

$$a_{12} = \frac{-c'_3}{\mathbf{g}(r_v + r_{vs})}$$

$$a_{21} = \frac{-c'_2}{\mathbf{g}(r_g + r_{gs})}$$

$$a_{22} = \frac{(1 - c'_3)}{\mathbf{g}(r_g + r_{gs})}$$

For the Matrix **B**:

$$b_{11} = \frac{(1 - c_2)}{r_v}$$

$$b_{12} = \frac{-c_3}{r_v}$$

$$b_{21} = \frac{-c_2}{r_g}$$

$$b_{22} = \frac{(1 - c_3)}{r_g}$$

and for the vector **d**:

$$d_1 = \frac{A_v}{rC_p} + \frac{c'_1 e_a}{\mathbf{g}(r_v + r_{vs})} + \frac{c_1 T_a}{r_v}$$

$$d_2 = \frac{A_g}{rC_p} + \frac{c'_1 e_a}{\mathbf{g}(r_g + r_{gs})} + \frac{c_1 T_a}{r_g}$$

This matrix equation could be linearised but the nonlinearity would remain in  $r_a$ . Hence, it is best to solve it as a fully nonlinear function zero search from a starting point such as  $T_v = T_g = T_a$ .

## 11.4 The Error Function and its Partial Derivatives

To find a zero of the vector function measuring the closure of the energy balance by Newton-Raphson we need the partial derivative (or Jacobian) matrix of the error vector function **e**:

$$\mathbf{e}(T_v, T_g) = \mathbf{A} \begin{Bmatrix} e_s(T_v) \\ e_s(T_g) \end{Bmatrix} + \mathbf{B} \begin{Bmatrix} T_v \\ T_g \end{Bmatrix} - \mathbf{d}$$

Now to get the partials:

First, we will assume that the following partials are available when their respective terms are computed:

$$\frac{\mathcal{J}R_{ng}}{\mathcal{J}T_x}, \quad \frac{\mathcal{J}R_{nv}}{\mathcal{J}T_x}$$

$$\Delta_x = \frac{\mathcal{J}e_s(T_x)}{\mathcal{J}T_x}$$

Also, we will assume that the partial  $\frac{\mathcal{J}r_a}{\mathcal{J}T_0}$  is computed when  $r_a$  is computed.

If the notation  $x$  means either vegetation ( $v$ ) or soil ( $g$ ) we have:

$$\frac{\mathcal{J}r_a}{\mathcal{J}T_x} = \frac{\mathcal{J}r_a}{\mathcal{J}T_0} \frac{\mathcal{J}T_0}{\mathcal{J}T_x}$$

so that to compute the partial we need:

$$\frac{\mathcal{J}T_0}{\mathcal{J}T_v} = \frac{\mathcal{J}c_1}{\mathcal{J}T_v} T_a + c_2 + \frac{\mathcal{J}c_2}{\mathcal{J}T_v} T_v + \frac{\mathcal{J}c_3}{\mathcal{J}T_v} T_g$$

$$\frac{\mathcal{J}T_0}{\mathcal{J}T_g} = \frac{\mathcal{J}c_1}{\mathcal{J}T_g} T_a + \frac{\mathcal{J}c_2}{\mathcal{J}T_g} T_v + c_3 + \frac{\mathcal{J}c_3}{\mathcal{J}T_g} T_g$$

from which we get that:

$$\frac{\mathcal{J}c_1}{\mathcal{J}T_x} = \frac{c_1}{r_a} (c_1 - 1) \frac{\mathcal{J}r_a}{\mathcal{J}T_x}$$

$$\frac{\mathcal{J}c_2}{\mathcal{J}T_x} = \frac{c_2^2 r_v}{r_a^2} \frac{\mathcal{J}r_a}{\mathcal{J}T_x}$$

$$\frac{\mathcal{J}c_3}{\mathcal{J}T_x} = \frac{c_3^2 r_g}{r_a^2} \frac{\mathcal{J}r_a}{\mathcal{J}T_x}$$

Define a function  $H$  by:

$$H = \frac{c_1}{r_a} (c_1 - 1) T_a + \frac{c_2^2 r_v}{r_a^2} T_v + \frac{c_3^2 r_g}{r_a^2} T_g$$

Then it follows by substitution that:

$$\frac{\mathbb{I}r_a}{\mathbb{I}T_x} = \frac{c_x \frac{\mathbb{I}r_a}{\mathbb{I}T_0}}{1 - H \frac{\mathbb{I}r_a}{\mathbb{I}T_0}}$$

where  $c_x$  is  $c_2$  if  $x=v$  and  $c_3$  if  $x=g$ .

Note also that:

$$\begin{aligned} \frac{\mathbb{I}c'_1}{\mathbb{I}T_x} &= \frac{c'_1}{r_a} (c'_1 - 1) \frac{\mathbb{I}r_a}{\mathbb{I}T_x} \\ \frac{\mathbb{I}c'_2}{\mathbb{I}T_x} &= \frac{c'^2_2 (r_v + r_{vs})}{r_a^2} \frac{\mathbb{I}r_a}{\mathbb{I}T_x} \\ \frac{\mathbb{I}c'_3}{\mathbb{I}T_x} &= \frac{c'^2_3 (r_g + r_{gs})}{r_a^2} \frac{\mathbb{I}r_a}{\mathbb{I}T_x} \end{aligned}$$

These formulae provide basic tools for computing the derivatives.

The three vector/matrix terms have partials as follows for the matrix A:

$$\frac{\mathbb{I}A}{\mathbb{I}T_x} = -\frac{1}{\mathbf{g}} \left( \begin{array}{c} \frac{\mathbb{I}c'_2}{\mathbb{I}T_x} / (r_v + r_{vs}) \quad \frac{\mathbb{I}c'_3}{\mathbb{I}T_x} / (r_v + r_{vs}) \\ \frac{\mathbb{I}c'_2}{\mathbb{I}T_x} / (r_g + r_{gs}) \quad \frac{\mathbb{I}c'_3}{\mathbb{I}T_x} / (r_g + r_{gs}) \end{array} \right)$$

For the matrix B:

$$\frac{\mathbb{I}B}{\mathbb{I}T_x} = - \left( \begin{array}{c} \frac{\mathbb{I}c_2}{\mathbb{I}T_x} / r_v \quad \frac{\mathbb{I}c_3}{\mathbb{I}T_x} / r_v \\ \frac{\mathbb{I}c_2}{\mathbb{I}T_x} / r_g \quad \frac{\mathbb{I}c_3}{\mathbb{I}T_x} / r_g \end{array} \right)$$

For the vector d:

$$\frac{\mathbb{I}d}{\mathbb{I}T_x} = \frac{1}{rC_p} \left( \begin{array}{c} \mathbb{I}A_v \\ \mathbb{I}T_x \\ \mathbb{I}A_g \\ \mathbb{I}T_x \end{array} \right) + \left( \begin{array}{c} \frac{1}{\mathbf{g}} \frac{e_a}{r_v + r_{vs}} \frac{\mathbb{I}c'_1}{\mathbb{I}T_x} + \frac{T_a}{r_v} \frac{\mathbb{I}c_1}{\mathbb{I}T_x} \\ \frac{1}{\mathbf{g}} \frac{e_a}{r_g + r_{gs}} \frac{\mathbb{I}c'_1}{\mathbb{I}T_x} + \frac{T_a}{r_g} \frac{\mathbb{I}c_1}{\mathbb{I}T_x} \end{array} \right)$$

Now, writing the equations we need to solve in full we get:

$$\begin{aligned} \mathbf{e}_1 &= a_{11}e_s(T_v) + a_{12}e_s(T_g) + b_{11}T_v + b_{12}T_g - d_1 \\ \mathbf{e}_2 &= a_{21}e_s(T_v) + a_{22}e_s(T_g) + b_{21}T_v + b_{22}T_g - d_2 \end{aligned}$$

The Jacobian matrix has the form:

$$J = \begin{pmatrix} \frac{\partial e_1}{\partial T_v} & \frac{\partial e_1}{\partial T_g} \\ \frac{\partial e_2}{\partial T_v} & \frac{\partial e_2}{\partial T_g} \end{pmatrix}$$

To make the system manageable, we will define two new sets of quantities:

$$dA_{1x} = \frac{\partial a_{11}}{\partial T_x} e_s(T_v) + \frac{\partial a_{12}}{\partial T_x} e_s(T_g)$$

$$dA_{2x} = \frac{\partial a_{21}}{\partial T_x} e_s(T_v) + \frac{\partial a_{22}}{\partial T_x} e_s(T_g)$$

$$dB_{1x} = \frac{\partial b_{11}}{\partial T_x} T_v + \frac{\partial b_{12}}{\partial T_x} T_g$$

$$dB_{2x} = \frac{\partial b_{21}}{\partial T_x} T_v + \frac{\partial b_{22}}{\partial T_x} T_g$$

for x=1,2 where, x=1 is the same as x=v and x=2 is the same as x=g.

With these in place, the Jacobian can be assembled as follows:

$$\frac{\partial e_1}{\partial T_v} = J_{11} = a_{11}\Delta_1 + b_{11} - \frac{\partial d_1}{\partial T_v} + dA_{11} + dB_{11}$$

$$\frac{\partial e_1}{\partial T_g} = J_{12} = a_{12}\Delta_2 + b_{12} - \frac{\partial d_1}{\partial T_g} + dA_{12} + dB_{12}$$

$$\frac{\partial e_2}{\partial T_v} = J_{21} = a_{21}\Delta_1 + b_{21} - \frac{\partial d_2}{\partial T_v} + dA_{21} + dB_{21}$$

$$\frac{\partial e_2}{\partial T_g} = J_{22} = a_{22}\Delta_2 + b_{22} - \frac{\partial d_2}{\partial T_g} + dA_{22} + dB_{22}$$

With the function and Jacobian in place, Newtons method can be used to locate a zero of the function starting from an initial point such as  $T_v=T_g=T_a$ .

#### 11.4.1 Special Case (1) - PET

In the case of the Potential ET we will assume this means  $r_{sv}=r_{sg}=0$ .

That is the energy balance becomes:

$$A_v = \frac{rC_p}{g} \frac{(e_s(T_v) - e_0)}{r_v} + rC_p \frac{(T_v - T_0)}{r_v}$$

$$A_g = \frac{rC_p}{g} \frac{(e_s(T_g) - e_0)}{r_g} + rC_p \frac{(T_g - T_0)}{r_g}$$

It then also follows that  $c'_j = c_j$  for  $j = 1, 3$  and:

$$\mathbf{A} = \frac{1}{\mathbf{g}} \mathbf{B}$$

so that:

$$\mathbf{e}(T_v, T_g) = \mathbf{B} \begin{pmatrix} \frac{1}{\mathbf{g}} e_s(T_v) + T_v \\ \frac{1}{\mathbf{g}} e_s(T_g) + T_g \end{pmatrix} - \mathbf{d}$$

or

$$\begin{aligned} \mathbf{e}_1 &= b_{11} \left( \frac{1}{\mathbf{g}} e_s(T_v) + T_v \right) + b_{12} \left( \frac{1}{\mathbf{g}} e_s(T_g) + T_g \right) - d_1 \\ \mathbf{e}_2 &= b_{21} \left( \frac{1}{\mathbf{g}} e_s(T_v) + T_v \right) + b_{22} \left( \frac{1}{\mathbf{g}} e_s(T_g) + T_g \right) - d_2 \end{aligned}$$

The vector  $\mathbf{d}$  is now simplified so that:

$$\begin{aligned} d_1 &= \frac{A_v}{rC_p} + \frac{c_1}{r_v} \left( \frac{1}{\mathbf{g}} e_a + T_a \right) \\ d_2 &= \frac{A_g}{rC_p} + \frac{c_1}{r_g} \left( \frac{1}{\mathbf{g}} e_a + T_a \right) \end{aligned}$$

and the partials are:

$$\frac{\mathbf{d}}{\mathbf{T}_x} = \frac{1}{rC_p} \begin{pmatrix} \mathbf{A}_v \\ \mathbf{T}_x \\ \mathbf{A}_g \\ \mathbf{T}_x \end{pmatrix} + \frac{c_1}{\mathbf{T}_x} \begin{pmatrix} \frac{1}{\mathbf{g}} \frac{e_a}{r_v} + \frac{T_a}{r_v} \\ \frac{1}{\mathbf{g}} \frac{e_a}{r_g} + \frac{T_a}{r_g} \end{pmatrix}$$

so if we redefine:

$$\begin{aligned} dB_{11} &= \frac{\mathbf{b}_{11}}{\mathbf{T}_v \mathbf{g}} \left( \frac{1}{\mathbf{g}} e_s(T_v) + T_v \right) + \frac{\mathbf{b}_{12}}{\mathbf{T}_v \mathbf{g}} \left( \frac{1}{\mathbf{g}} e_s(T_g) + T_g \right) \\ dB_{12} &= \frac{\mathbf{b}_{11}}{\mathbf{T}_g \mathbf{g}} \left( \frac{1}{\mathbf{g}} e_s(T_v) + T_v \right) + \frac{\mathbf{b}_{12}}{\mathbf{T}_g \mathbf{g}} \left( \frac{1}{\mathbf{g}} e_s(T_g) + T_g \right) \\ dB_{21} &= \frac{\mathbf{b}_{21}}{\mathbf{T}_v \mathbf{g}} \left( \frac{1}{\mathbf{g}} e_s(T_v) + T_v \right) + \frac{\mathbf{b}_{22}}{\mathbf{T}_v \mathbf{g}} \left( \frac{1}{\mathbf{g}} e_s(T_g) + T_g \right) \\ dB_{22} &= \frac{\mathbf{b}_{21}}{\mathbf{T}_g \mathbf{g}} \left( \frac{1}{\mathbf{g}} e_s(T_v) + T_v \right) + \frac{\mathbf{b}_{22}}{\mathbf{T}_g \mathbf{g}} \left( \frac{1}{\mathbf{g}} e_s(T_g) + T_g \right) \end{aligned}$$

it follows that:

$$\begin{aligned}\frac{\mathcal{J}\mathbf{e}_1}{\mathcal{J}T_v} &= J_{11} = b_{11}\left(\frac{1}{g}\Delta_1 + 1\right) - \frac{\mathcal{J}d_1}{\mathcal{J}T_v} + dB_{11} \\ \frac{\mathcal{J}\mathbf{e}_1}{\mathcal{J}T_g} &= J_{12} = b_{12}\left(\frac{1}{g}\Delta_2 + 1\right) - \frac{\mathcal{J}d_1}{\mathcal{J}T_g} + dB_{12} \\ \frac{\mathcal{J}\mathbf{e}_2}{\mathcal{J}T_v} &= J_{21} = b_{21}\left(\frac{1}{g}\Delta_1 + 1\right) - \frac{\mathcal{J}d_2}{\mathcal{J}T_v} + dB_{21} \\ \frac{\mathcal{J}\mathbf{e}_2}{\mathcal{J}T_g} &= J_{22} = b_{22}\left(\frac{1}{g}\Delta_2 + 1\right) - \frac{\mathcal{J}d_2}{\mathcal{J}T_g} + dB_{22}\end{aligned}$$

These equation still need to be solved by nonlinear methods but the simplification will improve the stability over simply setting  $r_{sv}=r_{sg}=0$  in the general solver.

#### 11.4.2 Special Case (2) - Infinite resistance (no water!)

In the other special case,  $r_{sv}=r_{sg}=\infty$  which involves some significant simplifications.

In this case:

$$\begin{aligned}A_v &= rC_p \frac{(T_v - T_0)}{r_v} \\ A_g &= rC_p \frac{(T_g - T_0)}{r_g}\end{aligned}$$

and

$$\mathbf{A} = \mathbf{0}$$

so it follows that the equation to solve is:

$$\mathbf{e}(T_v, T_g) = \mathbf{B} \begin{pmatrix} T_v \\ T_g \end{pmatrix} - \mathbf{d}$$

or to find the zeros of:

$$\begin{aligned}\mathbf{e}_1 &= b_{11}T_v + b_{12}T_g - d_1 \\ \mathbf{e}_2 &= b_{21}T_v + b_{22}T_g - d_2\end{aligned}$$

The vector  $\mathbf{d}$  is now simplified so that:

$$d_1 = \frac{A_v}{rC_p} + \frac{c_1 T_a}{r_v}$$

$$d_2 = \frac{A_g}{rC_p} + \frac{c_1 T_a}{r_g}$$

and the partials are:

$$\frac{\mathcal{J}\mathbf{d}}{\mathcal{J}T_x} = \frac{1}{rC_p} \begin{pmatrix} \mathcal{J}A_v \\ \mathcal{J}T_x \\ \mathcal{J}A_g \\ \mathcal{J}T_x \end{pmatrix} + \frac{\mathcal{J}c_1}{\mathcal{J}T_x} \begin{pmatrix} T_a \\ r_v \\ T_a \\ r_g \end{pmatrix}$$

With these in place, the Jacobian can be assembled as follows:

$$\frac{\mathcal{J}\mathbf{e}_1}{\mathcal{J}T_v} = J_{11} = b_{11} - \frac{\mathcal{J}d_1}{\mathcal{J}T_v} + dB_{11}$$

$$\frac{\mathcal{J}\mathbf{e}_1}{\mathcal{J}T_g} = J_{12} = b_{12} - \frac{\mathcal{J}d_1}{\mathcal{J}T_g} + dB_{12}$$

$$\frac{\mathcal{J}\mathbf{e}_2}{\mathcal{J}T_v} = J_{21} = b_{21} - \frac{\mathcal{J}d_2}{\mathcal{J}T_v} + dB_{21}$$

$$\frac{\mathcal{J}\mathbf{e}_2}{\mathcal{J}T_g} = J_{22} = b_{22} - \frac{\mathcal{J}d_2}{\mathcal{J}T_g} + dB_{22}$$

Again, this must be solved by non-linear iteration but the solution is more stable and the iteration faster when the simplifications are built in.